Mathematical models of infectious diseases in ungulate populations

Xander O'Neill

A thesis submitted for the degree of
Doctor of Philosophy

School of Mathematics and Computer Science, Heriot-Watt University

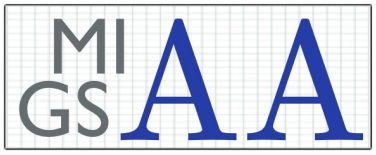

Maxwell Institute Graduate School in Analysis and its Applications

THE UNIVERSITY *of* EDINBURGH

School of Mathematics,
University of Edinburgh

October 13, 2021

Abstract

In this thesis we develop a suite of mathematical models to understand the epidemiological dynamics of infectious diseases in ungulate hosts. Using ordinary differential equation frameworks, we explored the key routes of transmission that promote the persistence of the highly virulent African swine fever (ASF) infection in wild boar and tested control strategies that could limit ASF outbreaks and its persistence. These modelling techniques were extended to investigate the impact of an ASF outbreak on endemic tuberculosis in wild boar. The generality of the model framework meant the results could add new perspective on the coexistence of multiple pathogens. Motivated by the work on the persistence of ASF, we used a suite of stochastic continuous-time Markov chain models to show that latent and chronic infection could have a significant impact on the mean time to pathogen extinction. We also developed a model framework to assess how hosts, including ungulates, contribute to tick-borne infections. This expands on previously studied models such that the regulation of tick density is dependent on the density of the specific hosts on which different tick stages feed. Our results outlined the effect host density and composition could have on tick-borne prevalence and incidence levels. The work in this thesis has highlighted how mathematical models are important tools for understanding epidemiological dynamics in wildlife systems with our work having had an impact on the management of key, current, endemic and emerging diseases in ungulates.

Dedications

This thesis is dedicated to my loving family and friends. Thank you for all your love, support and all the times where you "smile and wave", trying or pretending to understand my research.

Acknowledgments

Firstly, I would like to thank my supervisor Prof. Andy White, who has helped make this PhD rather enjoyable and with whom I enjoyed many trips abroad, had many Italian and Spanish beverages and met so many fantastic new people. His guidance and support was constant throughout and allowed me to expand my mathematical knowledge and develop more transferable skills. It will be a pleasure to work with him for future projects.

I would also like to thank both Christian Gortázar and Francisco Ruiz-Fons, who worked incredibly hard and provided us with all the biological information, without which it would have been extremely difficult to model the systems we did. It was always a pleasure to see them both and enjoy various culinary treats and home-cooked tapas.

Thank you to all the various people involved with MIGSAA, both the staff and the fellow students, and all the friends and colleagues at Heriot-Watt for helping make the experience that bit more welcoming and enjoyable.

Finally, I would like to thank my wonderful family and friends. You have all been incredibly supportive the past four years and even if you didn't quite understand my research you all kept me as sane as I can possibly be.

Xander O'Neill was supported by The Maxwell Institute Graduate School in Analysis and its Applications, a Centre for Doctoral Training funded by the UK Engineering and Physical Sciences Research Council (grant EP/L016508/01), the Scottish Funding Council, Heriot-Watt University and the University of Edinburgh. I would also like to acknowledge the contribution of the COST Action ASF-STOP CA15116, from the MCIU project CGL2017-89866-R and support from Fundación Biodiversidad, Ministerio de Transición Ecológica.

Declaration Statement

I declare that the thesis has been composed by myself and that the work has not been submitted for any other degree or professional qualification. I confirm that the work submitted is my own, except where work which has formed part of jointly-authored publications has been included. My contribution and those of the other authors to this work have been explicitly indicated below. I confirm that appropriate credit has been given within this thesis where reference has been made to the work of others.

The work presented in Chapter 2 was previously published in *Scientific Reports* as "Modelling the transmission and persistence of African swine fever in wild boar in contrasting European scenarios" by Xander O'Neill (author of thesis), Andy White (supervisor), Fran Ruiz-Fons and Christian Gortázar. This study was conceived by all of the authors. I carried out the mathematical modelling and analysis, numerical simulations and write up of the paper.

The work presented in Chapter 3 was previously published in *Transboundary and Emerging Diseases* as "The impact of an African swine fever outbreak on endemic tuberculosis in wild boar populations: A model analysis" by Xander O'Neill (author of thesis), Andy White (supervisor), Fran Ruiz-Fons and Christian Gortázar. This study was conceived by all of the authors. I carried out the mathematical modelling and analysis, numerical simulations and write up of the paper.

The work presented in Chapter 4 was previously published in *Mathematics* as "The influence of latent and chronic infection on pathogen persistence" by Xander O'Neill (author of thesis), Andy White (supervisor), Damian Clancy (second supervisor), Fran

Ruiz-Fons and Christian Gortázar. This study was conceived by all of the authors. I carried out the mathematical modelling and analysis, numerical simulations and write up of the paper.

Research Thesis Submission

Name*:*	Xander O'Neill		
School:	School of Mathematics		
Version: *(i.e. First, Resubmission, Final)*	Final	Degree Sought:	Doctor of Philosophy

Declaration

In accordance with the appropriate regulations I hereby submit my thesis and I declare that:

1. The thesis embodies the results of my own work and has been composed by myself
2. Where appropriate, I have made acknowledgement of the work of others
3. The thesis is the correct version for submission and is the same version as any electronic versions submitted*.
4. My thesis for the award referred to, deposited in the Heriot-Watt University Library, should be made available for loan or photocopying and be available via the Institutional Repository, subject to such conditions as the Librarian may require
5. I understand that as a student of the University I am required to abide by the Regulations of the University and to conform to its discipline.
6. I confirm that the thesis has been verified against plagiarism via an approved plagiarism detection application e.g. Turnitin.

ONLY for submissions including published works

7. Where the thesis contains published outputs under Regulation 6 (9.1.2) or Regulation 43 (9) these are accompanied by a critical review which accurately describes my contribution to the research and, for multi-author outputs, a signed declaration indicating the contribution of each author (complete)
8. Inclusion of published outputs under Regulation 6 (9.1.2) or Regulation 43 (9) shall not constitute plagiarism.

* *Please note that it is the responsibility of the candidate to ensure that the correct version of the thesis is submitted.*

Signature of Candidate*:*	XO'Neill	Date:	11/10/2021

Submission

Submitted By *(name in capitals):*	XANDER O'NEILL
Signature of Individual Submitting:	XO'Neill
Date Submitted:	11/10/2021

For Completion in the Student Service Centre (SSC)

Limited Access	Requested	Yes		No		Approved	Yes		No	
*E-thesis Submitted (**mandatory for final theses)***										
Received in the SSC by *(name in capitals):*						Date:				

Inclusion of Published Works

Declaration

This thesis contains one or more multi-author published works. In accordance with Regulation 6 (9.1.2) I hereby declare that the contributions of each author to these publications is as follows:

Citation details	O'Neill, X., White, A., Ruiz-Fons, F. and Gortázar, C., (2020). Modelling the transmission and persistence of African swine fever in wild boar in contrasting European scenarios. *Scientific reports*, 10(1), pp.1-10.
O'Neill, X.	This study was conceived by all of the authors. I carried out the mathematical modelling and analysis, numerical simulations and write up of the paper.
Signature:	XO'Neill
Date:	11/10/2021

Citation details	O'Neill, X., White, A., Ruiz-Fons, F. and Gortázar, C., (2021). The impact of an African swine fever outbreak on endemic tuberculosis in wild boar populations: A model analysis. *Transboundary and Emerging Diseases*. 00:1-11.
O'Neill, X.	This study was conceived by all of the authors. I carried out the mathematical modelling and analysis, numerical simulations and write up of the paper.
Signature:	XO'Neill
Date:	11/10/2021

Citation details	O'Neill, X., White, A., Clancy, D., Ruiz-Fons, F. and Gortázar, C., (2021). The Influence of Latent and Chronic Infection on Pathogen Persistence. *Mathematics*, 9(9), p.1007.
O'Neill, X.	This study was conceived by all of the authors. I carried out the mathematical modelling and analysis, numerical simulations and write up of the paper.
Signature:	XO'Neill
Date:	11/10/2021

Contents

Chapter 1

Introduction

1.1 Wildlife disease

The impact of infectious disease on wildlife species is pervasive, with many wildlife pathogens causing a deterioration of host health. Pathogen maintenance in wildlife populations can lead to infection spillover to livestock which can have consequential impacts on food productions [1]. Furthermore, wildlife pathogens are often zoonotic and can impact both human health and the economy. With a high proportion of emerging human pathogens originating from wildlife [2, 3] and an increasing trend in the number of emerging infectious disease events originating in wildlife, this poses a significant threat to global health [4, 2]. This threat is enhanced when considering the ever changing and adapting environments that may promote the evolution of pathogens whereby new strains can more effectively spread within a population [5, 6]. This has prompted a growing interest in the control and maintenance of disease in wildlife hosts. Methods commonly used include culling, vaccination, habitat management, fencing and arthropod vector control. However, whilst they may be effective, changes in wildlife management can also be considered drivers of pathogen emergence [4, 7]. Mathematical models are useful tools to further understand epidemiological and wildlife ecosystems and suggest potential methods of control to inform governments and policy makers prior to active management in the natural system.

An array of mathematical modelling approaches have been developed and used to ex-

plore and understand the spread and persistence of infectious disease [8]. These include the classical compartmental models first developed by Ross and Hudson (1917) [9] and brought to prominence by Anderson and May (1979) [10]. More recently individual-based models [11, 12, 13] Bayesian-Monte Carlo-Markov chain methods [14, 15] and Approximate Bayesian Computation [16] have been used to provide predictive assessments of epidemiological dynamics and disease management outcomes. Deterministic models can be more analytically tractable than their stochastic equivalents and are often suitable for understanding the key drivers of the epidemiological dynamics. However, wildlife systems are inherently probabilistic in nature, meaning stochastic models are often more representative, especially when considering pathogen persistence at low population levels [8]. Individual-based models (also known as agent-based models) often try to describe many of the processes of the real system and can therefore be over-complex and hard to parameterise and interpret [8]. Developing a model with the ability to describe the dynamics of a given system can be difficult, especially if data is scarce. In the case of wildlife infectious disease systems there is limited data available in comparison to data for livestock or human disease [8], making it harder to fit or parameterise complex models. In models where infection occurs through solely density-dependent transmission it has been shown that pathogens could not cause the extinction of a population, as the pathogen would die out at low levels of population density [10]. However, in some scenarios, such as the Tasmanian devil facial tumour disease, contact rates don't depend on host density and instead appear to be related to mating behaviours (frequency-dependent transmission) [3, 17] and in others, such as African swine fever, environmental transmission from infected carcasses can also play an important role in the transmission of disease [18, 19]. This can affect the long-term population dynamics. In selecting a model framework it is often a good strategy to choose the simplest model that still has the ability to answer and understand the key questions associated with the system of interest [20].

Two particular infectious diseases are discussed in this thesis: African swine fever (ASF), which affects both domestic pigs and wild boar (*Sus Scrofa*) and tuberculosis (TB), which can affect a wide range of wildlife hosts and humans, with an additional general

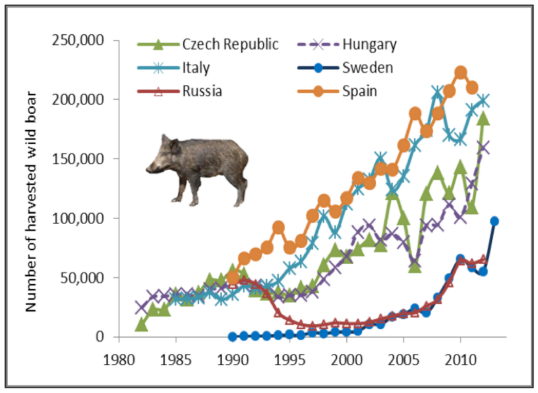

(a) The increasing trend in wild boar population density over the past 30-40 years [22].

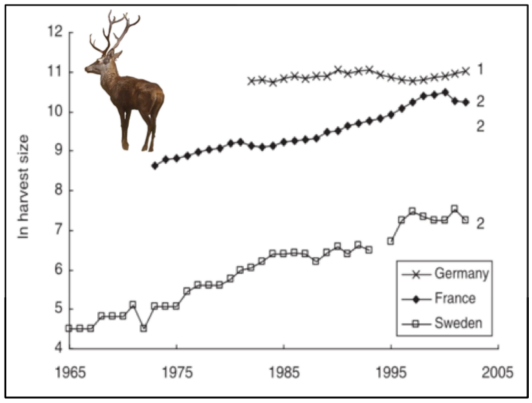

(b) The increasing trend in red deer population density over the past 30-40 years [23].

Figure 1.1: Trends in ungulate population densities.

study on tick-borne infectious diseases vectored in wildlife hosts that can be transmitted to humans. Ungulates such as wild boar and red deer are key host species for these infectious diseases, and there is evidence of an increasing trend in their population density [21, 22, 23, 24] (see Figure 1.1a and 1.1b). This could cause an increase in infection prevalence and an increased risk of infection spillover to other populations, including humans.

1.2 African swine fever

1.2.1 Background and motivation

African swine fever (ASF) virus, belonging to the Asfarviridae family, is a virulent virus affecting domestic pigs, wild boar (*Sus scrofa*) and African wild suids and is currently endemic in sub-Saharan Africa. In Europe the virus first emerged in 1957 in Portugal, spreading subsequently to Spain, France, Belgium, the Netherlands, Italy and Malta. The epidemic was eradicated in mainland Europe and Malta in 1999 through control of infected and at-risk domestic pig populations and by imposing strict biosecurity measures [25]. However, the infection still persists on Sardinia [26, 27]. A second epidemic started in Georgia in 2007. In the same year, ASF was reported in wild boar in the Russian Federation and by 2014 it had spread to Ukraine, Belarus, Estonia, Latvia, Lithuania and Poland [28], where ASF remains present. Recent outbreaks have been reported in the Czech Republic (the only successfully eradicated local outbreak), Bel-

gium (ongoing local outbreak), Slovakia and several south-east European countries [29]. In 2018, ASF was reported in China, where it has since spread to surrounding countries including Mongolia, Vietnam, Cambodia, North Korea, Laos, Myanmar, Philippines, South Korea, Timor-Leste, Indonesia, Papua New Guinea and India [30, 31, 32]. This suggests ASF is still spreading and therefore poses a substantial threat to some of Europe's most significant pig farming regions. ASF has a large economic impact in affected countries due to losses in pig production and food security threats and is listed as a notifiable disease by the World Organisation for Animal Health [33, 34].

Epidemic outbreaks of ASF typically lead to a population reduction of $85 - 95\%$ [28] with infection from highly virulent strains leading to near 100% mortality at the individual level [35, 36, 37, 38, 34]. However, a less common form of infection has been observed where individuals develop a persistent infection, which may be accompanied by signs of sub-acute or chronic disease [39, 40], with the potential for virus excretion and transmission with the resurgence of viraemia [41, 40]. ASF is highly contagious and potential transmission routes include direct transmission through close contact with infected individuals [42] and through environmental contamination due to the persistence of infection in carcasses, which can be contaminated with ASF for a considerable length of time [19]. In wildlife populations, commonly wild boar populations, the infectious disease dynamics do not exhibit a typical epidemic pattern for highly virulent, acute infections with self-limiting localized epidemics [35], and instead can persist in low density populations at low prevalence $(1 - 3\%)$ for several years following an epidemic [28]. Understanding the epidemiological dynamics of ASF in wild boar will be key to the management of infectious outbreaks.

Despite the documented importance of wild boar in the spread of ASF, an understanding of the epidemiological dynamics is incomplete and little is known about the key mechanisms that drive infection transmission and disease persistence [39, 40]. Understanding these key infection processes is critical to predicting the effectiveness of different control strategies, such as culling and carcass removal, to manage and eradicate ASF [43, 41]. Gaining a clear understanding of the infection and transmission

dynamics and developing strategies to control ASF outbreaks is a key, current priority [43]. The challenge is intensified due to the unprecedented increase of wild boar density over the last decades [21, 22, 24], which is likely to enhance their ability to contribute to ASF spread and maintenance (see Figure 1.1a).

1.2.2 Aims and objectives

In this thesis mathematical models are developed to explore the epidemiological dynamics of ASF in wild boar with the aim of understanding the drivers of ASF persistence (see Chapter 2). To do this the key potential transmission routes for ASF are incorporated into a deterministic ordinary differential equation (ODE) model which is then used to explore the impact of the different transmission routes on driving a disease outbreak and on the long-term persistence of infection. The model is then extended to consider scenarios that are representative of different European regions and to consider the impact of different control strategies on disease eradication. The work here, exploring mechanisms that promote the persistence of ASF, motivated a more general study examining how latent and chronic forms of infection affect disease persistence (see Chapter 4).

1.3 Tuberculosis

1.3.1 Background and motivation

Animal tuberculosis (TB) is a widespread multi-host disease caused by infection with *Mycobacterium bovis* and the closely related members of the *M. tuberculosis* complex (MTC) and leads to increased host mortality [44]. It was first discovered in the 19th century [45, 46] and has since spread globally to New Zealand, African, North America, Europe and Asia. The primary reservoir species vary with location and include European badgers (*Meles meles*) in the British Isles, cervids in North America, brushtail possums (*Trichosurus vulpecula*) in New Zealand and buffalo (*Syncerus caffer*) in South Africa, among others [47, 48, 49, 50]. In mainland Europe, and in particular on the Iberian Peninsula, wild ungulates such as the Eurasian wild boar (*Sus scrofa*) and red

deer (*Cervus elaphus*) act as the primary reservoir of infection [48, 51, 49, 52, 53]. Tuberculosis is considered to have infected over two billion people worldwide [54], killing two million people per year [55] and whilst it is primarily a pulmonary infection it can also affect the central nervous system and other organ systems [55]. It is therefore considered a global major health problem [56, 57].

TB has a significant economic impact on the livestock industry due to test and slaughter schemes and movement restrictions [48, 58, 59] and within the European Union, there has been funding and a long-term policy to reduce and eradicate TB [60]. Other intervention measures include reducing indirect contacts among host species [61, 50, 62], vaccinating [63, 64] and culling [65, 66, 50]. Nevertheless, there is an increasing prevalence of infection among cattle herds in Europe, with the EU herd prevalence at 0.4% in 2008 and at 0.9% in 2018 [67]. Whilst bovine TB has largely been eradicated in some European countries it still persists in the UK, Republic of Ireland, the Iberian peninsula and some other Mediterranean countries [48]. In the UK it persists in badgers with a prevalence range of $1.6 - 37.2\%$ and in Spain it persists in wild boar, at a prevalence of $46 - 52\%$ [68, 69], and red deer, with a prevalence of up to 27% [70].

A key issue for the control of TB is its persistence in wildlife reservoirs from which it can spillover to livestock [71, 49, 50]. As TB is a multi-host disease its epidemiology is more complex than single-host diseases. This provides a greater challenge in disease control as any measures to completely eradicate the infection must include all reservoirs [53]. Furthermore, due to the increasing habitat suitability and decreasing hunting pressure, the density of wild ungulates has seen an unprecedented increase over the last decades [72, 22, 23] (see Figure 1.1a and 1.1b) and this presents a further challenge for TB management.

1.3.2 Aims and objectives

A mathematical model is developed which combines and modifies the work in Chapter 2, exploring the dynamics and persistence of ASF in wild boar, with the model used Tanner et al. (2019) [66] for animal TB in wild boar (see Chapter 3). This work

explores the impact of an emerging disease (in this case African swine fever) on an endemic disease (TB) in a wild boar population. We aim to examine the role of the emerging disease to assess its impact in the control and eradication of TB in wild boar. Our model study adds new perspective to the theory on the coexistence of multiple pathogens. It includes co-infection of the host by different pathogens that infect the host through density-dependent and frequency-dependent mechanisms. In particular, the component of the pathogen reproductive ratio arising through frequency-dependent transmission does not depend on host density and we show that this transmission mechanism can promote pathogen coexistence and prevent the pathogen exclusion that arises due to disease-induced suppression of the host density.

1.4 Tick-borne disease

1.4.1 Background and motivation

Ticks are a parasitic invertebrate, of the class *Arachnida*, that survive by feeding on the blood of warm-blooded animals [73]. There exist two main sub-classes of ticks: Ixodid ticks (hard ticks) and Argasid ticks (soft ticks) both with a structured life cycle of progression from egg to larvae to nymph and finally to adult stages that can lay further eggs [73]. Progression between stages requires at least one blood meal with larvae generally feeding on small mammals, such as rabbits (*Oryctolagus cuniculus*), hares (*Lepus*) or birds; and adults generally feeding on large mammals, such as red deer (*Cervus elaphus*), wild boar (*Sus scrofa*) or humans (*Homo Sapien*), although this can vary depending on the type of tick considered [74, 75]. The interaction between ticks and hosts means they are a vector for the transmission of infectious disease [76]. Ticks can be infected with range of infections, ranging from bacterial diseases, such as Lyme disease or spotted fevers, to protozoa diseases, such as babesiosis, and to viral diseases, such as Crimean Congo Haemorrhagic fever virus [77, 78, 79]. Due to the increase in antimicrobial resistance among bacterial pathogens, there has been an increase in the number of zoonotic disease occurrences which could have a resulting strong impact on the animals and humans at risk [80, 79]. Both ticks and hosts can act as reservoirs for certain tick-borne infections [81] providing a challenge in the control and mainte-

nance of tick-borne disease. Wild ungulates are key hosts for ticks and tick disease and current evidence suggests a widespread increase in the density of wild ungulates across Europe (see Figure 1.1a and 1.1b). Since these are key hosts for ticks this could have an impact on tick density with a consequent impact on the prevalence and risk of zoonotic transmission of tick-borne infectious disease.

Mathematical models have been used to explore and understand the epidemiological dynamics of host-tick interactions and the persistence of tick-borne diseases [82, 83, 84]. Switkes et al. (2016) [84] developed a model for Crimean-Congo Haemorrhagic Fever virus (CCHFv) and explored thresholds for disease persistence, including the reproductive number of the virus, as well as the progression of the disease under a hypothetical outbreak. Tick-human transmission was identified as the main cause for the spread of CCHFv to humans. Norman et al. 1999 [82] developed a model to understand the persistence of the Louping-ill virus in grouse which was then extended and generalised by Rosá et al. (2003) [85]. In both studies a tick age-structured model was used where all stages could feed on either a viraemic or non-viraemic host and while the tick birth rate was linked to host density it was limited through self-regulation as tick density increased. These models therefore cannot capture the full impact of changes in host density on tick demography. Rosá and Pugliese (2007) [83] and Pugliese and Rosá (2008) [86] explored the impact of host population density on tick population dynamics and the persistence of tick-borne infections. They found that the effect that host densities have on tick-borne disease can depend strongly on how the tick population is regulated. While these studies consider the link between host density and tick density this is not their main focus and they do not fully recognise that different tick stages feed on different hosts whose densities may follow different trends (larval ticks will focus on small mammals and adult ticks will focus on large mammals).

1.4.2 Aims and objectives

A mathematical model is developed to investigate the effect host density has on tick density and consequently the impact of host density on the prevalence and spread of tick-borne diseases and their risk to humans (see Chapter 5). The models developed

by Rosá and Pugliese (2007) and Pugliese and Rosá (2008) are extended to explicitly link the development of specific tick stages to the specific hosts on which they feed. We show how variation in host density and host composition could explain the observed variation in prevalence and incidence of tick-borne disease.

1.5 Thesis methods

In all chapters systems of ordinary differential equations are used to formulate the respective models, with model results simulated using the in-built Matlab ODE solver *ode*45. This particular solver uses the Runge-Kutta 4^{th} and 5^{th} order numerical schemes with a variable time step to solve the system of equations over time [87]. The population densities at each time step are then stored and plotted to show the temporal dynamics of the system. For results where population density averages are calculated over a given time frame (see, for example, Figures 2.2 and 2.3 in Chapter 2), the specific densities for that particular time frame can be obtained and then averaged to produce the relevant results. Where steady state densities are plotted, (see, for example, Figures 5.5 and 5.6 in Chapter 5) the numerical simulations are run for a considerable period of time, $t = 150000$, to ensure that the population has settled to its steady state value. For Chapters 2 and 3 all rates are given per year and in Chapter 4 the model parameters can be considered generic and so rates are given per unit time. For Chapter 5 only steady state densities are considered. However, the model developed here uses parameters from Rosá and Pugliese (2007) [83] and so rates are given per year.

For Chapter 4, continuous-time Markov chain models are used to determine the mean time to pathogen extinction for different model frameworks [88, 89]. Here, we start with an initial population state (for example, 995 susceptible individuals and 5 infected individuals) and after a time step, dt, with a given probability, a transition event occurs where the population state changes. This process is repeated until the number of individuals that contribute to the infection reaches zero, indicating that the pathogen has gone extinct. The time taken to reach this state gives us the time to pathogen extinction for a single realisation. This process can then be repeated for many realisations,

and then averaged, to provide a mean time to pathogen extinction. The probability of a given transition event occurring is equal to the respective transition rate divided by the sum of all transition rates, R_T. The time step, dt, is a random variable selected from an exponential distribution with mean $\mu = R_T$. When calculating the mean time to pathogen extinction in Chapter 4 all realisations are run up to a large unit of time, for example $t = 1000$, where under all model frameworks the pathogen has gone extinct.

Steady state analysis can be seen within Chapter 3 and is used for the derivation of the reproductive numbers seen in this thesis. The reproductive number of a pathogen is the expected number of individuals that will become infected when a single infected individual is introduced into a disease-free population. Mathematically this can be calculated through the linearisation about the disease-free steady state or by using the Next Generation Matrix (NGM) approach [90, 91, 92]. When linearising about the steady state, an equality can be found where, if satisfied, the disease-free steady state becomes unstable. This equality can then be rearranged to give the reproductive number, R_0, where should $R_0 > 1$ the disease-free steady state is unstable and vice-versa.

1.6 Thesis organisation

The thesis is organised as follows:

Chapter 2 develops a mathematical model to explore the persistence of African swine fever in wild boar, aiming to understand how this highly virulent infection can persist following an outbreak.

Chapter 3 expands previously studied mathematical models to examine the impact of an emerging infection (African swine fever) on an endemic infection (tuberculosis) in a wild boar population.

Chapter 4 uses a suite of stochastic continuous-time Markov chain models to explore

how latent and chronic infections affect the mean time to extinction of an infectious disease.

Chapter 5 develops a mathematical model for the host-tick system where tick development is linked to the specific hosts on which each tick stage feeds and examines how host density and composition affects the prevalence of tick-borne infectious disease.

Chapter 6 discusses the key findings of the thesis and the over-arching impact of the research conducted.

The work in Chapters 2, 3 and 4 have appeared in peer-reviewed research publications. The work in Chapter 5 develops the methodology for work that we hope will lead to a further publication.

1.7 Code Repository

All code developed and used for this thesis can be obtained in the following code repository: https://github.com/XanderONeill/PhD_Thesis_Math_modelling

Chapter 2

Modelling the transmission and persistence of African swine fever in wild boar in contrasting European scenarios

The work in this chapter has been published in:

> O'Neill, X., White, A., Ruiz-Fons, F. and Gortázar, C., 2020. Modelling the transmission and persistence of African swine fever in wild boar in contrasting European scenarios. *Scientific reports*, 10(1), pp.1-10. https://doi.org/10.1038/s41598-020-62736-y

but has been modified to provide a clearer explanation of the persistence of ASF in different model scenarios.

Abstract

African swine fever (ASF) is a severe viral disease that is currently spreading among domestic pigs and wild boar (*Sus scrofa*) in large areas of Eurasia. Wild boar play a key role in the spread of ASF, yet despite their significance, little is known about the key mechanisms that drive infection transmission and disease persistence. A mathematical model of the wild boar ASF system is developed that captures the observed drop in population density, the peak in infected density and the persistence of the virus observed in ASF outbreaks. The model results provide insight into the key processes that drive the ASF dynamics and show

that environmental transmission is a key mechanism determining the severity of an infectious outbreak and that direct frequency-dependent transmission and transmission from individuals that survive initial ASF infection but eventually succumb to the disease are key for the long-term persistence of the virus. By considering scenarios representative of Estonia and Spain we show that the faster degradation of carcasses in Spain, due to elevated temperature and abundant obligate scavengers, may reduce the severity of the infectious outbreak. Our results also suggest that the higher underlying host density and longer breeding season associated with supplementary feeding leads to a more pronounced epidemic outbreak and persistence of the disease in the long-term. The model is used to assess disease control measures and suggests that a combination of culling and infected carcass removal is the most effective method to eradicate the virus without also eradicating the host population, and that early implementation of these control measures will reduce infection levels whilst maintaining a higher host population density and, in some situations, prevent ASF from establishing in a population.

2.1 Introduction

African swine fever (ASF) virus, belonging to the Asfarviridae family, is a virulent virus affecting domestic pigs, wild boar (*Sus scrofa*) and African wild suids. Infection from highly virulent strains leads to near 100% mortality at the individual level [36, 37, 38, 34], and outbreaks typically lead to significant population loss [28]. ASF has a large economic impact in affected countries due to losses in pig production and food security threats and is listed as a notifiable disease by the World Organisation for Animal Health [33, 34]. Gaining a clear understanding of the infection and transmission dynamics and developing strategies to control ASF outbreaks is a key, current priority [43].

African swine fever is endemic in wild suids and domestic pigs in sub-Saharan Africa. The virus first emerged in Europe in 1957 in Portugal, spreading subsequently to Spain, France, Belgium, the Netherlands, Italy and Malta. The epidemic was eradicated in mainland Europe and Malta in 1999 through control of infected and at-risk domestic pig populations and by imposing strict biosecurity measures [25]. However, the infection still persists on Sardinia [26, 27]. A second epidemic started in Georgia in 2007. In

the same year, ASF was reported in wild boar in the Russian Federation and by 2014 it had spread to Ukraine, Belarus, Estonia, Latvia, Lithuania and Poland [28], where ASF remains present. Recent outbreaks have been reported in the Czech Republic (the only successfully eradicated local outbreak), Belgium (ongoing local outbreak), Slovakia and several south-east European countries [29]. This suggests ASF is still spreading and therefore poses a substantial threat to some of Europe's most significant pig farming regions. The presence of ASF infection in wild boar populations represents a current and significant disease management challenge across Eurasia [43]. The challenge is intensified as the density of wild boar has experienced an unprecedented increase over the last decades [22], which is likely to enhance their ability to contribute to ASF spread and maintenance.

Despite the documented importance of wild boar in the spread of ASF, an understanding of the epidemiological dynamics is incomplete and little is known about the key mechanisms that drive infection transmission and disease persistence [39, 40]. ASF typically leads to an acute infection with close to 100% individual mortality around $4-9$ days following exposure [35, 36]. A less common form of infection is possible, where individuals do not die but develop a persistent infection, which may be accompanied by signs of sub-acute or chronic disease [39, 40]. This invariably leads to death, with the potential to excrete virus in association with the resurgence of viraemia [41, 40]. Such individuals are termed type 1 'survivors' by Ståhl et al. [40] since they survive the initial ASF infection and we will call such individuals 'survivors' in this study. Infection can lead to a population reduction of $85-95\%$ in the initial epidemic phase [28]. The disease does not exhibit a typical epidemic pattern for highly virulent, acute infections with self-limiting localized epidemics [35], and instead can persist in low density populations at low prevalence $(1-3\%)$ for several years following an epidemic [28]. ASF is highly contagious and potential transmission routes include direct transmission through close contact with infected individuals [42] - which may occur within social groups and more widely if social groups congregate at feeding stations or water holes. Transmission may also occur via environmental contamination due to the persistence of infection in carcasses. Such carcasses can be contaminated with ASF virus for a considerable length

of time [19] and contact with carcasses poses a significant risk of transmission [39, 35]. Understanding these key infection processes is critical to predicting the effectiveness of different control strategies, such as culling and carcass removal, to manage and eradicate ASF [43, 41].

Mathematical models have played a key role in understanding the processes that drive epidemiological dynamics in wildlife populations [10, 93]. In the context of ASF, statistical spatial models have shown that survivor individuals and infectious residue from dead animals may be important for the spread and persistence of ASF [94]. Statistical models have also been fitted to data to examine the spread of ASF in the Russian Federation [37, 34], the impact of control zones on the (hypothetical) persistence of ASF in Denmark [95], and to examine the between farm spread of ASF in domestic pigs in Sardinia [96], suggesting wild boar management may be a key component in reducing spread in farmed populations. Model studies have also been used to undertake a risk assessment for the spread of ASF. These studies have used statistical data fitting approaches to determine the risk of ASF introduction through contaminated pork products [97, 98], have linked ASF infection data to meteorological records to make global predictions of ASF outbreaks [99], and have identified risk factor indicators to predict the spread of ASF in Europe [100, 101], with wild boar density classified as a key indicator. These model approaches have not focused on determining the underlying epidemiological processes responsible for infection. A stochastic model (based on a process based deterministic model), that focused on direct transmission of infection, was developed to assess the impact of the implementation of different disease control strategies [33]. Here the focus was not on understanding the importance of the key epidemiological processes but on assessing the effectiveness of a hypothetical vaccine and of biosecurity control measures, modelled implicitly as a reduction in infection transmission. They showed that these strategies could reduce population mortality due to ASF, particularly if the control measures were applied soon after the initial outbreak [33].

In this study we develop a deterministic model of ASF in wild boar to uncover the key

transmission and infection maintenance processes. The model includes direct transmission, transmission from infected carcasses and the possibility of survivor individuals, all of which have been implicated in ASF outbreaks and persistence [35, 19, 41, 40]. We compare the model results to key observed criteria for the epidemiological dynamics of ASF in Estonia to determine the important processes that drive the infection and to fit model parameters. The fitted model will then be used to test the effectiveness of disease management by explicitly including the impact of culling and carcass removal. We will also consider a model set-up that represents conditions in Spain, where wild boar densities are considerably higher than in Estonia and where the persistence of carcasses is reduced due to climatic conditions and the presence of abundant obligate scavengers, such as vultures. The results will highlight the usefulness of mathematical modelling for disease management and provide important new information to understand the epidemiological dynamics of ASF and to inform policy to control its spread.

2.2 Methodology

Detailed data on the local, temporal population and epidemiological dynamics for ASF are not available. Instead, we use information from published studies to develop and fit a model to key epidemiological criteria observed for ASF in wild boar in eastern Europe. These criteria are:

1. An $85-95\%$ drop in total population density after an epidemic [28, 102].

2. A peak in the number of infected individuals approximately 6 months after the virus is initially discovered [28]. In the model results this criterion is specified as a peak in infected density in a $4-10$ month period following the initial infection.

3. The persistence of the virus several years after the initial epidemic [28]. In the model results this criterion is specified as having a $1-3\%$ prevalence 3 years after the initial epidemic.

2.2.1 Mathematical modelling

We develop a model for the temporal dynamics of ASF in wild boar, which is an extension of classical, compartmental disease modelling frameworks [103, 93], and of models for disease transmission in wild boar [66, 104]. We consider a model that separates wild boar into two age classes: piglets (hosts aged $0-10$ months on average, subscript P) and yearlings/adults (known hereafter as adults, subscript A). We do this as there are key differences in reproduction, natural mortality and mortality due to hunting between these age-classes. We further classify the population in terms of the key infection status of individuals. This is through the classes S, uninfected and susceptible to infection; I, infected and able to transmit the virus; C, survivor individuals which do not transmit the virus but can revert to the infected (I) class and D, infected carcasses which can transmit the virus. The model is detailed below:

$$\begin{aligned}
\frac{dS_P}{dt} &= a(t)A - \beta_F \frac{S_P}{N} I - \beta_E S_P D - \alpha S_P - b_P S_P - b_C S_P, \\
\frac{dS_A}{dt} &= -\beta_F \frac{S_A}{N} I - \beta_E S_A D + \alpha S_P - b_A S_A - b_H S_A - b_C S_A, \\
\frac{dI_P}{dt} &= \beta_F \frac{S_P}{N} I + \beta_E S_P D - \alpha I_P - \gamma I_P + \kappa C_P - b_P I_P - b_C I_P, \\
\frac{dI_A}{dt} &= \beta_F \frac{S_A}{N} I + \beta_E S_A D + \alpha I_P - \gamma I_A + \kappa C_A - b_A I_A - b_H I_A - b_C I_A, \\
\frac{dC_P}{dt} &= \gamma(1-\rho) I_P - \kappa C_P - \alpha C_P - b_P C_P - b_C C_P, \\
\frac{dC_A}{dt} &= \gamma(1-\rho) I_A - \kappa C_A + \alpha C_P - b_A C_A - b_H C_A - b_C C_A, \\
\frac{dD}{dt} &= \gamma\rho I + b_P I_P + b_A I_A - dD - rD.
\end{aligned} \tag{2.1}$$

Here, $I = I_P + I_A$ denotes the total infected population, $A = S_A + I_A + C_A$ denotes the total adult population and $N = S_P + S_A + I_P + I_A + C_P + C_A$ denotes the total population of (living) wild boar. We base our model on the system in Estonia and parameterise the model where possible from published data. Adults give birth to susceptible piglets during a defined breeding season with seasonal birth rate $a(t)$. We consider two forms for $a(t)$, a 'natural' population and a population which receives supplementary feeding (see Figure A.1 in the Supplementary Information). The matu-

ration of piglets to adults occurs at rate $\alpha = 12/10$ which reflects an average maturation time of 10 months [105]. In the absence of the disease wild boar suffer mortality at rate b_P, b_A and b_H representing natural death of piglets and adults and mortality due to hunting respectively. For Estonia the total annual adult mortality is 53%, of which 93% is due to hunting and 7% due to other forms of mortality [106] giving $b_H = 0.69$ and $b_A = 0.05$. Piglet annual mortality increases from 50% at low density to 95% at high density due to crowding effects and is given by $b_P = (b_0 + b_1 N)$ where $b_0 = \log(2)$ and $b_1 = \sigma \frac{(\overline{a(t)} - b_A - b_H)\alpha - b_0(b_A + b_H)}{(b_A + b_H)K}$ where $\overline{a(t)}$ represents the average annual birth rate, K the carrying capacity, defined as the average annual population size in the absence of ASF, and σ denotes a scaling term to ensure that the average population density equals the carrying capacity. We assume a carrying capacity, K, of $2km^{-2}$ in natural populations and $4km^{-2}$ under supplementary feeding. To allow consideration of disease control measures, we include culling, at rate b_C and the removal of carcasses, at rate r.

For the infection dynamics, a susceptible can become infected due to direct contact with an infected individual via frequency-dependent transmission, β_F or due to environmental transmission through contact with an infected carcass, β_E. A proportion, ρ, of infected individuals suffer disease-induced mortality at rate $\gamma = 365/5$, reflecting an average lifespan of 5 days for an individual with ASF [36]. A proportion $1-\rho$ of infected can enter the survivor class, which does not incur disease-induced mortality. Survivors can revert to the infected class (where they incur disease-induced mortality) at rate $\kappa = 12/6$ implying that the average time spent in the survivor class is 6 months [36]. Individuals that die whilst infected are classed as infected carcasses and can transmit infection for on average 8 weeks [107, 19], giving a decay rate of carcasses $d = 52/8$. Note, we also examine the impact of a range of average times spent in the survivor class and a range of carcass degradation rates.

To initiate the model we introduce a low level of infection (I is set to 0.2% of the carrying capacity, K) to a population at its carrying capacity. We make no assumptions about the source of the initial infection, which could include contact with an infected individual from a neighbouring population or human-mediated introduction. We as-

sume the model (Equations 2.1) includes the key mechanisms responsible for infection transmission within a population following the initial infection and undertake an exploration in parameter space to determine the combinations of transmission terms (β_E and β_F) and the proportion of survivors ($1-\rho$) that can satisfy the epidemiological criteria for ASF outlined in Section 2.2. We aim to interpret the results in terms of the epidemiological mechanisms responsible for ASF dynamics and maintenance, examine the epidemiological consequences of these results and test the impact of disease control measures in the form of increased carcass removal and culling. We also examine the potential impact of ASF and disease control in other regions that may have higher density populations of wild boar (i.e., Spain), higher populations of obligate scavengers and higher temperatures which significantly contribute to faster carcass degradation and virus decay compared to Estonia. We adjust the model to represent the situation in Spain by considering carrying capacities of $5km^{-2}$ in natural populations and $10km^{-2}$ under supplementary feeding [108]. Total annual adult mortality is now 56%, of which 60% is due to hunting and 40% due to other forms of mortality [44]. This gives $b_H = 0.49$ and $b_A = 0.33$. To represent increased temperature and increased activity from obligate scavengers (e.g., vultures) [109], we assume that carcasses transmission can occur at all times of the year and an individual infected carcass can transmit infection for on average one week (giving $d = 52$). In all modelling results we introduce ASF at low density (0.2%) into a disease-free population at its carrying capacity.

2.3 The drivers for the epidemiological dynamics of ASF

We undertake a sensitivity analysis to determine the range of parameters that produce model outputs satisfying the epidemiological criteria observed for ASF and outlined in Section 2.2 (further details of the sensitivity to model parameters are provided in the Supplementary Information, Section A.2). A key finding is that frequency-dependent transmission, environmental transmission and the progression from an infected state to the survivor state are required to satisfy the criteria for ASF (Figure A.2). Importantly, this suggests that survivor individuals may play a key role in the long-term

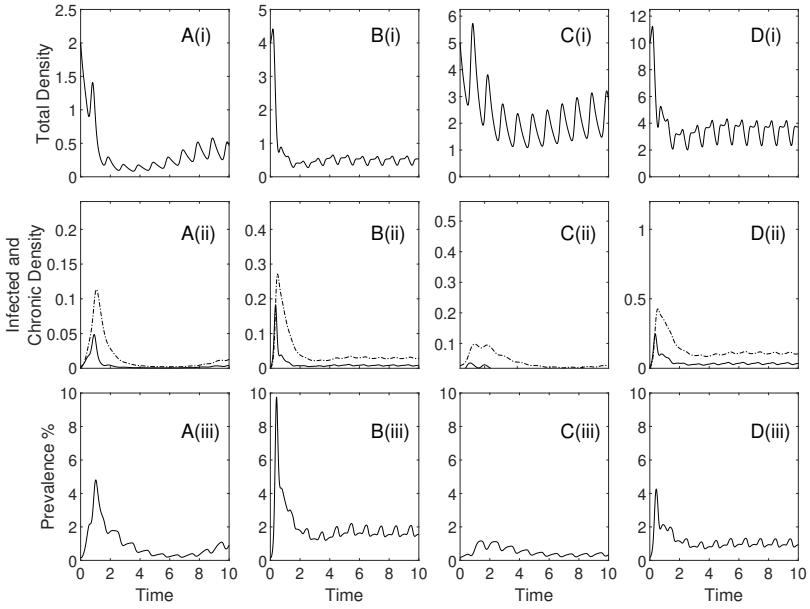

Figure 2.1: Population densities and prevalence over time for the model described by Equations (2.1). All results were obtained using MATLAB software, specifically the built-in ODE solver packages. Total densities are given in (i), infected (solid line) and survivor (dashed line) densities in (ii), with prevalence, defined as I/N, in (iii). The plots in A and B represent the scenario for Estonia, under natural conditions and with supplementary feeding respectively. In C and D, we show the model results for the scenario that represents Spain, under natural conditions and with supplementary feeding respectively. For Estonia we have $d = 52/8$, with $K = 2$ (A) and $K = 4$ (B). For Spain $d = 52$ with $K = 5$ (C) and $K = 10$ (D). Other parameters are $\beta_F = 63, \beta_E = 2, \rho = 0.85, b_C = 0$ and $r = 0$ (see Section 2.2 and Section A.1).

persistence of ASF. For parameters that satisfy the criteria the epidemiological dynamics are similar and shown for representative parameters in Figure 2.1A. This highlights the crash in total host density (Figure 2.1Ai), the epidemic outbreak in infected hosts and consequently in survivor individuals (Figure 2.1Aii) and a peak and persistence of low prevalence infection following the outbreak (Figure 2.1Aiii). While there are more acute (infected) cases than survivor cases over the course of the epidemic, the density of the infected class (I) may be lower than the density of the survivor class (C) due to the high rate of disease-induced mortality for I (which results in infected carcasses D). The epidemiological dynamics arise from the following processes:

1. Density-dependent environmental transmission is the key process driving the initial population crash. Model results when environmental transmission is excluded (Figure A.3A) show no epidemic outbreak, and as a result no drop in population density. When environmental transmission is high (Figure A.3C) the crash in population density is severe and drops below the level defined by our epidemiological

criteria.

2. Frequency-dependent transmission and the progression and subsequent reversion from survivor to infected individuals allows the infection to be sustained at low density. Without survivor individuals the disease is self-limiting and fades out after the epidemic (Figure A.5), whilst with low frequency-dependent transmission the disease does not persist in the long-term at low population density (Figure A.4). If frequency-dependent transmission is high the population exhibits pathogen driven extinction (Figure A.4C) and if a high proportion of infected individuals survive the initial infection and enter the survivor class the population does not exhibit the required reduction in density.

In our model study survivor individuals revert to the infected state after an average of six months, but there is uncertainty in this duration [110]. We use the model to show that the epidemiological criteria for ASF can be satisfied for a range of durations in the survivor class (from 2 months to 9 months, see Figure A.6). In order to satisfy the epidemiological criteria when the length of time in the survivor class decreases, the proportion of individuals that survive the infection must increase, leading to an increase in the density of survivor individuals.

2.4 The dynamics of ASF in different regions

The model sensitivity analysis was undertaken to match observed epidemiological dynamics for natural populations in Estonia and provide a default set of infection parameters. We use these parameters to examine the impact of ASF for additional scenarios in Estonia that simulate when wild boar are supplementary fed (Figure 2.1B) and for scenarios representative of Spain for natural (Figure 2.1C) and supplementary fed (Figure 2.1D) populations.

In Estonia (with both natural conditions and supplementary feeding) and in Spain under supplementary feeding there is an initial epidemic outbreak. This causes an $85-95\%$ population reduction in Estonia (Figure 2.1A(i), B(i)) and a $60-70\%$ reduction in Spain (Figure 2.1D(i)). In Spain, under natural conditions, the infectious outbreak develops

more slowly and the drop in population density is more gradual compared to the other scenarios. Nevertheless, the infection still leads to a $60 - 70\%$ reduction in population density (Figure 2.1C(i)). In all scenarios the infected steady state is stable under pertubations (determined by running the model simulations for large times) resulting in the infection persisting at low prevalence after the initial infectious outbreak (Figure 2.1). Under natural conditions the disease persistence has a low but initially declining prevalence of infection (Figure 2.1A, C), but with the inclusion of supplementary feeding the infection persists with a slightly higher level of prevalence (Figure 2.1B, D). The addition of feeding also leads to a more severe infectious outbreak with a rapid initial drop in population density. In the long-term, the disease is more likely to fade out in the absence of feeding, due to the lower ASF prevalence levels, and more likely to persist at low prevalence with the inclusion of supplemented feeding, where the population is likely to be regulated by the disease.

2.5 The impact of different control methods

We consider two control methods: culling and the removal of infected carcasses, and initially focus on the scenario in Estonia under natural conditions. When culling alone is used (Figure 2.2, with $r = 0$) an increase in the rate of culling reduces the total density as well as the infected, survivor and infected carcass densities. The disease persists at low population density indicating that culling may not be effective at eradicating the disease without also eradicating the population. When carcass removal alone is used (Figure 2.3, with $b_C = 0$), we see an increase in total population density as the carcass removal rate is increased. This occurs as the removal of carcasses reduces environmental transmission and so reduces the population level mortality due to ASF. At low levels of carcass removal, the increase in total population supports an increase in the number of infected individuals but as the carcass removal rate increases further the infected level peaks and then decreases. Note that high levels of carcass removal can eliminate infected carcasses yet ASF is still supported at low density through frequency-dependent transmission and survivor individuals. While the impact on population density is low it emphasizes that carcass removal alone may not be sufficient to eradicate ASF.

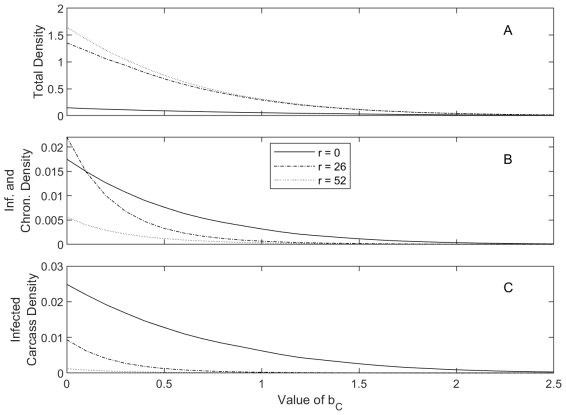

Figure 2.2: Population response to a varying culling intensity, b_C, with three different carcass removal rates $r = 0$ (solid line), $r = 26$ (dashed) and $r = 52$ (dotted), for the model represented by Equations (2.1). The total density, N, is given in A, with infected and survivor density in B and carcass density in C. Results are shown for the scenario that represents natural conditions in Estonia (see Figure 2.1 for parameters) and show the average densities between the years 2 and 3 following disease introduction. Control measures were implemented as soon as the virus is first discovered, defined as the time when carcass levels first reach a density of 0.02. The value b_C corresponds to a culling proportion equal to $1 - e^{-b_C}$, per year, of the total population.

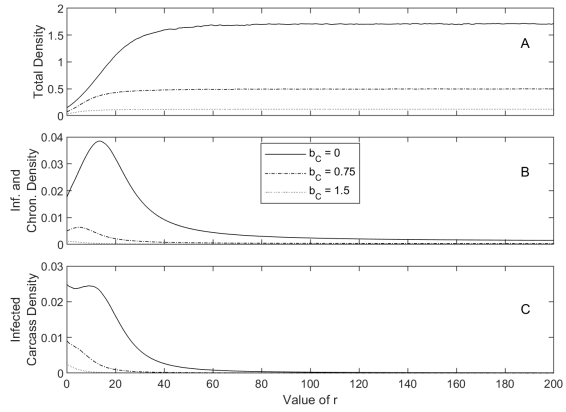

Figure 2.3: Population response to a varying carcass removal rate, r, with three different culling intensities $b_C = 0$ (solid line), $b_C = 0.75$ (dashed) and $b_C = 1.5$ (dotted), for the model represented by Equations (2.1). The total density, N, is given in A, with infected and survivor density in B and carcass density in C. Results are shown for the scenario that represents natural conditions in Estonia (see Figure 2.1 for parameters) and show the average densities between the years 2 and 3 following disease introduction. Control measures were implemented as soon as the virus is first discovered, defined as the time when carcass levels first reach a density of 0.02. The value r corresponds to an average removal time, in years, of $1/r$.

When we consider a combination of disease control methods (Figure 2.2 and 2.3) model results indicate that it is possible to eradicate all sources of infection without eradicating the host population. In particular, varying the culling rate for fixed levels of carcass removal show a clear difference in the culling threshold for disease eradication

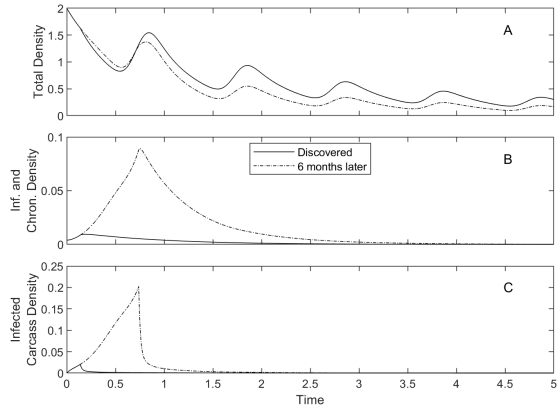

Figure 2.4: Population response to the combination of culling, at fixed rate $b_C = 0.75$, and carcass removal, at fixed rate $r = 52$, for the model represented by Equations (2.1) and for parameters that represent the scenario in Estonia under natural conditions (see Figure 2.1 for parameters).The total density, N, is given in A, with infected and survivor densities in B and prevalence in C. The results are shown for two different control implementation times: when the virus is first discovered (solid line), and six months after the virus was discovered (dashed line).

and population eradication (Figure 2.2). Varying the carcass removal rate for fixed levels of culling shows that the disease can be eradicated while maintaining a positive host population level (Figure 2.3). Model results suggest that a combination of control measures would be effective at controlling ASF. The impacts of these disease control methods show similar trends for the scenarios that represent Estonia with feeding and for parameters representative of Spain (see Figures A.7, A.8, A.11, A.12, A.15 and A.16). However, the elevated rate of natural carcass removal in Spain means that the infection can be eradicated through culling only and more generally this makes the virus easier to control in Spain compared to Estonia. Nonetheless, in all scenarios the removal of carcasses (applied when the infection is detected) cannot eradicate the disease, although a high level of removal does reduce the level of infection and impact on host population density. Here our model results suggest that a combination of control procedures will be the most effective method to eradicate the disease while maintaining a viable population of wild boar.

We also test the impact of the timing of the implementation of control (Figure 2.4). Applying control as soon as the disease is discovered in a population is significantly more effective than if control is applied later, when the infection is at epidemic levels. In particular, the early application of control reduces the level of infected individuals

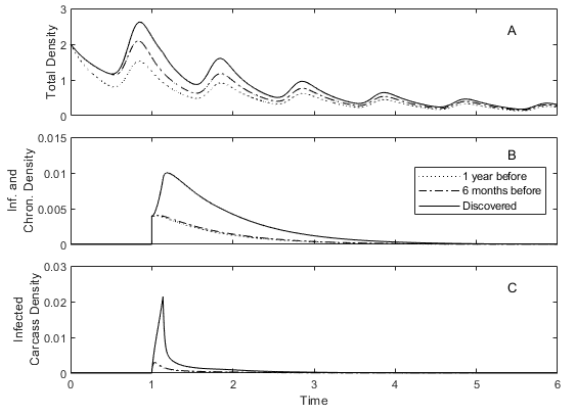

Figure 2.5: Population response to the combination of culling, at fixed rate $b_C = 0.75$, and carcass removal, at fixed rate $r = 52$, for the model represented by Equations (2.1) and for parameters that represent the scenario in Estonia under natural conditions (see Figure 2.1 for parameters).The total density, N, is given in A, with infected and survivor densities in B and prevalence in C. The results are shown for three different control implementation times: one year before the onset of the virus (dotted line), six months before the onset of the virus (dashed line), and when the virus is first discovered (solid line).

while maintaining a higher host population density. This reduction in the level of infected individuals is further enhanced if control is applied prior to the introduction of infection (Figure 2.5) and these lower levels of infection are likely to reduce the risk of infectious spread to other populations. In the general control methods reduce the population density and the rate of transmission to a level that cannot support ASF. This trend is seen across the different scenarios considered in this study (Figures A.9, A.13 and A.17). It should be noted however, for Spain, where there is assumed to be high levels of 'natural' carcass degradation, that high levels of culling can reduce the host density to a level that cannot support the disease and could prevent ASF from establishing if applied prior to an infectious outbreak (see Figures A.11 and A.15 with r = 0).

2.6 Discussion

There is limited information regarding the key processes responsible for disease transmission and the mechanisms that allow the virus to persist at low density in wild boar populations whilst maintaining a high disease-induced mortality rate. We have developed an age-structured mathematical model that includes a range of potential transmission mechanisms with the aim of understanding the epidemiological dynamics

of ASF in wild boar. The model captures the observed drop in population density [28, 102], the peak in infected density [28] and the persistence of the virus [28] and gives an insight into the key processes that drive these dynamics.

Our model results indicate that environmental transmission from infected carcasses to susceptible individuals and frequency-dependent transmission from infected to susceptible individuals are key factors in producing a disease outbreak and the persistence of the disease at low population levels, respectively. These mechanisms have been highlighted as key factors in driving ASF dynamics in warthogs [39, 42], with persistence linked to the long-term survival of the virus in the environment [35, 111, 19]. Gallardo et al. 2015 [110] suggests that sub-clinically infected, chronically infected or survivor pigs are likely to play an important role in disease persistence in endemic areas and in sporadic outbreaks or ASF introduction into disease-free zones. Our model analysis clarifies the potential role of hosts that can survive the initial ASF infection but that may revert to an infected state indicating that they are necessary for the persistence of ASF in low density host populations. A key message is that all three routes of infection: direct and environmental transmission and the role of survivors, that delay the resurgence of viraemia, are essential to capture the population crash associated with the initial ASF epidemic and long-term persistence of ASF that regulates the host at low density. The long-term persistence of ASF makes the virus difficult to eradicate and increases the opportunity of infectious spread to neighbouring populations.

Recent studies have highlighted the potential role of chronically infected and survivor individuals in the transmission of ASF [112, 110, 40]. Eblé et al. [112] showed that chronically (or sub-chronically) infected domestic pigs of the Netherlands '86 strain of ASF (a low virulence strain) could transmit the infection through contact to susceptible pigs leading to acute infection. Also, Ståhl et al. [40] suggests there are two types of individuals that may survive initial infection: (i) those that do not initially die of the disease but develop a persistent infection and can succumb to the disease and excrete virus in association with the resurgence of viraemia and (ii) those that show no clinical signs of infection, that can clear the infection and would not present prolonged virus

excretion. The significance of these types is likely to vary between hosts and strains of the virus [112, 40]. Our model study considers individuals that survive an initial infected and infectious stage and that can later revert to the infected class that can transmit the virus (type (i) in the Ståhl et al. [40] definition of survivor pigs). In the absence of this survivor stage our results indicate that the disease is self-limiting and fades out after the initial epidemic, which is typical of high virulence infection [35]. The survivor stage therefore adds a delay that allows the infection to persist in the long-term.

While Ståhl et al. [40] suggest that there is evidence for individuals that survive ASF infection they also question whether such survivors would play a role in the persistence of ASF. We therefore used the model to further explore ASF transmission mechanisms that could lead to the long-term persistence of ASF. In our model study survivor individuals cannot transmit the infection, whereas there is evidence that they can excrete the virus and therefore have the potential to transmit infection [112, 40]. An extension of our model study, which also included infected transmission from the survivor class, showed that the rate of transmission must be low compared to that of acutely infected individuals (Figure A.21) but that its inclusion allowed the model to match the epidemiological criteria for ASF with a reduced overall density of survivor individuals (Figure A.22). There is also evidence of variability in the degradation of wild boar carcasses where in some cases skeletonization can take several months and is dependent on factors such as insect activity, scavenger activity and weather conditions [113]. An extension of the model showed that the epidemiological criteria for ASF could not be satisfied for a range of carcass degradation rates in the absence of survivor individuals (representing an average degradation length from 1 week to 40 weeks). When carcass degradation is slow and environmental transmission is 'high', it is possible to satisfy our epidemiological criteria points (1) and (2) related to the drop in population density and timing of the peak outbreak of ASF but not the persistence of ASF in the long-term since ASF fades-out after the outbreak (Figure A.23). When carcass degradation is slow and environmental transmission is 'low', it is possible to satisfy point (3) of our epidemiological criteria related to the long-term persistence of ASF but the decrease in host density is slow and the peak in the outbreak of ASF occurs several years after the

initial introduction of the infection. While we recognise that models are a simplified representation of the real world and that there is uncertainty in the criteria we use to define the epidemiological dynamics of ASF, our modelling results combined with recent empirical assessments [112, 40], suggest that a more detailed analysis of the role of survivor individuals in ASF epidemiology should be undertaken.

The results allow us to compare the epidemiology of ASF in scenarios that represent different regions or countries. For Estonia and other northern European regions, it is assumed that degradation of infected carcasses is slow [19]. Consequently, direct environmental transmission is the key infection mechanism that drives an epidemic outbreak and rapid population crash.

In Spain or other southern European countries, degradation of infected carcasses is likely to be faster due to elevated temperatures and the potential role of obligate scavengers. It was recently suggested that in northern Europe scavengers represent a minor risk factor for spreading ASF but may contribute to reducing virus persistence [114]. Here, the model predicts that the epidemic outbreak will be less severe and the wild boar population loss from ASF infection will be reduced due to the high degradation rate of infected carcasses. Our results can inform the ongoing debate regarding vulture conservation [115]. We acknowledge that the role of scavengers and temperature on carcass degradation in Spain is uncertain and likely to vary across regions and habitat type. In open areas there is evidence that vultures can clean a carcass in a matter of hours [107]. If the degradation rate is suitably rapid (on average 1 day) then the infection cannot persist (Figure A.19). However, in covered or wooded habitats a carcass may go undetected and could degrade more slowly. As this degradation rate decreases, the results in Spain become more similar to those in Estonia with a predicted population crash of $85 - 95\%$ following ASF introduction (Figure A.20). This suggests that there may be considerable local and regional variation in the impact of ASF. We do not include the impact of obligate scavengers in Estonia (since they are not present) but there may be an impact from the partial consumption of carcasses from other scavengers (such as wolves, birds or insects [113]). The impact of such activity would be

similar to the impact of increased carcass removal through control.

It is noteworthy that in both Estonia and Spain the higher underlying host density and longer breeding season associated with supplementary feeding leads to a more pronounced epidemic outbreak and persistence of the disease in the long-term when compared to natural populations. This increased disease risk in supplementary fed populations fits with similar empirical findings regarding other viral and bacterial infections of wild boar [116, 117]. Therefore, wild boar feeding should be limited as a means of ASF prevention, at least in open, unfenced areas.

Recent assessments on the spread and control of ASF advocate the use of hunting, culling and the active removal of carcasses as potential methods by which to control the infection [43]. Our study indicates that multiple control methods should be applied in parallel to eradicate ASF without eradicating the population. This will be of particular relevance in regions where wild boar hunting is an important industry that supports rural communities [118]. Furthermore, the control methods are more effective if implemented at the onset of infection (or prior to the arrival of infection in the case of culling) as they reduce the size of the infectious outbreak, thereby reducing the risk of spread to neighbouring populations. This supports the finding of Barongo et al. [33], who tested the impact of the timing of biosecurity measures on the control of ASF indicting that a rapid response was more effective.

The use of culling as a method to control infectious disease has had varying levels of success [119, 4]. For some circumstances the culling of a population can affect the behaviour of the wildlife species of concern and can disrupt the social interactions within groups and between groups [120, 121, 122, 123, 124]. This can lead to increased wildlife movement and a resulting increase in disease spread [123]. A recent theoretical paper has shown that in hosts challenged by highly virulent pathogens that do not confer long-lived immunity there is only a narrow gap between the thresholds in the culling rate that eradicate the disease or that eradicate the population [104]. ASF is highly virulent with little prospect of post infection recovery to immunity. Our model study indicates

that in Estonia, culling alone is unlikely to eradicate the disease without eradicating the host population, whereas in Spain culling could potentially eradicate the disease without eradicating the host. The difference is that in Estonia infected carcasses remain in the environment, acting as a long-term source of infection and increasing the difficulty of eradicating the disease. We also consider the potential of disease control through the removal of infected carcasses. Carcass removal reduces density-dependent environmental transmission and thereby reduces the population crash at the onset of infection. This allows an increased density of hosts to be supported in the long-term. For some scenarios however, the lower level of transmission combined with the increased density of hosts means the density of infected individuals can increase in response to control. In all cases carcass removal alone, instigated when the infection is detected, cannot eradicate the virus. When culling and carcass removal control methods are combined the model predicts that disease eradication can occur without the eradication of the host population. Here the increase in mortality due to culling is balanced by the reduction in transmission due to carcass removal and therefore a reduction in disease-induced mortality at the population level [104].

The threat posed by ASF to wild and domestic swine is significant [33, 34], and understanding the transmission dynamics is key for developing strategies to control ASF [43]. Our model study considers the dynamics and impacts of ASF control measures for different population scenarios that are representative of different geographical regions and different wild boar management strategies. Our findings have uncovered the role of different infection transmission routes in determining the epidemiological dynamics and in particular we suggest that a small proportion of survivor individuals that can subsequently revert to the infected class can play a key role in the long-term persistence of infection. The model results also suggest that ASF eradication requires a combination of control measures applied at the onset of (or prior to) detection of infection. This study highlights the role that mathematical modelling can play in understanding and developing management strategies to control important infectious diseases.

Appendix A: Supplementary material for Chapter 2

A.1 The birth rate function, $a(t)$

We use either uni-modal or bi-modal birth functions, Figure A.1, to represent the reproductive conditions when there is a natural population, Figure A.1A, and a population with supplementary feeding, Figure A.1B. In the former case each female adult is expected to produce 6 offspring with a peak of reproduction in March. As we assume a 50/50 male/female split, we assume each adult, on average, to produce 3 offspring. With additional feeding, we expect two peaks in reproduction, one in March and one in September, and an increase in the offspring per female to 12 individuals.

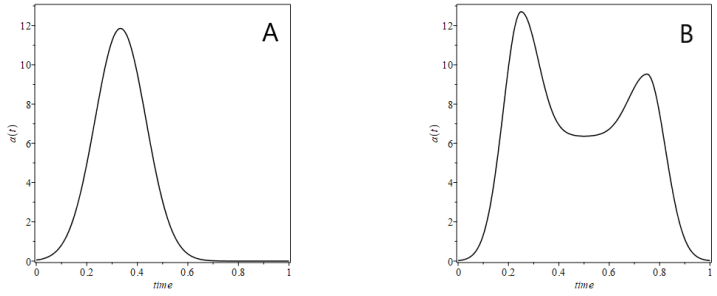

Figure A.1: The average reproductive rate, $a(t)$, for adult wild boar over a period of 1 year, where January is given by $t = 0$, in natural conditions (A) and with supplementary feeding (B) respectively. Under natural conditions we assume each adult individual produces an average of 3 piglets per year, and with supplementary feeding an average of 6 piglets per year.

A.2 Drivers for the epidemiological dynamics of African swine fever

We undertake a sensitivity analysis to find the transmission parameters and the proportion transitioning to the survivor state that satisfy the criteria outlined in Section 2.2 of the main paper (Figure A.2). In particular the epidemiological criteria are only satisfied for a limited range of transmission coefficients and proportions transitioning to survivors.

Density-dependent environmental transmission is the key process driving the initial population crash. Model results when environmental transmission is excluded (Figure A.3A) show no epidemic outbreak, and as a result no drop in population density and when environmental transmission is high (Figure A.3C) the crash in population is severe and drops below the level defined by our epidemiological criteria.

Frequency-dependent transmission and the progression and subsequent reversion from survivor to infected individuals allows the infection to be sustained at low density. Without these processes the disease is self-limiting and fades out after the epidemic (Figure A.4 and A.5). If frequency-dependent transmission is high the population exhibits

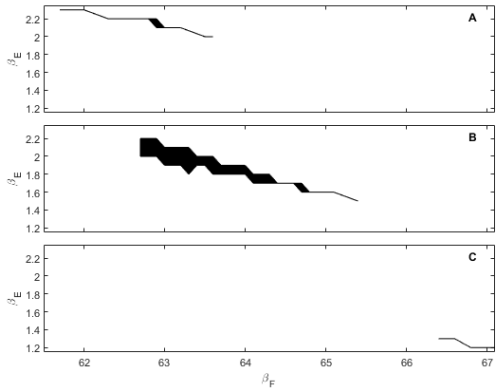

Figure A.2: A selection of valid transmission coefficients satisfying the epidemiological criteria outlined in Section 2.2 of the main paper for the model represented by Equations (2.1) and for parameters that represent Estonia under natural conditions with no control measures. We also test the significance of when the infection is introduced and the results shown are for parameters that satisfy the epidemiological criteria when an outbreak may occur at any time of the year. The shaded regions indicate parameters that satisfy the epidemiological criteria for $\rho = 0.83$ in A; $\rho = 0.85$ in B; $\rho = 0.9$ in C. The other parameters used are outlined in Section 2.2.1.

pathogen driven extinction (Figure A.4C) and if a high proportion of infected individuals progress to the survivor phase the population does not exhibit such a marked crash.

In our model study survivor individuals revert to the infected state after an average of six months, but there is uncertainty in this duration [110]. We use the model to show that the epidemiological criteria for ASF can be satisfied for a range of durations in the survivor class (from 2 months to 9 months, see Figure A.6). In order to satisfy

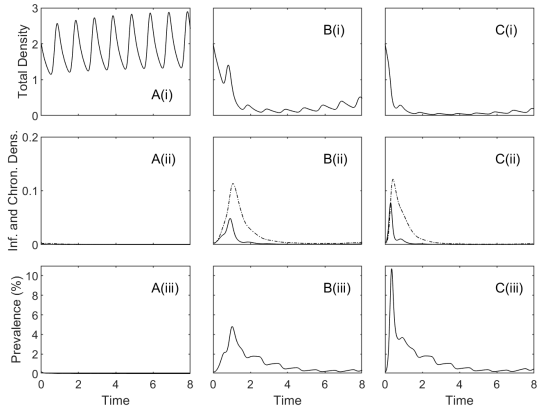

Figure A.3: Model results for the scenario that represents Estonia under natural conditions for different environmental transmission coefficients: $\beta_E = 0$ (A), $\beta_E = 2$ (B) and $\beta_E = 6$ (C), with other parameters set to default values (in particular $\beta_F = 63$ and $\rho = 0.85$). Plots in (i) give the total densities, (ii) the infected (solid line) and survivor (dashed) densities and (iii) the prevalence. Other parameters are as discussed in Section 2.2.1. When environmental transmission is low there is no population crash (A) and when it is high the crash is too severe (C).

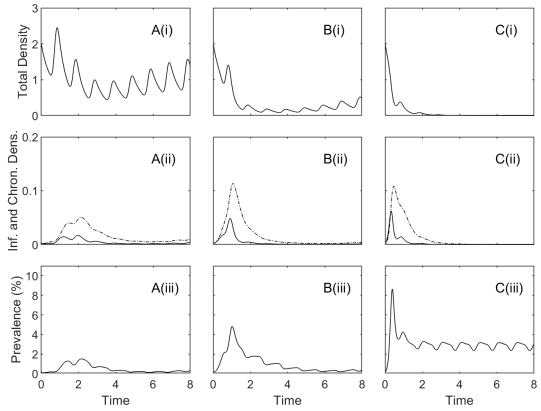

Figure A.4: Model results for the scenario that represents Estonia under natural conditions for different frequency-dependent transmission coefficients: $\beta_F = 50$ (A), $\beta_F = 63$ (B) and $\beta_F = 76$ (C), with other parameters set to default values (in particular $\beta_E = 2$ and $\rho = 0.85$). Plots in (i) give the total densities, (ii) the infected (solid line) and survivor (dashed) densities and (iii) the prevalence. Other parameters are as discussed in Section 2.2.1. When frequency-dependent transmission is low the prevalence following an outbreak is too low (A) and when it is high the population exhibits pathogen driven extinction (C).

the epidemiological criteria when the length of time in the survivor class decreases, the proportion of individuals that survive the infection must increase, leading to an increase in the density of survivor individuals.

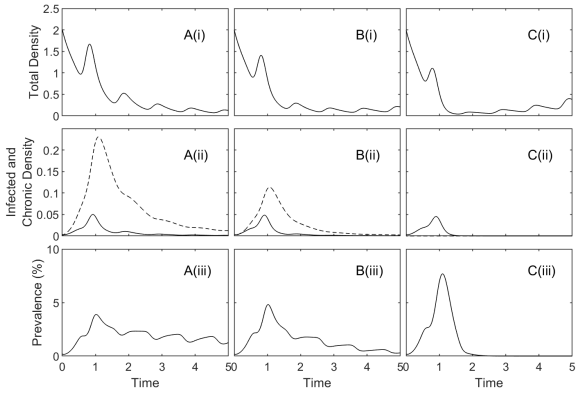

Figure A.5: Model results for the scenario that represents Estonia under natural conditions for different values of $\rho = 0.7$ (A), $\rho = 0.85$ (B) and $\rho = 1$ (C), with other parameters set to default values (in particular $\beta_F = 63$ and $\beta_E = 2$). Plots in (i) give the total densities, (ii) the infected (solid line) and survivor (dashed) densities and (iii) the prevalence. Other parameters are as discussed in Section 2.2.1. If the proportion that transition to the survivor state is high then the population crash is too slow (A) and if it is too low the disease fades out after the infectious outbreak (C).

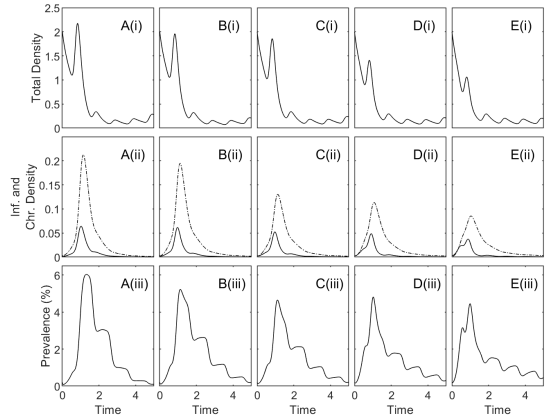

Figure A.6: Population densities and prevalence over time for the model described by Equations (2.1). Total densities are given in (i), infected (solid line) and survivor (dashed line) densities in (ii), with prevalence, defined as I/N, in (iii). Simulations were completed for the situation representative of Estonia under natural conditions for different values of the survivor reversion rate κ, with results for $\kappa = 12/2, 12/3, 12/4, 12/6$ and $12/9$ given in figures A, B, C, D and E, respectively. This corresponds to an average time in the survivor class of $2, 3, 4, 6$ and 9 months, respectively. The transmission parameters are (β_F, β_E, ρ) are given by $(40, 4, 0.61), (50, 3.1, 0.7), (58, 2.1, 0.8), (63, 2, 0.85)$ and $(67.5, 1.7, 0.89)$ for figures $A - E$, respectively, so that the epidemiological criteria, described in Section 2.2, are satisfied. All other parameters are as discussed in Figure 2.1.

A.3 The impact of control in Estonia with supplemented feeding

Figures A.7, A.8, A.9 and A.10 explore the impact of culling and carcass removal on the epidemiological dynamics for the parameters representing the scenario in Estonia where wild boar receive supplementary feeding.

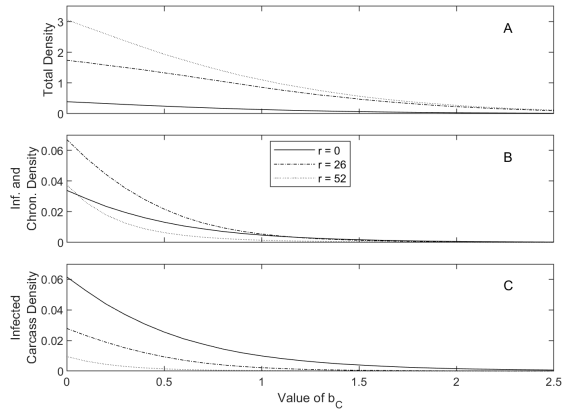

Figure A.7: Population response to a varying culling intensity, b_C, with three different carcass removal rates $r = 0$ (solid line), $r = 26$ (dashed) and $r = 52$ (dotted), for the model represented by Equations (2.1). The total density, N, is given in A, with infected and survivor density in B and carcass density in C. Results are shown for the scenario that represents Estonia with supplementary feeding (see Figure 2.1 for parameters) and show the average densities between the years 2 and 3 following disease introduction. Control measures were implemented as soon as the virus is first discovered, defined as the time when carcass levels first reach a density of 0.02.

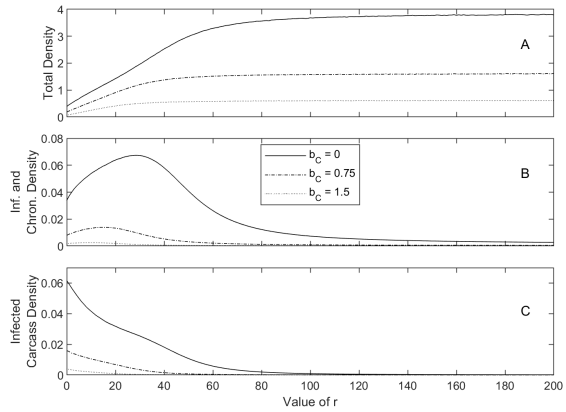

Figure A.8: Population response to a varying carcass removal rate, r, with three different culling intensities $b_C = 0$ (solid line), $b_C = 0.75$ (dashed) and $b_C = 1.5$ (dotted), for the model represented by Equations (2.1). The total density, N, is given in A, with infected and survivor density in B and carcass density in C. Results are shown for the scenario that represents Estonia with supplementary feeding (see Figure 2.1 for parameters) and show the average densities between the years 2 and 3 following disease introduction. Control measures were implemented as soon as the virus is first discovered, defined as the time when carcass levels first reach a density of 0.02.

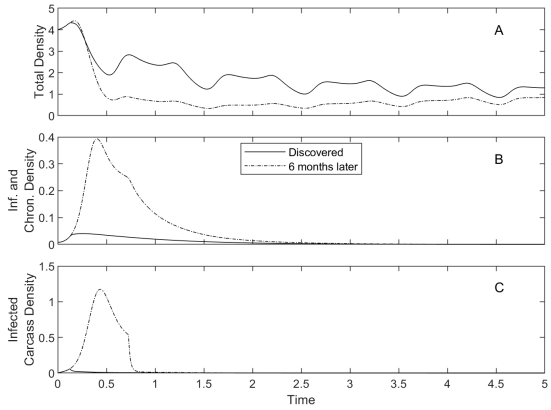

Figure A.9: Population response to the combination of culling, at fixed rate $b_C = 0.75$, and carcass removal, at fixed rate $r = 52$, for the model represented by Equations (2.1) and for parameters that represent the scenario of Estonia with supplementary feeding (see Figure 2.1 for parameters).The total density, N, is given in A, with infected and survivor densities in B and prevalence in C. The results are shown for two different control implementation times: when the virus is first discovered (solid line), and six months after the virus was discovered (dashed line).

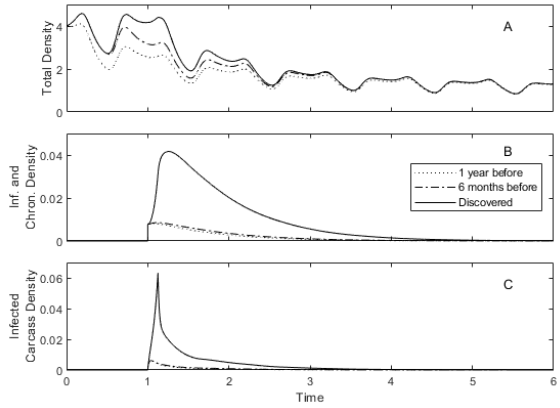

Figure A.10: Population response to the combination of culling, at fixed rate $b_C = 0.75$, and carcass removal, at fixed rate $r = 52$, for the model represented by Equations (2.1) and for parameters that represent the scenario of Estonia with supplementary feeding (see Figure 2.1 for parameters).The total density, N, is given in A, with infected and survivor densities in B and prevalence in C. The results are shown for three different control implementation times: one year before the onset of the virus (dotted line), six months before the onset of the virus (dashed line), and when the virus is first discovered (solid line).

A.4 The impact of control in Spain under natural conditions

Figures A.11, A.12, A.13 and A.14 explore the impact of culling and carcass removal on the epidemiological dynamics for the parameters representing the scenario in Spain where wild boar do not receive supplementary feeding.

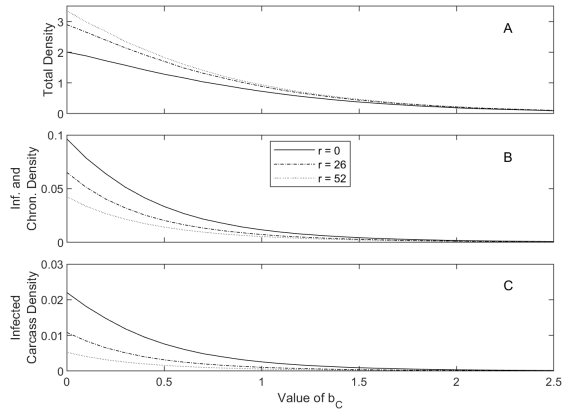

Figure A.11: Population response to a varying culling intensity, b_C, with three different carcass removal rates $r = 0$ (solid line), $r = 26$ (dashed) and $r = 52$ (dotted), for the model represented by Equations (2.1). The total density, N, is given in A, with infected and survivor density in B and carcass density in C. Results are shown for the scenario that represents Spain under natural conditions (see Figure 2.1 for parameters) and show the average densities between the years 2 and 3 following disease introduction. Control measures were implemented as soon as the virus is first discovered, defined as the time when carcass levels first reach a density of 0.02.

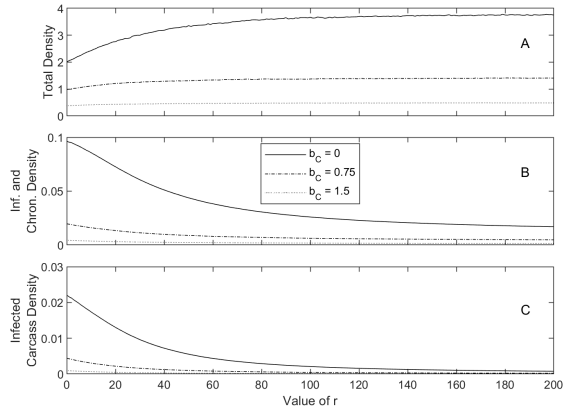

Figure A.12: Population response to a varying carcass removal rate, r, with three different culling intensities $b_C = 0$ (solid line), $b_C = 0.75$ (dashed) and $b_C = 1.5$ (dotted), for the model represented by Equations (2.1). The total density, N, is given in A, with infected and survivor density in B and carcass density in C. Results are shown for the scenario that represents Spain under natural conditions (see Figure 2.1 for parameters) and show the average densities between the years 2 and 3 following disease introduction. Control measures were implemented as soon as the virus is first discovered, defined as the time when carcass levels first reach a density of 0.02.

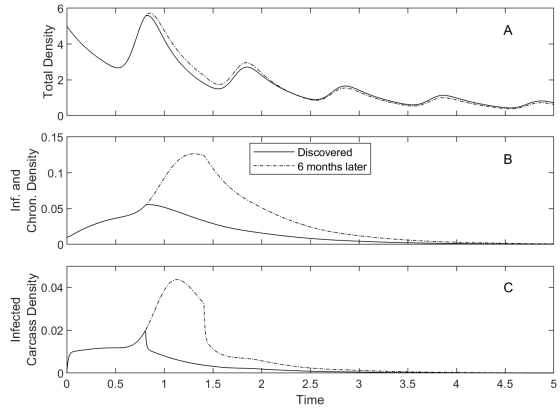

Figure A.13: Population response to the combination of culling, at fixed rate $b_C = 0.75$, and carcass removal, at fixed rate $r = 52$, for the model represented by Equations (2.1) and for parameters that represent the scenario in Spain under natural conditions (see Figure 2.1 for parameters).The total density, N, is given in A, with infected and survivor densities in B and prevalence in C. The results are shown for two different control implementation times: when the virus is first discovered (solid line), and six months after the virus was discovered (dashed line).

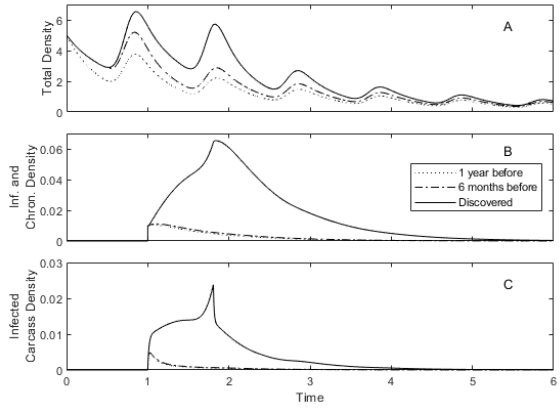

Figure A.14: Population response to the combination of culling, at fixed rate $b_C = 0.75$, and carcass removal, at fixed rate $r = 52$, for the model represented by Equations (2.1) and for parameters that represent the scenario in Spain under natural conditions (see Figure 2.1 for parameters).The total density, N, is given in A, with infected and survivor densities in B and prevalence in C. The results are shown for three different control implementation times: one year before the onset of the virus (dotted line), six months before the onset of the virus (dashed line), and when the virus is first discovered (solid line).

A.5 The impact of control in Spain with supplemented feeding

Figures A.15, A.16, A.17 and A.18 explore the impact of culling and carcass removal on the epidemiological dynamics for the parameters representing the scenario in Spain where wild boar receive supplementary feeding.

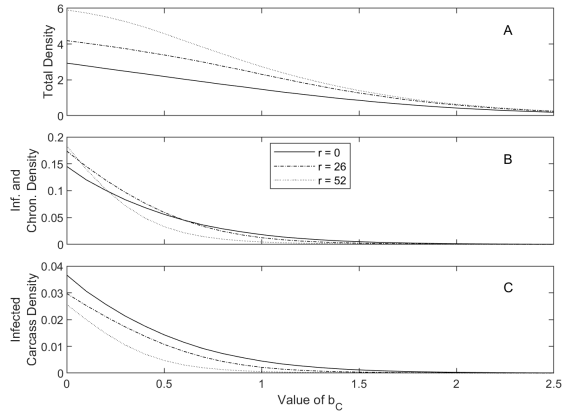

Figure A.15: Population response to a varying culling intensity, b_C, with three different carcass removal rates $r = 0$ (solid line), $r = 26$ (dashed) and $r = 52$ (dotted), for the model represented by Equations (2.1). The total density, N, is given in A, with infected and survivor density in B and carcass density in C. Results are shown for the scenario that represents Spain with supplementary feeding (see Figure 2.1 for parameters) and show the average densities between the years 2 and 3 following disease introduction. Control measures were implemented as soon as the virus is first discovered, defined as the time when carcass levels first reach a density of 0.02.

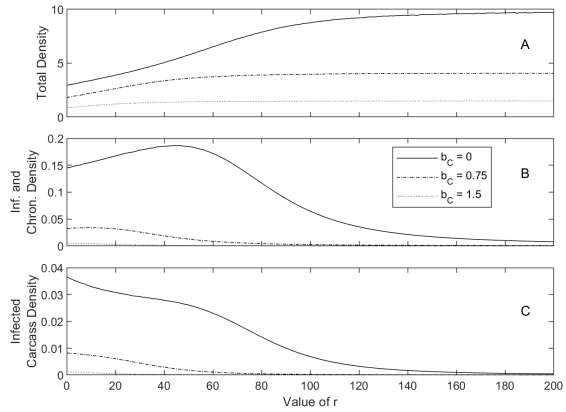

Figure A.16: Population response to a varying carcass removal rate, r, with three different culling intensities $b_C = 0$ (solid line), $b_C = 0.75$ (dashed) and $b_C = 1.5$ (dotted), for the model represented by Equations (2.1). The total density, N, is given in A, with infected and survivor density in B and carcass density in C. Results are shown for the scenario that represents Spain with supplementary feeding (see Figure 2.1 for parameters) and show the average densities between the years 2 and 3 following disease introduction. Control measures were implemented as soon as the virus is first discovered, defined as the time when carcass levels first reach a density of 0.02.

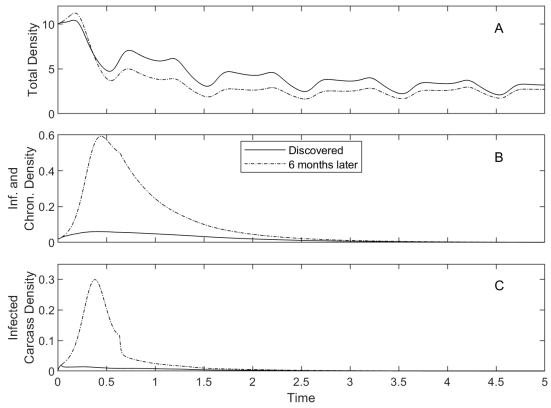

Figure A.17: Population response to the combination of culling, at fixed rate $b_C = 0.75$, and carcass removal, at fixed rate $r = 52$, for the model represented by Equations (2.1) and for parameters that represent the scenario of Spain with supplementary feeding (see Figure 2.1 for parameters).The total density, N, is given in A, with infected and survivor densities in B and prevalence in C. The results are shown for two different control implementation times: when the virus is first discovered (solid line), and six months after the virus was discovered (dashed line).

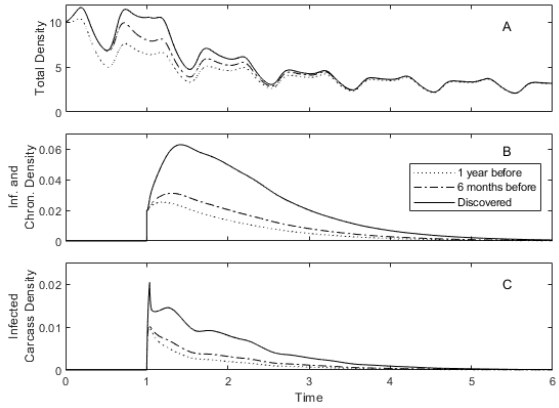

Figure A.18: Population response to the combination of culling, at fixed rate $b_C = 0.75$, and carcass removal, at fixed rate $r = 52$, for the model represented by Equations (2.1) and for parameters that represent the scenario of Spain with supplementary feeding (see Figure 2.1 for parameters).The total density, N, is given in A, with infected and survivor densities in B and prevalence in C. The results are shown for three different control implementation times: one year before the onset of the virus (dotted line), six months before the onset of the virus (dashed line), and when the virus is first discovered (solid line).

A.6 The impact of a varying degradation rate in Spain under natural conditions

Figures A.19 and A.20 explore the impact of a varying degradation rate, d, for the parameters and scenario representative of Spain under natural conditions in the absence of control.

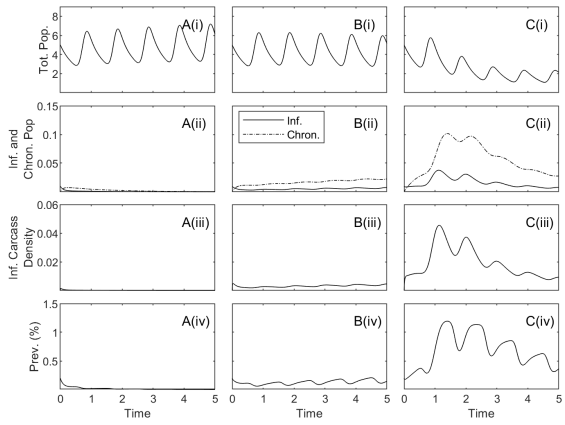

Figure A.19: Model simulations for the scenario representative of Spain under natural conditions with no control measures (see Figure 2.1 for parameters). The degradation rate varies from 1 day ($d = 365$), A, to 1/2 a week ($d = 104$), B, and to 1 week ($d = 52$), C, with C being our default. The total density, N, is given in (i), with infected (solid line) and survivor densities (dashed line) in (ii), infected carcass densities in (iii) and prevalence in (iv).

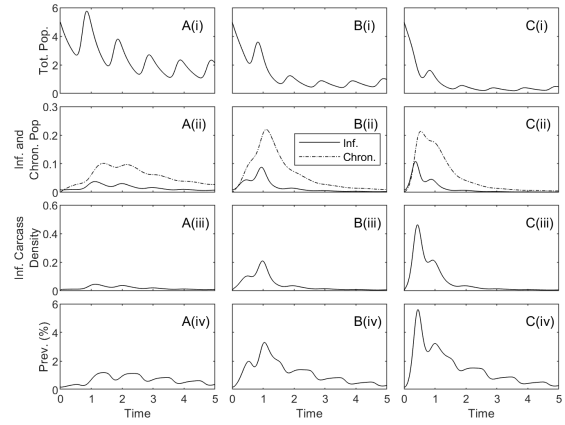

Figure A.20: Model simulations for the scenario representative of Spain under natural conditions with no control measures (see Figure 2.1 for parameters). The degradation rate varies from 1 week ($d = 52$), A, to 2 weeks ($d = 26$), B, and to 4 weeks ($d = 13$), C, with A being our default. The total density, N, is given in (i), with infected (solid line) and survivor densities (dashed line) in (ii), infected carcass densities in (iii) and prevalence in (iv).

A.7 Transmission from survivor individuals

Figures A.21 and A.22 explore the range of parameters which satisfy the epidemiological criteria for ASF (Section 2.2) when survivor individuals can also transmit the infection. We assume that survivor individuals transmit at rate $\beta_C = F\beta_F$ which is a fraction, F, of the rate of transmission from infected individuals. For both our default parameters and those which consider a reduced level of β_F the rate of transmission from survivor individuals needs to be low for the dynamics to satisfy the epidemiological criteria of ASF (Figure A.21). The inclusion of transmission from survivor individuals allowed

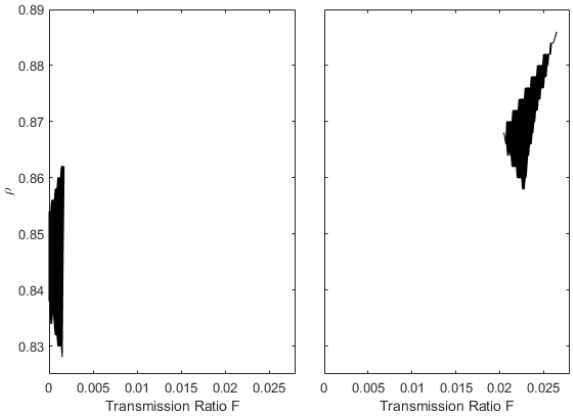

Figure A.21: A selection of valid transmission coefficients satisfying the epidemiological criteria outlined in Section 2.2 of the main paper for the model that represents Estonia under natural conditions and which additionally includes transmission from survivor individuals with transmission rate $\beta_C = F\beta_F$. Parameters are as in Section 2.2.1 with $\beta_F = 63$ in (A) and $\beta_F = 56$ in (B).

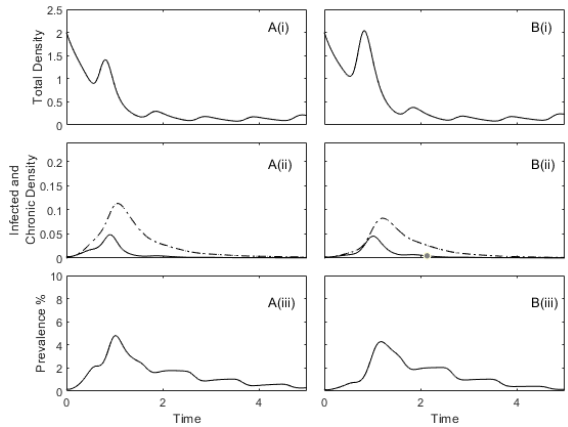

Figure A.22: Population densities and prevalence over time for the model representative of Estonia under natural conditions. In (A) the model is described by Equations (2.1) with parameters as outlined in Section 2.2.1 and in (B) the model additionally includes transmission from survivor individuals with transmission rate $\beta_C = F\beta_F$ and parameters as outlined in Section 2.2.1 except for $\beta_F = 56$ and $F = 0.025$. The total density, N, is given in (i), with infected (solid line) and survivor densities (dashed line) in (ii), and prevalence in (iii).

the model to match the epidemiological criteria for ASF with a reduced overall density of survivors (Figure A.22). Note, if the transmission rate from survivor individuals is similar to that of acutely infected individuals, then it leads to population extinction.

A.8 Varying carcass degradation rates without a survivor population

We used the model to test whether the epidemiological criteria for ASF could be satisfied for a range of carcass degradation rates (representing an average degradation time from 1 week to 40 weeks) in the absence of a survivor class. However, the epidemiological criteria could not be satisfied. When carcass degradation is slow and environmental transmission is 'high', it is possible to satisfy our epidemiological criteria points (1) and (2) related to the drop in population density and timing of the peak outbreak of ASF but not the persistence of ASF in the long-term since ASF fades-out after the outbreak (Figure A.23). This result only occurred for degradation lengths of less than 26 weeks. When carcass degradation is slow and environmental transmission is 'low', it is possible to satisfy point (3) of the epidemiological criteria related to the long-term

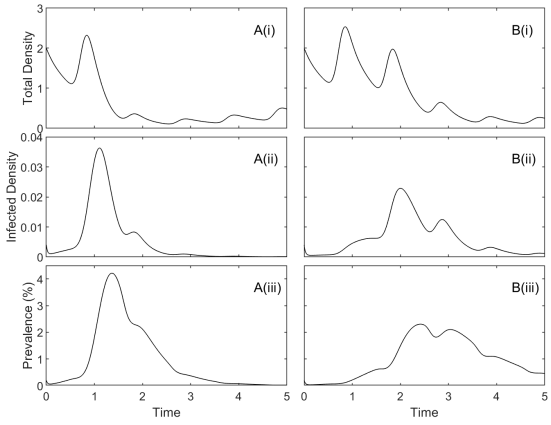

Figure A.23: Population densities and prevalence over time for the model described by Equations (2.1), with the total densities given in (i), infected density in (ii), and prevalence, defined as I/N, in (iii). Simulations were run for the situation representative of Estonia under natural conditions but without the presence of a survivor class ($\rho = 1$). Note, in the absence of a survivor class the three epidemiological criteria defined in Section 2.2 cannot be satisfied. For plots in (A) we use parameters $(\beta_F = 42, \beta_E = 2, d = 20)$ satisfying the first two elements of the epidemiological criteria but that could not satisfy the third and in (B) we use parameters $(\beta_F = 42, \beta_E = 1, d = 40)$ that could satisfy the third element in the epidemiological criteria but not the first two. All other parameters are as in Figure 2.1.

persistence of ASF but the decrease in host density is slow and the peak in the outbreak of ASF occurs several years after the initial introduction of the infection. This result only worked for degradation lengths of more than 37 weeks.

Chapter 3

The impact of an African swine fever outbreak on endemic tuberculosis in wild boar populations: a model analysis

The work in this chapter has been published in:

O'Neill, X., White, A., Ruiz-Fons, F. and Gortázar, C., 2021. The impact of an African swine fever outbreak on endemic tuberculosis in wild boar populations: A model analysis. *Transboundary and Emerging Diseases.* 00:1–11. https://doi.org/10.1111/tbed.14052

but with some of the supplementary information material moved into the main chapter, providing details on the full TB and ASF model and the coexistence of multiple pathogens through the inclusion of frequency-dependent transmission.

Abstract

A mathematical model is developed and analysed to examine the impacts of African swine fever (ASF) introduction into a wild boar population that supports endemic animal tuberculosis (TB). TB is a widespread infectious disease caused by the *Mycobacterium tuberculosis* bacteria belonging to the *Mycobacterium tuberculosis complex* (MTC) that can persist in reservoir wildlife hosts. Wild boar (*Sus scrofa*) are a key reservoir for MTC and an increasing trend in wild boar density is expected to lead to an increase in TB prevalence with spillover to livestock.

MTC infection is presently controlled through a variety of strategies, including culling. African swine fever (ASF) is a virulent, viral infection which affects wild boar and is spreading across Eurasia and Oceania. ASF infection leads to near 100% mortality at the individual level, can cause a dramatic decrease in population density and may therefore lead to TB control. We extend an established model that captures the key demographic and infection processes for TB in wild boar to consider the impact of ASF introduction on wild boar populations that support different levels of endemic TB. Our model results indicate that an ASF infection will reduce wild boar population density and lead to a decrease in the prevalence of TB. If ASF persists in the local host population the model predicts the long-term decline of TB prevalence in wild boar. If ASF is eradicated, or fades-out in the local host population, the model predicts a slower recovery of TB prevalence in comparison to wild boar density after an ASF epidemic. This may open a window of opportunity to apply TB management to maintain low TB prevalence.

3.1 Introduction

Animal tuberculosis (TB) is a widespread multi-host disease caused by infection with *Mycobacterium bovis* and the closely related members of the *M. tuberculosis complex* (MTC) and leads to increased host mortality [44]. TB has a significant economic impact on the livestock industry due to test and slaughter schemes and movement restrictions [48, 58, 59] and within the European Union there has been funding and a long-term policy to reduce and eradicate TB [60]. Other intervention measures include reducing indirect contacts among host species [61, 62], vaccinating [63], and culling [65, 66]. Nevertheless, there is an increasing prevalence of infection among cattle herds in Europe, with the EU herd prevalence at 0.4% in 2008 and at 0.9% in 2018 [67]. A key issue for the control of TB is its persistence in wildlife reservoirs from which it can spillover to livestock [71]. The primary reservoir species vary with location and include European badgers (*Meles meles*) in the British Isles, cervids in North America, brushtail possums (*Trichosurus vulpecula*) in New Zealand and buffalo (*Syncerus caffer*) in South Africa, among others [47, 48]. In mainland Europe, and in particular on the Iberian Peninsula, wild ungulates such as the Eurasian wild boar (*Sus scrofa*) and red deer (*Cervus elaphus*) act as the primary reservoir of infection [48, 51, 52, 53]. Due to increasing

habitat suitability and decreasing hunting pressure, the density of wild ungulates has seen an unprecedented increase over the last decades [72, 22, 23] and this presents a challenge for TB management.

Wildlife species can harbour multiple infectious agents and this can be facilitated by the increase in density of wild ungulates. In Eurasian wild boar, the spread of African swine fever (ASF) is a cause for current concern as it leads to high levels of mortality and has the potential to spillover to domestic pigs resulting in subsequent losses in pig production [33, 125, 126, 127]. As such, ASF is listed as a notifiable disease by the World Organisation for Animal Health (OIE). Outbreaks are currently causing global concern; in Europe an outbreak in Georgia and the Russian Federation in 2007 had spread to Ukraine, Belarus, Estonia, Latvia, Lithuania and Poland [35, 28, 34] and recent outbreaks have been reported in the Czech Republic, Belgium, Germany, Poland and Slovakia and several south-east European countries [128, 129, 130, 131]. In Asia, ASF was reported in China in 2018 and has subsequently spread throughout the region (up to Mongolia in the north and to Indonesia in the south) [132]. ASF is likely to continue to spread and therefore have a widespread global impact on domestic pig production and wild boar abundance. Rapid control measures are instigated to manage and eradicate ASF in wild boar [125, 28]. The measures will depend on the route of entry of infection, i.e., a widespread epidemic wave or a focal introduction, and include implementation of a combination of zoning, fencing and carcass removal, feeding bans, specific hunting regulations and depopulation actions [125, 28, 130].

The persistence of infectious disease is known to be linked to host population density with the potential for disease eradication if the host population decreases below a threshold density [10]. This has underpinned the use of culling as a management strategy to control wildlife diseases [133, 104, 134]. Since ASF outbreaks typically lead to significant reductions in host population density, which may be exacerbated due to ASF control measures (although intensified hunting in newly ASF-infected areas may be outweighed by the ASF induced population crash [135]). This is likely to have impacts for the prevalence and persistence of co-infecting pathogens, such as MTC. With

the continued spread of ASF it is therefore important to examine the potential impact of an ASF outbreak on the persistence of TB.

Mathematical models have played a key role in understanding the processes that drive epidemiological dynamics in wildlife populations [10, 93]. In this study we develop a mathematical model for a wild boar host population that can be co-infected with TB and ASF. Given the marked effect of ASF on wild boar population density and knowing that wild boar culling can contribute to TB control, we hypothesize that ASF emergence will have a significant impact on wild boar TB. Therefore, our aim is to understand the consequences of an ASF outbreak on the prevalence and persistence of endemic TB in wild boar. To do this we incorporate the disease dynamics for ASF, detailed in O'Neill et al. [18], into a model of TB in wild boar [66]. Our model system is parameterised to be representative of the wild boar TB system in different regions in Spain. However, the findings apply in general as we examine the impact of ASF in regions of high density and high endemic TB prevalence and in regions of low density and low endemic TB prevalence. Degradation of ASF in wild boar carcasses can play a key role in the ASF epidemiological dynamics [39, 18, 19], and so we explore the outcome with two different rates of degradation, a high and a low rate. In particular, the high rate represents the rapid degradation of the infection as seen in places with high temperatures or with abundant obligate scavengers, such as vultures. We then consider how disease control measures introduced to eradicate ASF will impact the dynamics of TB. Beyond assessing the potential impact of ASF on the epidemiological dynamics of TB our findings add new perspective to the theory on the interaction and coexistence of multiple pathogens in a single host species.

3.2 Methodology

We extend the model of Tanner et al. 2019 [66], which represents the dynamics of tuberculosis in wild boar, to include co-infection of African swine fever, as represented by O'Neill et al. 2020 [18]. A full model description is presented by Equations (3.2 and B.1-B.4) in Section 3.2.2 and the Supplementary Information. Here we describe the key

infection processes for TB, in Section 3.2.1, and for ASF, in Section 3.2.2.

3.2.1 The Wild Boar Tuberculosis model

The model of Tanner et al. 2019 [66] considers a wild boar host population that is split into three age-classes: piglets (P), yearlings (Y) and adults (A). The three different age classes are required as each class has distinct properties in terms of their demographic and infection dynamics. This model framework has been used successfully to understand the impact of vaccination and predation on TB prevalence in the wild boar TB system [63, 66]. The age-classes are further split into susceptible (subscript S), infected (subscript I) and generalised (subscript G) classes to reflect the TB disease status of the population. Generalised individuals can also release free-living TB pathogen particles, with density F, into the environment. The model is given below:

$$
\begin{aligned}
\frac{dP_S}{dt} &= b(Y+A)(1-qN) - \beta_{DP}P_S\frac{G}{N} - \omega\beta_{FP}P_SF - (m+d)P_S,\\
\frac{dP_I}{dt} &= \beta_{DP}P_S\frac{G}{N} + \omega\beta_{FP}P_SF - (\epsilon_P+m+d)P_I,\\
\frac{dP_G}{dt} &= \epsilon_P P_I - (\alpha+m+d)P_G,\\
\frac{dY_S}{dt} &= mP_S - \beta_{DY}Y_S\frac{G}{N} - \omega\beta_{FY}Y_SF - (c+m+d)Y_S,\\
\frac{dY_I}{dt} &= mP_I + \beta_{DY}Y_S\frac{G}{N} + \omega\beta_{FY}Y_SF - (\epsilon_Y+c+m+d)Y_I,\\
\frac{dY_G}{dt} &= mP_G + \epsilon_Y Y_I - (\alpha+c+m+d)Y_G,\\
\frac{dA_S}{dt} &= mY_S - \beta_{DA}A_S\frac{G}{N} - \omega\beta_{FA}A_SF - (c+d)A_S,\\
\frac{dA_I}{dt} &= mY_I + \beta_{DA}A_S\frac{G}{N} + \omega\beta_{FA}A_SF - (\epsilon_A+c+d)A_I,\\
\frac{dA_G}{dt} &= mY_G + \epsilon_A A_I - (\alpha+c+d)A_G,\\
\frac{dF}{dt} &= \lambda G - \mu_F F.
\end{aligned}
\tag{3.1}
$$

Here, $N = P + Y + A$ represents the total wild boar population, where $P = P_S + P_I + P_G; Y = Y_S + Y_I + Y_G; A = A_S + A_I + A_G$ and G is the total number of generalised individuals, $G = P_G + Y_G + A_G$. Yearlings and adults give birth to susceptible piglets

at rate b. This takes two values, $b = \log 4$ and $b = \log 7$, for scenarios representative of low and high TB prevalence regions, respectively. The total population is regulated through a crowding parameter, q, that acts on the birth rate, and is related to the carrying capacity, K, since $q = \frac{1}{K}\left(1 - \frac{d(d+m)}{mb}\right)$. We choose the values, $K = 5.95$ or $K = 27$, for low and high prevalence TB regions, respectively. Maturity from piglets to yearlings and yearlings to adults occurs at rate m and piglets, yearlings and adults may die of natural causes at rate d. This set-up for the demographic dynamics has previously been used to assess wild boar TB interactions [63, 104].

The model assumes infection can occur through direct frequency-dependent interactions (since wild boar tend to congregate in social groups) between susceptible and generalised individuals with transmission coefficients β_{DP}, β_{DY} and β_{DA}, for piglets, yearling and adults respectively, or through environmental contact with the free-living MTC, with transmission coefficients β_{FP}, β_{FY} and β_{FA}. Piglets and yearlings are assumed to be three times more susceptible to infection than adults [136]. Infected individuals are not infectious but can progress to the generalised (infectious) class at rates ϵ_P, ϵ_Y and ϵ_A, for the different age-classes, respectively. In low prevalence regions, where resources are not limited, it is assumed that $\epsilon_P = \epsilon_Y = \epsilon_A$ [66]. However, for high prevalence regions, where resources (particularly water) are scarce and overall health is impaired (similar to conditions in central and southern Spain), it is assumed that piglets and yearlings progress from the infected to the generalised class at three times the rate of adults ($\epsilon_P = \epsilon_Y = 3\epsilon_A$) [66]. The model assumes that free-living MTC is shed from generalised wild boar at rate λ and decays at rate μ_FF. The level of environmental transmission is scaled through the parameter ω which increases when environmental conditions become more severe to reflect, for example, aggregation at limited water holes. Finally, it is assumed that all wild boar in the generalised class suffer disease-induced mortality at rate α and that all adult and yearling classes are culled due to hunting at constant rate c.

In this study we consider two parameter sets that include a range of wild boar densities and TB prevalences found in Spain: (i) where the wild boar density is $4km^{-2}$ and TB is endemic with a prevalence of 10%, representative of regions in northern Spain, or

similar, where water is not a limiting factor and no feeding takes place [137] and (ii) where the wild boar density is $12km^{-2}$ and TB is endemic with a prevalence of 60%, representative of regions in central Spain, or similar, where wild boar are supplementary fed but where water resources are scarce in summer [138]. A full description of the parameters and their values (which are taken from Tanner et al. 2019 [66], except where stated) is given in the Supplementary Information.

3.2.2 The Wild Boar African Swine Fever and Tuberculosis model

We extend the wild boar TB dynamics to include co-infection with ASF following the methodology presented in O'Neill et al. 2020 [18] that develops a wild boar ASF model. The O'Neill et al., 2020 [18] model framework has been used successfully to examine the epidemiological dynamics of ASF in wild boar populations and to assess the effectiveness of control strategies to manage and eradicate ASF. For the ASF epidemiological dynamics we consider the following classes: S, uninfected and susceptible to infection; I, infected and able to transmit the virus; C, survivor individuals which do not transmit the virus but can revert to the infected (I) class and D, infected carcasses which can transmit the virus. The definition of survivor individuals arises from the type 1 'survivors' definition used in Ståhl et al. [40] where such individuals will invariably die but have the potential to excrete virus in association with the resurgence of viraemia. An overview of the ASF infection dynamics is shown schematically in Figure 3.1.

ASF infection is assumed to affect all age-classes of wild boar equally [18]. It is assumed a susceptible can become infected with ASF due to direct contact with an infected individual via frequency-dependent transmission, β_F or due to environmental transmission through contact with an infected carcass, β_E. A proportion, ρ, of infected individuals suffer disease-induced mortality at rate $\gamma = 365/5$, reflecting an average lifespan of 5 days for an individual with ASF [36]. A proportion, $1-\rho$, of infected individuals can instead enter the survivor class, which does not incur disease-induced mortality. Survivor individuals can revert to the infected class at rate $\kappa = 12/6$ implying that on average individuals remain survivors for 6 months [36]. Host individuals that die due

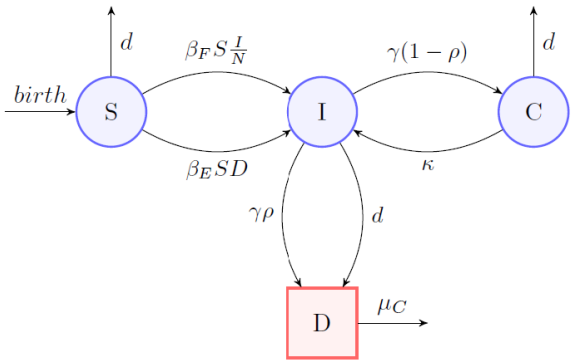

Figure 3.1: A visual representation of the wild boar ASF model presented in O'Neill et al. (2020). The nodes represent the different ASF infection classes: S, ASF susceptible, I, ASF infected, C, ASF survivor individuals and D, infected carcasses. The arrows show the possible entry and exit routes into and out of each respective class.

to the infection become infected carcasses which degrade at rate μ_C. Further details of the wild boar ASF model can be found in O'Neill et al. 2020 [18].

The combined TB and ASF infection model considers a wild boar host population that is split into three age-classes: piglets (P), yearlings (Y) and adults (A). The age-classes are split into TB susceptible (first subscript S), TB infected (first subscript I) and TB generalised (first subscript G) classes to reflect the TB disease status of the population. They are then further split into ASF susceptible (second subscript S), ASF infected, (second subscript I) and ASF survivor individuals (second subscript C) classes to reflect the ASF disease status of the population. Generalised individuals can also release free-living TB pathogens with density F into the environment and when ASF infected individuals die, either naturally or through disease-induced mortality, they enter the infected carcass class D. The combined TB and ASF infection model is shown for the piglet population in Equations (3.2), with the TB and ASF infection model for the remaining wild boar populations, and details of the parameter values, shown in the Supplementary Information. Note, in the TB and ASF full model we do not assume direct interference between competing pathogens. However, there will be indirect interference due to parasite induced changes in host population density.

$$\frac{dP_{SS}}{dt} = b(Y+A)(1-qN) - \beta_{DP}P_{SS}\frac{G}{N} - \omega\beta_{FP}P_{SS}F$$

$$
\begin{aligned}
&\quad - \beta_F P_{SS}\frac{I}{N} - \beta_E P_{SS} D - m P_{SS} - d_p P_{SS} - b_C P_{SS},\\
\frac{dP_{IS}}{dt} &= \beta_{DP} P_{SS}\frac{G}{N} + \omega\beta_{FP} P_{SS} F - \epsilon_P P_{IS}\\
&\quad - \beta_F P_{IS}\frac{I}{N} - \beta_E P_{IS} D - m P_{IS} - d_p P_{IS} - b_C P_{IS},\\
\frac{dP_{GS}}{dt} &= \epsilon_P P_{IS} - \alpha P P_{GS}\\
&\quad - \beta_F P_{GS}\frac{I}{N} - \beta_E P_{GS} D - m P_{GS} - d_p P_{GS} - b_C P_{GS},\\
\frac{dP_{SI}}{dt} &= -\beta_{DP} P_{SI}\frac{G}{N} - \omega\beta_{FP} P_{SI} F\\
&\quad + \beta_F P_{SS}\frac{I}{N} + \beta_E P_{SS} D - \gamma P_{SI} + \kappa P_{SC} - m P_{SI} - d_p P_{SI} - b_C P_{SI},\\
\frac{dP_{II}}{dt} &= \beta_{DP} P_{SI}\frac{G}{N} + \omega\beta_{FP} P_{SI} F - \epsilon_P P_{II}\\
&\quad + \beta_F P_{IS}\frac{I}{N} + \beta_E P_{IS} D - \gamma P_{II} + \kappa P_{IC} - m P_{II} - d_p P_{II} - b_C P_{II},\\
\frac{dP_{GI}}{dt} &= \epsilon_P P_{II} - \alpha P_{GI}\\
&\quad + \beta_F P_{GS}\frac{I}{N} + \beta_E P_{GS} D - \gamma P_{GI} + \kappa P_{GC} - m P_{GI} - d_p P_{GI} - b_C P_{GI},\\
\frac{dP_{SC}}{dt} &= -\beta_{DP} P_{SC}\frac{G}{N} - \omega\beta_{FP} P_{SC} F\\
&\quad + \gamma(1-\rho) P_{SI} - \kappa P_{SC} - m P_{SC} - d_p P_{SC} - b_C P_{SC},\\
\frac{dP_{IC}}{dt} &= \beta_{DP} P_{SC}\frac{G}{N} + \omega\beta_{FP} P_{SC} F - \epsilon_P P_{IC}\\
&\quad + \gamma(1-\rho) P_{II} - \kappa P_{IC} - m P_{IC} - d_p P_{IC} + -b_C P_{IC},\\
\frac{dP_{GC}}{dt} &= \epsilon_P P_{IC} - \alpha P_{GC}\\
&\quad + \gamma(1-\rho) P_{GI} - \kappa P_{GC} - m P_{GC} - d_p P_{GC} + -b_C P_{GC}.
\end{aligned}
\tag{3.2}
$$

The key control methods adopted to manage and eradicate ASF are dramatic depopulation (to reduce direct transmission) and the removal of infected carcasses (to reduce environmental transmission) [125, 28, 18]. In the model we include wild boar depopulation by assuming culling is applied at rate b_C, across all age and infection classes (see Equations 3.2, B.1 and B.2). The culling rate, b_C, corresponds to a culling proportion equal to $1 - e^{-b_C}$, per year. The removal of ASF infected carcasses is modelled as an additional loss term in the infected carcass class, D, with removal rate, r (see Equation B.3). The value r corresponds to an average time till the removal of a carcass of $1/r$ years.

3.3 The impact of African swine fever on endemic tuberculosis

We undertake model simulations for the introduction of ASF into the TB endemic system, for scenarios that are representative of TB infection status found in Spain, including regions of high and low TB prevalence and regions of high and low ASF infected carcass degradation rates.

For the scenario with high TB prevalence and a high rate of ASF infected carcass degradation the introduction of ASF leads to a rapid population reduction of 85% (Figure 3.2). There is a peak in ASF infection around 3 months after its introduction and in the model ASF persists at low prevalence (0.8%) in the long-term. The impact and persistence of ASF leads to a reduction in the host population density which in turn leads to a decrease in TB prevalence. Note, the decrease in TB prevalence is slow and in the long-term TB prevalence stabilises to a reduced level. For the scenario with high TB prevalence and a low rate of ASF infected carcass degradation the introduction of ASF leads to a near eradication of the host population, with a 99% reduction in the host population density (Figure 3.3). The impact of ASF is more severe as the low rate of carcass degradation increases the potential for ASF transmission. ASF

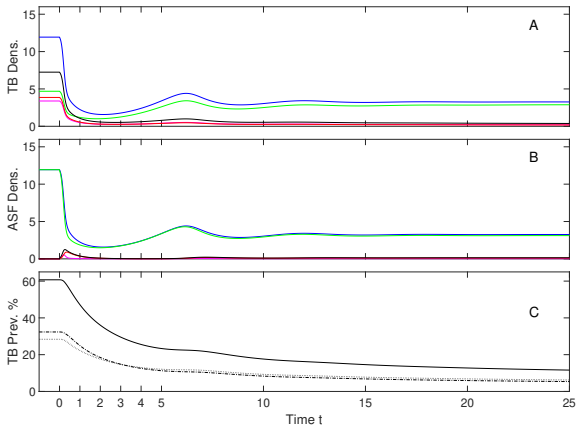

Figure 3.2: Population densities and prevalence for the model described by the Equations (3.2–B.4), for the scenario with high carcass degradation rate and a high tuberculosis prevalence. Results are shown over a 25-year period. (A) shows total host density (blue), hosts susceptible to TB (green), hosts infected with TB (magenta), hosts with generalized TB infection (red) and the combined infected and generalized hosts (black). (B) shows the total host density (blue), hosts susceptible to ASF (green), hosts infected with TB (magenta), ASF survivor density (red) and the infected carcass density (black). (C) shows TB prevalence with infected prevalence, I_{TB}/N, (dotted); generalized prevalence, G/N, (dot-dash) and total prevalence, $(I_{TB}+G)/N$, (solid). We used default parameter values and $K = 27, b = \ln 7, c_\epsilon = 3, \omega = 1$ and $d = 52$.

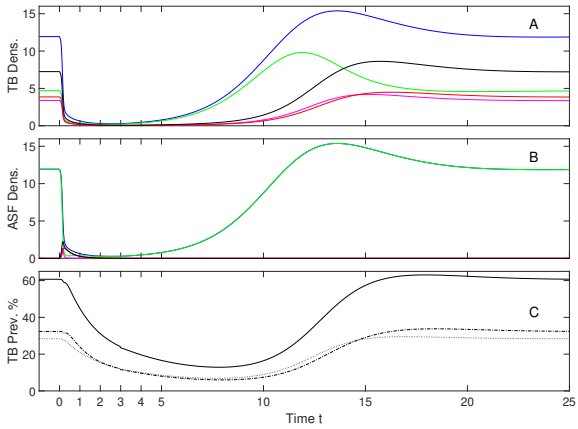

Figure 3.3: Population densities and prevalence for the model described by the Equations (3.2–B.4), for the scenario with low carcass degradation rate and a high tuberculosis prevalence. Results are shown over a 25-year period. (A) shows total host density (blue), hosts susceptible to TB (green), hosts infected with TB (magenta), hosts with generalized TB infection (red) and the combined infected and generalized hosts (black). (B) shows the total host density (blue), hosts susceptible to ASF (green), hosts infected with TB (magenta), ASF survivor density (red) and the infected carcass density (black). (C) shows TB prevalence with infected prevalence, I_{TB}/N, (dotted); generalized prevalence, G/N, (dot-dash) and total prevalence, $(I_{TB}+G)/N$, (solid). We used default parameter values and $K = 27, b = \ln 7, c_\epsilon = 3, \omega = 1$ and $d = 13$.

infection peaks after 2 months and persists for 2 years but the model results indicate local disease fade-out. In the long-term this allows the host population to return to the density prior to the ASF outbreak. The impact on TB is a gradual reduction in prevalence from 60% to less than 20% within 8 years, and then an increase in TB prevalence back to 60% at a rate that lags behind the increase in population density.

Although ASF leads to near eradication of the population, the TB prevalence does not drop below 20%. TB is not eradicated in the model as the component of the effective reproductive ratio that arises through the frequency-dependent transmission is independent of host density and is greater than 1 (see Section 3.5 for more details).

In the low TB prevalence (and lower initial host density), high carcass degradation rate scenario ASF establishes slowly and becomes endemic at low prevalence (Figure 3.4). This leads to a slow decrease in the host population of around 35% which then leads to a slow decrease in TB prevalence. In the long-term TB would be eradicated as the TB infection parameters for this scenario mean that the reduction in host population density due to endemic ASF is sufficient to reduce the effective reproductive ratio for TB below 1 (see Section 3.5). The low TB prevalence and low carcass degradation rate scenario (Figure 3.5) is similar to the equivalent

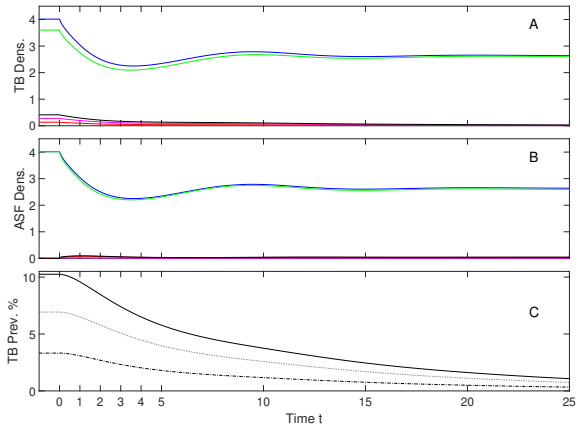

Figure 3.4: Population densities and prevalence for the model described by the Equations (3.2–B.4), for the scenario with high carcass degradation rate and a low tuberculosis prevalence. Results are shown over a 25-year period. (A) shows total host density (blue), hosts susceptible to TB (green), hosts infected with TB (magenta), hosts with generalized TB infection (red) and the combined infected and generalized hosts (black). (B) shows the total host density (blue), hosts susceptible to ASF (green), hosts infected with TB (magenta), ASF survivor density (red) and the infected carcass density (black). (C) shows TB prevalence with infected prevalence, I_{TB}/N, (dotted); generalized prevalence, G/N, (dot-dash) and total prevalence, $(I_TB + G)/N$, (solid). We used default parameter values and $K = 5.95, b = \ln 4, c_\epsilon = 1, \omega = 0.1$ and $d = 52$.

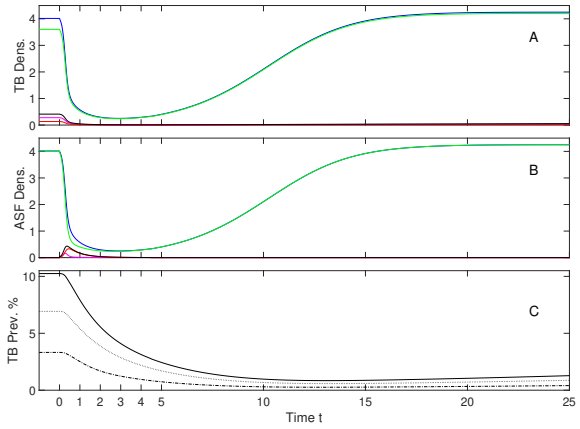

Figure 3.5: Population densities and prevalence for the model described by the Equations (3.2–B.4), for the scenario with low carcass degradation rate and a low tuberculosis prevalence. Results are shown over a 25-year period. (A) shows total host density (blue), hosts susceptible to TB (green), hosts infected with TB (magenta), hosts with generalized TB infection (red) and the combined infected and generalized hosts (black). (B) shows the total host density (blue), hosts susceptible to ASF (green), hosts infected with TB (magenta), ASF survivor density (red) and the infected carcass density (black). (C) shows TB prevalence with infected prevalence, I_{TB}/N, (dotted); generalized prevalence, G/N, (dot-dash) and total prevalence, $(I_{TB} + G)/N$, (solid). We used default parameter values and $K = 5.95, b = \ln 4, c_\epsilon = 1, \omega = 0.1$ and $d = 13$.

high TB prevalence case with an ASF outbreak followed by rapid population crash and fade out of ASF before the population then recovers. There is a reduction in TB prevalence to low levels and a slow increase in TB prevalence following population recovery. The slow decrease and then increase in TB prevalence is due to the effective reproductive ratio for TB dropping

below 1 for low host population densities and increasing above 1 as the host population returns to its density prior to the ASF outbreak. A common finding across all scenarios is that the epidemiological dynamics of ASF are rapid whereas those of TB are slow and highlights a difference between acute and chronic infections.

3.4 Applying ASF control

Due to the economic and population impact of ASF on wildlife and domestic hosts control measures to eradicate ASF are applied following its detection. In ASF endemic regions, such as the Baltic countries, infected wild boar are recorded for several years after the initial introduction and suggest there could be poorly understood pathways that facilitate the persistence of the virus at very low densities [130, 18]. ASF maintenance could also be caused by continued new introductions of the virus from adjacent affected regions and countries [130]. Recommended measures under these epidemiological circumstances include continued active and passive disease surveillance, intense efforts of carcass detection and removal, and continuous and intensive hunting of wild boar to maintain low population densities, both to slow down the speed of infection spread and to monitor progress through active disease surveillance [130]. We repeat the scenarios outlined in Section 3.3 but with the inclusion of ASF control measures. We consider two control measures: the culling of the host population (with culling rate b_C) and the removal of ASF infected carcasses (with removal rate r). The measures are implemented as soon as ASF enters the population and cease when ASF has been eradicated from the population (defined as the time when the total number of ASF infected and survivor individuals, $I + C$, is less than 0.1% of the initial host density).

For control that focuses on carcass removal (a high carcass removal rate, $r = 200$ and low culling rate $b_C = 0.2$) the results are similar regardless of the ASF and TB scenario. We show results for the high TB prevalence and low carcass degradation rate scenario (Figure 3.6). Results for other scenarios can be found in the Supplementary Information (Figure B.1). ASF control prevents a severe ASF infectious outbreak and ASF is eradicated within 3 years. There is an approximate 40% drop in total population and only 10% drop in TB prevalence. This method of control eradicated ASF without a significant drop in host population density and therefore will have little impact on TB prevalence.

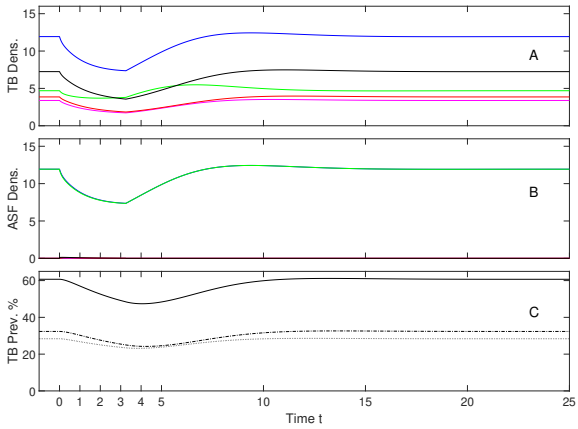

Figure 3.6: Population densities and prevalence for the model described by the Equations (3.2–B.4), for the scenario with low carcass degradation rate and a high tuberculosis prevalence under specific ASF control measures. Results are shown over a 25-year period. (A) shows total host density (blue), hosts susceptible to TB (green), hosts infected with TB (magenta), hosts with generalized TB infection (red) and the combined infected and generalized hosts (black). (B) shows the total host density (blue), hosts susceptible to ASF (green), hosts infected with TB (magenta), ASF survivor density (red) and the infected carcass density (black). (C) shows TB prevalence with infected prevalence, I_{TB}/N, (dotted); generalized prevalence, G/N, (dot-dash) and total prevalence, $(I_{TB}+G)/N$, (solid). Parameters are as in Figure 3.3, with the culling parameter $b_C = 0.2$ and carcass removal rate $r = 200$.

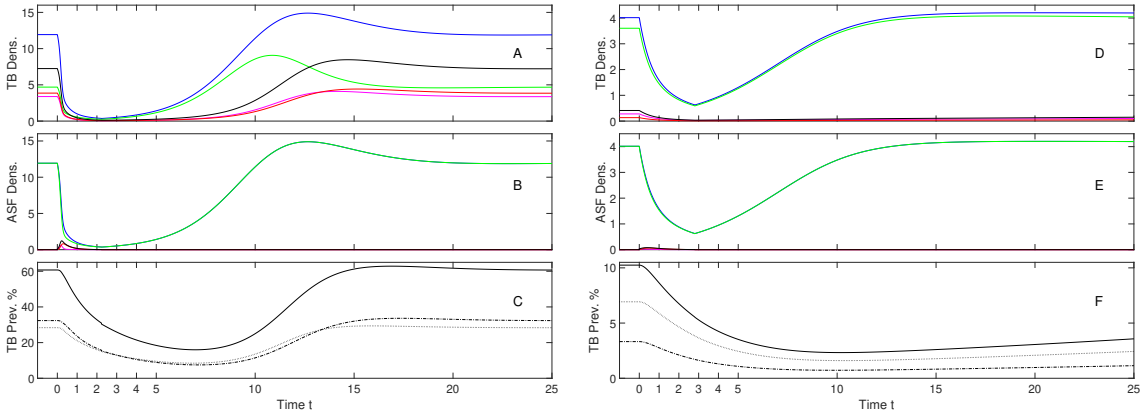

Figure 3.7: Population densities and prevalence for the model described by the Equations (3.2–B.4), for the scenario with low carcass degradation rate and either a high tuberculosis prevalence (A–C) or a low tuberculosis prevalence (D–F), under specific ASF control measures. Results are shown over a 25-year period. (A & D) show total host density (blue), hosts susceptible to TB (green), hosts infected with TB (magenta), hosts with generalized TB infection (red) and the combined infected and generalized hosts (black). (B & E) show the total host density (blue), hosts susceptible to ASF (green), hosts infected with TB (magenta), ASF survivor density (red) and the infected carcass density (black). (C & F) show TB prevalence with infected prevalence, I_{TB}/N, (dotted); generalized prevalence, G/N, (dot-dash) and total prevalence, $(I_{TB}+G)/N$, (solid). For A–C, parameters are as in Figure 3.3, and for D–F, parameters are as in Figure 3.5. For all plots, the culling parameter $b_C = 0.7$ and carcass removal rate $r = 26$ are used.

For the culling-based control measure (a low carcass removal rate, $r = 26$ and high culling rate $b_C = 0.7$) the outcome depends on whether the initial TB prevalence is high or low but is independent of the natural carcass degradation rate. We show results representative of a low

carcass degradation rate with results representative of a high carcass degradation rate given in the Supplementary Information (Figure B.2). For scenarios representative of a high TB prevalence region there is a rapid reduction in host population density, of approximately 95%, and a more gradual reduction in TB prevalence (Figure 3.7). Once ASF is eradicated the total population recovers but the increase in prevalence of TB to its original value lags behind that of the increase in host population. For scenarios representative of a low TB prevalence region (Figure 3.7), there is an approximate drop of 80% in the total population and slow decrease in TB prevalence. Following ASF eradication the host population recovers to its original density but TB prevalence increases slowly.

3.5 TB infection at low host density

In many classical infection models [10, 93], the basic reproductive ratio (R_0) of the disease depends on the density of susceptible individuals. Therefore, it is possible to reduce R_0 below 1 and eradicate the infection by reducing the population density. In the TB and ASF model we observe that ASF may lead to a drop in the population to low levels and yet TB is not eradicated. We investigate the reason for this observation by considering a reduced model that captures the key TB infection dynamics and by undertaking numerical simulations of the full TB model.

This reduced model neglects age-classes and considers a susceptible population (S), an infected population (I), a generalised population (G) and the free-living TB particles (F), and is given in Equations (3.3) below:

$$\begin{aligned}
\frac{dS}{dt} &= w(S,I,G,F) = bN(1-qN) - \beta_D S\frac{G}{N} - \omega\beta_F SF - dS,\\
\frac{dI}{dt} &= x(S,I,G,F) = \beta_D S\frac{G}{N} + \omega\beta_F SF - \epsilon I - dI,\\
\frac{dG}{dt} &= y(S,I,G,F) = \epsilon I - \alpha G - dG,\\
\frac{dF}{dt} &= z(S,I,G,F) = \lambda G - \mu_F F.
\end{aligned} \tag{3.3}$$

Here, $N = S + I + G$ is the total population density, with transmission coefficients β_D and β_F representing the direct contact and free-living contact transmissions respectively. All other parameters are as discussed in the full TB model. The model therefore captures the key

infection processes of TB in the absence of age-classes.

3.5.1 Steady state and stability analysis of the reduced model

The system of equations (3.3) has three steady states: the trivial steady state $(S, I, G, F) = (0, 0, 0, 0)$, the disease-free steady state $(K, 0, 0, 0)$, where $K = (b - d)/bq$ and the endemic steady state (S_e, I_e, G_e, F_e). Stability of the steady states can be determined by calculating the eigenvalues of the Jacobian, J (Equation 3.4).

$$J(S, I, G, F) = \begin{pmatrix} \frac{\partial w}{\partial S} & \frac{\partial w}{\partial I} & \frac{\partial w}{\partial G} & \frac{\partial w}{\partial F} \\ \frac{\partial x}{\partial S} & \frac{\partial x}{\partial I} & \frac{\partial x}{\partial G} & \frac{\partial x}{\partial F} \\ \frac{\partial y}{\partial S} & \frac{\partial y}{\partial I} & \frac{\partial y}{\partial G} & \frac{\partial y}{\partial F} \\ \frac{\partial z}{\partial S} & \frac{\partial z}{\partial I} & \frac{\partial z}{\partial G} & \frac{\partial z}{\partial F} \end{pmatrix} \tag{3.4}$$

The Jacobian evaluated at the disease-free steady state is given by:

$$J(K, 0, 0, 0) = \begin{pmatrix} d - b & 2d - b & 2d - b - \beta_D & -\omega\beta_F K \\ 0 & -\epsilon - d & \beta_D & \omega\beta_F K \\ 0 & \epsilon & -\alpha - d & 0 \\ 0 & 0 & \lambda & -\mu_F \end{pmatrix}, \tag{3.5}$$

which gives the characteristic polynomial:

$$(\gamma - d + b)(\gamma^3 + a_1\gamma^2 + a_2\gamma + a_3) = 0, \tag{3.6}$$

where:

$$\begin{aligned} a_1 &= \mu_F + \alpha + 2d + \epsilon, \\ a_2 &= (\alpha + d)(d + \epsilon + \mu_F) + \mu_F(d + \epsilon) - \epsilon\beta_D, \end{aligned} \tag{3.7}$$

$$a_3 = \mu_F(\alpha + d)(d + \epsilon) - \beta_D \epsilon \mu_F - \lambda \epsilon \omega \beta_F K.$$

From this characteristic polynomial we can already determine one of the eigenvalues $\gamma_1 = d - b$, which we assume to be negative (otherwise the trivial steady state would be stable). Using the Routh-Hurwitz stability criterion on the remaining cubic polynomial we determine that the remaining requirements for stability are that all our coefficients a_i are positive, and that $a_1 a_2 > a_3$. Given that all parameters are positive, a_1 is therefore positive. The condition $a_3 > 0$ requires that the following inequality holds:

$$\mu_F(\alpha + d)(d + \epsilon) - \beta_D \epsilon \mu_F - \lambda \epsilon \omega \beta_F K > 0. \tag{3.8}$$

The inequality (3.8) implies $(\alpha + d)(d + \epsilon) - \lambda \epsilon \beta_F K / \mu_F > \epsilon \beta_D$ and therefore if (3.8) holds it is clear that $a_2 > 0$.

The condition $a_1 a_2 > a_3$ can be written as:

$$(\alpha + d)(d + \epsilon + \mu_F) + \mu_F(d + \epsilon) + \mu_F^2 + \frac{\lambda \epsilon \omega \beta_F K}{(\alpha + 2d + \epsilon)} > \epsilon \beta_D, \tag{3.9}$$

and this holds if (3.8) holds.

Finally, we can rearrange (3.8) to represent the basic reproductive ratio, R_0, of the disease as follows:

$$R_0 = \frac{\lambda \omega \beta_F K}{\mu_F(\alpha + d)(d + \epsilon)} + \frac{\epsilon \beta_D \mu_F}{\mu_F(\alpha + d)(d + \epsilon)} < 1. \tag{3.10}$$

Note, the first term in R_0 relates to (density dependent) environmental transmission and the magnitude of this decreases with host density. The second term relates to frequency dependent direct transmission and does not depend on host density (K). If the second term has a magnitude greater than unity then $R_0 > 1$ regardless of host density and the disease-free steady state will be unstable at all host densities.

3.5.2 Simulated steady states in the full TB model

We now explore the full TB model to understand the relationship between host density and the persistence of TB. The results for the full TB model, in the absence of ASF, in both high and low TB prevalence scenarios indicate that the disease does not die out as the host density

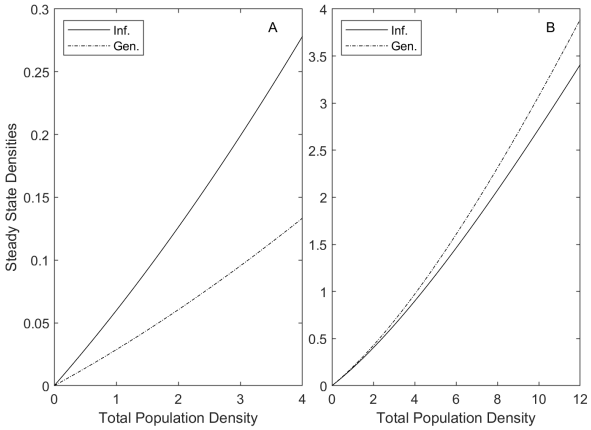

Figure 3.8: Stable steady state population densities plotted against the total population density for the model described by Equations (3.1). The scenarios are representative of low TB prevalence (A) or high TB prevalence (B) with infected steady state densities (solid line) and generalised densities(dot-dash). Parameters are taken from the full TB model as discussed in Section B.1.2.

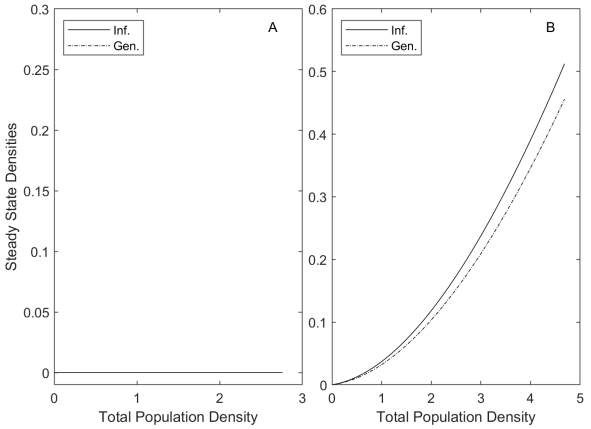

Figure 3.9: Stable steady state population densities plotted against the total population density for the model described by Equations (3.1) but with an additional mortality term from ASF. This additional mortality term is given by $\gamma\rho P_{ASF}$ where γ is the mortality rate due to ASF, ρ the proportion that enter the infected carcass class and P_{ASF} the endemic prevalence value of ASF in each scenario. The scenarios are representative of low TB prevalence (A) or high TB prevalence (B) with infected steady state densities (solid) and generalised steady state densities (dot-dash). Parameters are taken from the full TB model as discussed in Section B.1.2, with additional mortality of 0.0029γ and 0.0071γ included for low and high TB prevalence cases respectively.

decreases (Figure 3.8). This indicates that the frequency dependence direct transmission term of the effective reproductive ratio is greater than unity and so the disease does not die out as host density become small. However, in the scenarios when ASF is introduced into a TB endemic population, TB is eradicated in the low TB prevalence scenario (Figure 3.4) and close to eradication in the high TB prevalence scenario (Figure 3.2). In these scenarios ASF remains endemic in the population, with prevalence of 0.29% and 0.71% in the low and high TB prevalence cases respectively. This imposes an addition mortality on the host population of

0.0029γ and 0.0071γ in the low and high TB prevalence cases, respectively, and this will affect the effective reproductive ratio of TB. If we include this additional mortality we see that TB is eradicated in the low TB prevalence case (Figure 3.9A) but not in the high TB prevalence case (Figure 3.9B). This indicates that the frequency dependence direct transmission term of the effective reproductive ratio is less than unity in the low TB prevalence case but greater than unity in the high TB prevalence case.

3.6 Discussion

The insight gained from our mathematical model confirmed the hypothesis that the emergence of ASF could have a significant impact on the prevalence of TB in wild boar, with a reduction in TB prevalence in response to an ASF outbreak. If ASF persists in the local host population the model predicts the long-term decline of TB prevalence in wild boar. If ASF fades-out in the local host population the model predicts a slower recovery of TB prevalence in comparison to wild boar density after an ASF epidemic. This may open a window of opportunity to apply TB management to maintain low TB prevalence. Whilst there are ongoing efforts to prevent ASF re-emergence in Spain, after its successful eradication in 1995 [139], and elsewhere across the globe, the ongoing ASF spread in Eurasia [140, 100] means this option for TB management may be realised.

Our model study adds new perspective to the theory on the coexistence of multiple pathogens. Classical infectious disease model studies [10, 141], that include multiple pathogens which exclusively infect the host and that consider density-dependent infection transmission, indicate that the pathogen with the greatest reproductive ratio can out-compete the other pathogen. Exclusion of competing pathogens occurs as disease-induced mortality suppresses the host density to levels where only one pathogen can persist [142]. Coexistence of multiple pathogens requires co-infection or super-infection mechanisms that include trade-offs balancing the pathogens' ability to transmit the infection against disease-induced mortality [143, 144, 145, 146]. Our study includes co-infection of the host by different pathogens that infect the host through density-dependent and frequency-dependent mechanisms. In particular, the component of the pathogen reproductive ratio arising through frequency-dependent transmission does not depend on host density (see Section 3.5) and we show that this transmission mechanism can promote pathogen coexistence and prevent the pathogen exclusion that arises

due to disease-induced suppression of the host density.

ASF infection leads to high levels of disease-induced mortality in wild boar and an ASF outbreak can cause a rapid and significant decline in population density [28, 36, 37, 18, 38]. Therefore, an ASF outbreak in wild boar populations that support endemic TB will act in a similar manner to host population culling and can have an impact on TB prevalence and MTC infection levels [66, 104]. Our model results indicate that an ASF infection will reduce wild boar population density and lead to a decrease in the prevalence of TB. The decrease in population density leads to a rapid decrease in the number of TB infected individuals but with the decrease in TB prevalence occurring on a longer time scale. This is due to ASF infecting all TB classes equally, TB being a chronic long-lived infection compared to ASF and due to the direct, frequency-dependent transmission of TB at low wild boar density. When ASF persists in the host population a reduction in wild boar population density is seen due to the increase in population level mortality. This leads to a long-term reduction in TB prevalence and the potential for TB eradication. In some model scenarios where ASF transmission in the environment (from infected carcasses) is high, the ASF outbreak causes a severe reduction in host population density and while ASF persists in the medium term it can fade-out, in the local host population, in the long-term. This further highlights the importance of environmental transmission from infected carcasses in the persistence of ASF and the role obligate scavengers may play in reducing environmental transmission [39, 18, 19]. Infection fade-out is common for highly virulent, acute infections [35, 147, 148, 89] and may occur locally for ASF but is unlikely to do so over a regional scale due to the spatial spread of infection (for example, ASF has persisted at the regional scale in Baltic countries since 2014, [149]). Model results indicate that following ASF fade-out the local wild boar population density will increase and slowly return to pre-ASF infection levels. The increase in MTC infection lags behind the increase in population density and therefore the return to pre-ASF infection levels of TB is predicted to occur on a longer time scale. This should not be misinterpreted for TB control as TB will still increase in the long-term. However, the slow increasing rate of TB infection may open a window of opportunity to apply TB management and maintain low TB prevalence. This could include bio-safety measures that reduce wildlife-cattle contact rates [61], the culling of wild boar [65] or the introduction of TB vaccinations for wild boar [63]. We recognise that our model only considers a single host system and in a natural system there are several species that can act as a TB reservoir [48, 51, 52]. Therefore, there is the potential for inter-species trans-

mission which could accelerate the increase in TB prevalence during the wild boar population recovery phase. However, there is evidence that wild boar are the key reservoir species for TB in Spain [52, 53] and that a decrease in wild boar TB infection levels leads to a reduction in TB prevalence in other wildlife [65, 66].

ASF infection has widespread and severe impacts on wild boar and domestic pig production [33, 127] and is listed as a notifiable disease by the World Organisation of Animal Health (OIE) [126, 34]. Control measures to manage ASF are likely to be introduced following detection [150, 126] and while these would diminish the impact of an ASF outbreak they may also limit host population mortality and therefore the impact of ASF on TB control. Furthermore, resources that are used to target TB control may be redistributed to focus on ASF management and this could have unforeseen consequences for TB management. A consequence of the Foot-and-Mouth outbreak in the UK in 2001 [151] and a likely consequence of the effort to tackle COVID-19 [152], is a shift in resources to control the emerging disease at the expense of a reductions in the direct efforts to control endemic disease. Therefore, any efforts to control emerging pathogens should be considered as part of a joint strategy to control the multiple pathogens that share a host.

In this study we have used a mathematical modelling framework to assess the potential impact of an ASF outbreak on the epidemiological dynamics of wild boar. We have made particular reference to the situation in Spain where wild boar are the key reservoir host for TB. However, the key findings that ASF can lead to a marked reduction in host density and hence a rapid reduction in TB infected individuals but a more gradual reduction in TB prevalence generalise beyond the system in Spain. Our results highlight the interaction and impact of co-infecting pathogens on the population and epidemiological dynamics of their host and the need to consider multiple pathogens when attempting to control a primary infectious outbreak.

Appendix B: Supplementary material for Chapter 3

B.1 Methodology

B.1.1 The TB and ASF model

The model considers a wild boar host population that is split into three age-classes: piglets (P), yearlings (Y) and adults (A). The age-classes are split into TB susceptible (first subscript S), TB infected (first subscript I) and TB generalised (first subscript G) classes to reflect the TB disease status of the population. They are then further split into ASF susceptible (second subscript S), ASF infected, (second subscript I) and ASF survivor individuals (second subscript C) classes to reflect the ASF disease status of the population. Generalised individuals can also release free-living TB pathogens with density F into the environment and when ASF infected individuals die, either naturally or through disease-induced mortality, they enter the infected carcass class D. The full TB and ASF wild boar model is given by Equations (3.2 and B.1-B.11):

Yearlings:

$$\begin{aligned}
\frac{dY_{SS}}{dt} &= mP_{SS} - cY_{SS} - \beta_{DY}Y_{SS}\frac{G}{N} - \omega\beta_{FY}Y_{SS}F \\
&\quad - \beta_F Y_{SS}\frac{I}{N} - \beta_E Y_{SS}D - mY_{SS} - d_Y Y_{SS} - b_C Y_{SS}, \\
\frac{dY_{IS}}{dt} &= mP_{IS} - cY_{IS} + \beta_{DY}Y_{SS}\frac{G}{N} + \omega\beta_{FY}Y_{SS}F - \epsilon_Y Y_{IS} \\
&\quad - \beta_F Y_{IS}\frac{I}{N} - \beta_E Y_{IS}D - mY_{IS} - d_Y Y_{IS} - b_C Y_{IS}, \\
\frac{dY_{GS}}{dt} &= mP_{GS} - cY_{GS} + \epsilon_Y Y_{IS} - \alpha Y_{GS}
\end{aligned}$$

$$
\begin{aligned}
&\quad - \beta_F Y_{GS}\frac{I}{N} - \beta_E Y_{GS} D - mY_{GS} - d_Y Y_{GS} - b_C Y_{GS},\\
\frac{dY_{SI}}{dt} &= mP_{SI} - cY_{SI} - \beta_{DY} Y_{SI}\frac{G}{N} - \omega\beta_{FY} Y_{SI} F\\
&\quad + \beta_F Y_{SS}\frac{I}{N} + \beta_E Y_{SS} D - \gamma Y_{SI} + \kappa Y_{SC} - mY_{SI} - d_Y Y_{SI} - b_C Y_{SI},\\
\frac{dY_{II}}{dt} &= mP_{II} - cY_{II} + \beta_{DY} Y_{SI}\frac{G}{N} + \omega\beta_{FY} Y_{SI} F - \epsilon_Y Y_{II}\\
&\quad + \beta_F Y_{IS}\frac{I}{N} + \beta_E Y_{IS} D - \gamma Y_{II} + \kappa Y_{IC} - mY_{II} - d_Y Y_{II} - b_C Y_{II},\\
\frac{dY_{GI}}{dt} &= mP_{GI} - cY_{GI} + \epsilon_Y Y_{II} - \alpha Y_{GI}\\
&\quad + \beta_F Y_{GS}\frac{I}{N} + \beta_E Y_{GS} D - \gamma Y_{GI} + \kappa Y_{GC} - mY_{GI} - d_Y Y_{GI} - b_C Y_{GI},\\
\frac{dY_{SC}}{dt} &= mP_{SC} - cY_{SC} - \beta_{DY} Y_{SC}\frac{G}{N} - \omega\beta_{FY} Y_{SC} F\\
&\quad + \gamma(1-\rho) Y_{SI} - \kappa Y_{SC} - mY_{SC} - d_Y Y_{SC} - b_C Y_{SC},\\
\frac{dY_{IC}}{dt} &= mP_{IC} - cY_{IC} + \beta_{DY} Y_{SC}\frac{G}{N} + \omega\beta_{FY} Y_{SC} F - \epsilon_Y Y_{IC}\\
&\quad + \gamma(1-\rho) Y_{II} - \kappa Y_{IC} - mY_{IC} - d_Y Y_{IC} - b_C Y_{IC},\\
\frac{dY_{GC}}{dt} &= mP_{GC} - cY_{GC} + \epsilon_Y Y_{IC} - \alpha Y_{GC}\\
&\quad + \gamma(1-\rho) Y_{GI} - \kappa Y_{GC} - mY_{GC} - d_Y Y_{GC} - b_C Y_{GC}.
\end{aligned}
\tag{B.1}
$$

Adults:

$$
\begin{aligned}
\frac{dA_{SS}}{dt} &= mY_{SS} - cA_{SS} - \beta_{DA} A_{SS}\frac{G}{N} - \omega\beta_{FA} A_{SS} F\\
&\quad - \beta_F A_{SS}\frac{I}{N} - \beta_E A_{SS} D - d_A A_{SS} - b_C A_{SS},\\
\frac{dA_{IS}}{dt} &= mY_{IS} - cA_{IS} + \beta_{DA} A_{SS}\frac{G}{N} + \omega\beta_{FA} A_{SS} F - \epsilon_A A_{IS}\\
&\quad - \beta_F A_{IS}\frac{I}{N} - \beta_E A_{IS} D - d_A A_{IS} - b_C A_{IS},\\
\frac{dA_{GS}}{dt} &= mY_{GS} - cA_{GS} + \epsilon_A A_{IS} - \alpha A_{GS}\\
&\quad - \beta_F A_{GS}\frac{I}{N} - \beta_E A_{GS} D - d_A A_{GS} - b_C A_{GS},\\
\frac{dA_{SI}}{dt} &= mY_{SI} - cA_{SI} - \beta_{DA} A_{SI}\frac{G}{N} - \omega\beta_{FA} A_{SI} F\\
&\quad + \beta_F A_{SS}\frac{I}{N} + \beta_E A_{SS} D - \gamma A_{SI} + \kappa A_{SC} - d_A A_{SI} - b_C A_{SI},\\
\frac{dA_{II}}{dt} &= mY_{II} - cA_{II} + \beta_{DA} A_{SI}\frac{G}{N} + \omega\beta_{FA} A_{SI} F - \epsilon_A A_{II}\\
&\quad + \beta_F A_{IS}\frac{I}{N} + \beta_E A_{IS} D - \gamma A_{II} + \kappa A_{IC} - d_A A_{II} - b_C A_{II},
\end{aligned}
\tag{B.2}
$$

$$\begin{aligned}
\frac{dA_{GI}}{dt} &= mY_{GI} - cA_{GI} + \epsilon_A A_{II} - \alpha A_{GI} \\
&\quad + \beta_F A_{GS}\frac{I}{N} + \beta_E A_{GS} D - \gamma A_{GI} + \kappa A_{GC} - d_A A_{GI} - b_C A_{GI}, \\
\frac{dA_{SC}}{dt} &= mY_{SC} - cA_{SC} - \beta_{DA} A_{SC}\frac{G}{N} - \omega\beta_{FA} A_{SC} F \\
&\quad + \gamma(1-\rho)A_{SI} - \kappa A_{SC} - d_A A_{SC} - b_C A_{SC}, \\
\frac{dA_{IC}}{dt} &= mY_{IC} - cA_{IC} + \beta_{DA} A_{SC}\frac{G}{N} + \omega\beta_{FA} A_{SC} F - \epsilon_A A_{IC} \\
&\quad + \gamma(1-\rho)A_{II} - \kappa A_{IC} - d_A A_{IC} - b_C A_{IC}, \\
\frac{dA_{GC}}{dt} &= mY_{GC} - cA_{GC} + \epsilon_A A_{IC} - \alpha A_{GC} \\
&\quad + \gamma(1-\rho)A_{GI} - \kappa A_{GC} - d_A A_{GC} - b_C A_{GC}.
\end{aligned}$$

Carcass and Free-Living:

$$\begin{aligned}
\frac{dD}{dt} &= d_P(P_{SI} + P_{II} + P_{GI}) + d_Y(Y_{SI} + Y_{II} + Y_{GI}) \\
&\quad + d_A(A_{SI} + A_{II} + A_{GI}) + \gamma\rho(I) - \mu_C D - rD, \qquad \text{(B.3)} \\
\frac{dF}{dt} &= \lambda G - \mu_F F. \qquad \text{(B.4)}
\end{aligned}$$

Other Variables:

$$\begin{aligned}
P_T &= P_{SS} + P_{IS} + P_{GS} + P_{SI} \qquad \text{(Total Piglet Density)} \qquad \text{(B.5)} \\
&\quad + P_{II} + P_{GI} + P_{SC} + P_{IC} + P_{GC}, \\
Y_T &= Y_{SS} + Y_{IS} + Y_{GS} + Y_{SI} \qquad \text{(Total Yearling Density)} \qquad \text{(B.6)} \\
&\quad + Y_{II} + Y_{GI} + Y_{SC} + Y_{IC} + Y_{GC}, \\
A_T &= A_{SS} + A_{IS} + A_{GS} + A_{SI} \qquad \text{(Total Adult Density)} \qquad \text{(B.7)} \\
&\quad + A_{II} + A_{GI} + A_{SC} + A_{IC} + A_{GC}, \\
N &= P_T + Y_T + A_T, \qquad \text{(Total Density)} \qquad \text{(B.8)} \\
I &= P_{SI} + P_{II} + P_{GI} + Y_{SI} \qquad \text{(Total ASF Infected Density)} \qquad \text{(B.9)} \\
&\quad + Y_{II} + Y_{GI} + A_{SI} + A_{II} + A_{GI}, \\
I_{TB} &= P_{IS} + P_{II} + P_{IC} + Y_{IS} \qquad \text{(Total TB Infected Density)} \qquad \text{(B.10)} \\
&\quad + Y_{II} + Y_{IC} + A_{IS} + A_{II} + A_{IC},
\end{aligned}$$

$$G = P_{GS} + P_{GI} + P_{GC} + Y_{GS} \qquad \text{(Total TB Generalised Density)} \qquad \text{(B.11)}$$
$$+ Y_{GI} + Y_{GC} + A_{GS} + A_{GI} + A_{GC}.$$

Here, P_T, Y_T and A_T represent the total piglet, yearling and adult density respectively, and are given in Equations (B.5-B.7). The total density of wild boar is given by $N = P_T + Y_T + A_T$, the total number of ASF infected individuals by I (Equation B.9), the total number of TB infected individuals by I_{TB} (Equation B.10) and the total number of TB generalised individuals by G (Equation B.11).

B.1.2 TB parameter values

Parameter values for wild boar demographics and TB transmission are taken from Tanner et al. [66] with adjustments to represent the different scenarios in TB prevalence used in our study (see Table B.1). For the scenario representative of lower TB prevalence, the wild boar density is assumed to be $4km^{-2}$ with a prevalence of 10% and in the scenario representative of higher TB prevalence the density is assumed to be $12km^{-2}$ with a prevalence of 60%. We therefore adjusted the birth rate, carrying capacity and transmission coefficients seen in Tanner et al. [66] as necessary.

B.1.3 ASF parameter values

To obtain parameter values for the ASF infection terms we followed the methodology outlined in O'Neill et al. [18]. In particular, we assumed the absence of TB, that $b = \ln 4, K = 2$ and $d = 52/8$ (which are representative of the parameters in Estonia that are considered in O'Neill et al. [18]) with other parameters as in Section B.1.2. We then explored the parameter space for values of β_F, β_E and ρ that satisfied the epidemiological criteria for ASF described in O'Neill et al. [18]. Namely that there was an $85 - 95\%$ drop in total population density after an ASF epidemic, a peak in the number of ASF infected individuals approximately 6 months after the virus is initially discovered and the persistence of ASF at low prevalence several years after the initial epidemic. The parameters used in this study are as detailed in Table B.2.

Table B.1: TB model parameter values

$b = \log 4$ or $\log 7$	Reproduction rate of yearlings and adults. In low tuberculosis prevalent regions this is set to $\log 4$ and in high prevalent regions it is set to $\log 7$.
$d = \frac{1}{7}$	Natural death rate of piglets, yearlings and adults.
$m = 1$	Average rate of maturity from piglet to yearling and from yearling to adult.
$K = 5.95$ or 27	The carrying capacity, defined as the total population density in the absence of disease and culling. In lower prevalence regions this is set to 5.95, whilst in high prevalence regions this is set to 27.
$q = \frac{1}{K}\left(1 - \frac{d(d+m)}{mb}\right)$	Susceptibility to crowding term limiting the total population to the carrying capacity K in the disease-free steady state and is derived from steady-state analysis of the model without infection or culling.
$c = 0.3$	Culling rate of the yearling and adult populations.
$\beta_{DA} = 1.12$	TB transmission rate for adults from direct contact with generalised individuals.
$\beta_{DP} = \beta_{DY} = c_\beta \beta_{DA}$	TB transmission rate for piglets and yearlings from contact with generalised individuals. The disease transmission for piglets and yearlings is assumed three times higher than that of adults ($c_\beta = 3$).
$\beta_{FA} = \frac{13}{54}$	TB transmission rate for adults from contact with free-living TB particles.
$\beta_{FP} = \beta_{FY} = c_\beta \beta_{FA}$	TB transmission rate for piglets and yearlings from contact with free-living TB particles. The disease transmission for piglets and yearlings is assumed three times higher than that of adults ($c_\beta = 3$).
$\omega = 0.1$ or 1	Scaling for the level of environmental TB transmission in regions of low TB prevalence $\omega = 0.1$ or regions of high TB prevalence $\omega = 1$.
$\epsilon_A = \frac{2}{3}$	Rate that infected adults become generalised.
$\epsilon_P = \epsilon_Y = c_\epsilon \epsilon_A$	Rate that infected piglets and infected yearlings become generalised. In low prevalence regions this rate is assumed equal to that of adults ($c_\epsilon = 1$) and in high prevalence regions this assumed three times higher than that of adults ($c_\epsilon = 3$).
$\alpha = 1$	Mortality rate of generalised individuals from TB infected. Mortality due to generalised TB is assumed to take on average one year.
$\lambda = 1$	Rate at which generalised individuals shed the virus into the environment.
$\mu_F = 6$	Decay rate of the free-living TB particles found within the environment. The average lifespan of a TB particle is assumed to be 2 months.

Table B.2: ASF model parameter values

$\beta_F = 56$	African swine fever transmission coefficient from contact with ASF infected individuals. All age classes have equal rate of transmission from the susceptible class of infection to the infected class.
$\beta_E = 2.9$	African swine fever transmission coefficient from contact with ASF infected carcasses. All age classes have equal rate of transmission from the susceptible class of infection to the infected class.
$\gamma = 365/5$	Mortality rate of ASF infected individuals. Mortality due to ASF is assumed to take on average five days.
$\rho = 0.85$	The proportion of the ASF mortality cases which die from the disease. The proportion $1 - \rho = 0.15$ of infected individuals enter the survivor class, where they can no longer transmit the disease but can revert to an infected state.
$\kappa = 2$	The rate that the survivor individuals revert to an infected state. This is assumed to take an average of 6 months [Gallardo et al., 2015].
$\mu_C = 52/1$ or $52/4$	The natural carcass degradation rate. This is assumed to take the value $\mu_C = 52/1$ for regions representative of high carcass degradation, such as areas with abundant obligate scavengers, or the value $\mu_C = 52/4$ for regions representative of low carcass degradation, such as woodland regions.
$b_C = 0.2$ or 0.7	The culling rate used under different control measures. For the scenario focused on carcass removal the culling rate takes the value $b_C = 0.2$, with $b_C = 0.7$ used under a culling focused control measure.
$r = 200$ or 26	The removal rate of carcasses under different control measures. For the scenario focused on carcass removal the removal rate takes the value $r = 200$, with $r = 26$ used under a culling focused control measure.

B.1.4 ASF control measures

In the model we include wild boar depopulation by assuming culling is applied at rate b_C, across all age and infection classes (see Equations 3.2-B.2). The culling rate, b_C, corresponds to a culling proportion equal to $1 - e^{-b_C}$, per year. The removal of ASF infected carcasses is modelled as an additional loss term in the infected carcass class, D, with removal rate, r (see Equation B.3). The value r corresponds to an average time till the removal of a carcass of $1/r$ years. Parameter values for these are provided in Table B.2. For scenarios where control measures are not implemented both rates are set to zero.

B.2 Results when control measures are applied to other model scenarios

Figure B.1 explores the impact of a carcass removal focused control measure (a high carcass removal rate, $r = 200$ and low culling rate $b_C = 0.2$) on scenarios representative of a high TB prevalence, high carcass degradation region, a low TB prevalence, high carcass degradation region and a low TB prevalence, low carcass degradation region.

Figure B.2 explores the impact of a culling-based control measure (a low carcass removal rate, $r = 26$ and high culling rate $b_C = 0.7$) on scenarios representative of a high TB prevalence, high carcass degradation region and a low TB prevalence, high carcass degradation region.

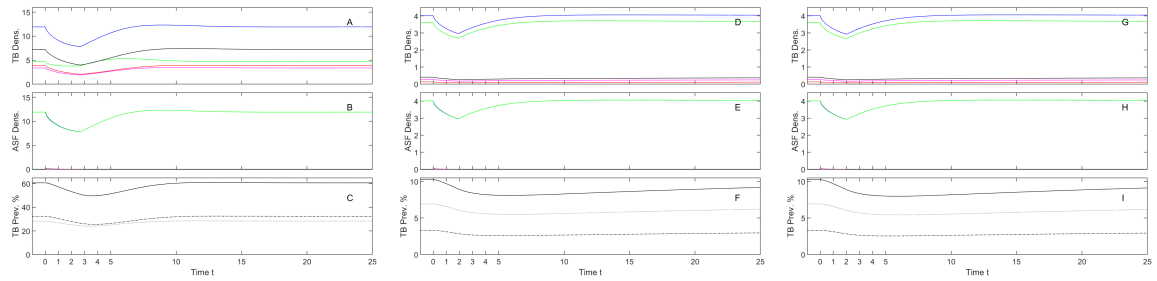

Figure B.1: Population densities and prevalence for the model described by the Equations (3.2-B.4) for the following scenarios under specific ASF control measures: (A-C) a high carcass degradation rate and a high TB prevalence, (D-F) a high carcass degradation rate and a low TB prevalence and (G-I) a low carcass degradation rate and a low TB prevalence. Results are shown over a 25-year period. (A,D&G) show total host density (blue), hosts susceptible to TB (green), hosts infected with TB (magenta), hosts with generalised TB infection (red) and the combined infected and generalised hosts (black). (B,E&H) show the total host density (blue), hosts susceptible to ASF (green), hosts infected with TB (magenta), ASF survivor density (red) and the infected carcass density (black). (C,F&I) show TB prevalence with infected prevalence, I_{TB}/N, (dotted); generalised prevalence, G/N, (dot-dash) and total prevalence, $(I_{TB}+G)/N$, (solid). For (A-C) parameters are as in Figure 3.2, for (D-F) parameters are as in Figure 3.4 and for (G-I) parameters are as in Figure 3.5. For all plots, the culling parameter $b_C = 0.2$ and carcass removal rate $r = 200$ are used.

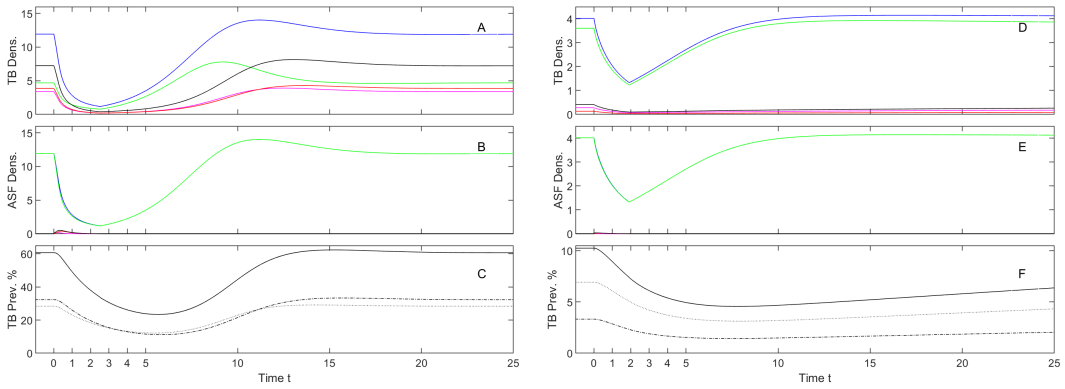

Figure B.2: Population densities and prevalence for the model described by the Equations (3.2-B.4), for the scenarios with high carcass degradation rate and either a high tuberculosis prevalence (A-C) or a low tuberculosis prevalence (D-F), under specific ASF control measures. Results are shown over a 25-year period. (A&D) show total host density (blue), hosts susceptible to TB (green), hosts infected with TB (magenta), hosts with generalised TB infection (red) and the combined infected and generalised hosts (black). (B&E) show the total host density (blue), hosts susceptible to ASF (green), hosts infected with TB (magenta), ASF survivor density (red) and the infected carcass density (black). (C&F) show TB prevalence with infected prevalence, I_{TB}/N, (dotted); generalised prevalence, G/N, (dot-dash) and total prevalence, $(I_{TB}+G)/N$, (solid). For A-C parameters are as in Figure 3.2 and for D-F parameters are as in Figure 3.4. For all plots, the culling parameter $b_C = 0.7$ and carcass removal rate $r = 26$ are used.

Chapter 4

The influence of latent and chronic infection on pathogen persistence

The work in this chapter has been published in:

O'Neill, X., White, A., Clancy, D., Ruiz-Fons, F. and Gortázar, C., 2021. The Influence of Latent and Chronic Infection on Pathogen Persistence. *Mathematics*, 9(9), p.1007. https://doi.org/10.3390/math9091007

Here we present the published version and its accompanied supplementary information.

Abstract

We extend the classical compartmental frameworks for susceptible-infected-susceptible (SIS) and susceptible-infected-recovered (SIR) systems to include an exposed/latent class or a chronic class of infection. Using a suite of stochastic continuous-time Markov chain models we examine the impact of latent and chronic infection on the mean time to extinction of the infection. Our findings indicate that the mean time to pathogen extinction is increased for infectious diseases which cause exposed/latent infection prior to full infection and that the extinction time is increased further if these exposed individuals are also capable of transmitting the infection. A chronic infection stage can decrease or increase the mean time to pathogen extinction and in particular this depends on whether chronically infected individuals incur disease-induced mortality and whether they are able to transmit the infection. We relate our findings to specific infectious diseases that exhibit latent and chronic infectious stages and argue that infectious diseases with these characteristics may be more difficult to manage and control.

4.1 Introduction

Mathematical models of infectious disease are key tools for understanding the epidemiological dynamics and persistence of infections in humans and animals [153, 93]. Model systems have been used to determine the expected persistence time of infection [154, 155, 156], and thereby provide insight into ways of reducing the impact and spread of pathogens and inform policy for infectious disease management [157, 8].

Following an outbreak, an infection may fade-out due to random fluctuations in the number of infected individuals. This can lead to epidemic fade-out where, after a major outbreak, the population is depleted to a level where the number of infected individuals is low and pathogen extinction (zero sources of infection) occurs due to stochasticity, or endemic fade-out where pathogen extinction occurs due to stochasticity from a relatively stable endemic state [153, 155]. Analysis of endemic fade-out focuses on the expected time to pathogen extinction, τ, beginning from the quasi-stationary distribution of the number of susceptible and infectious individuals. The expected pathogen extinction time increases as the population size increases whilst also depending on the relative timescales of infection and demographic processes [155, 158]. The analysis of an epidemic fade-out is more complicated and arises when population numbers drop to low levels following an epidemic outbreak which can temporarily limit transmission. Persistence through the outbreak depends on the replenishment of susceptible individuals and the tail of infecteds following the outbreak [155, 158].

The mean time to pathogen extinction has been calculated for SIS (susceptible-infected-susceptible) and SIR (susceptible-infected-recovered) model frameworks that assume density-dependent transmission and a constant population size (and therefore omit the impact of disease-induced mortality on regulating host density). For an SIS framework, where the basic reproductive number of the infection (also defined as the number of secondary cases when a single infected individual is introduced into a disease-free population) , $\mathcal{R}_0$, is assumed to be greater than unity, the mean time to pathogen extinction is given by $\tau \sim \frac{C}{\sqrt{N}} e^{AN}$, where the coefficients A and C depend on model parameters but are independent of the total population, N, [159, 160]. The expression also holds

for SIR model frameworks but with A computed numerically and indicates that recovery from infection to immunity reduces the persistence time of infection compared to SIS dynamics where recovery replenishes the susceptible pool [161, 162]. These model studies emphasize the importance of the infection processes in determining the persistence of a pathogen.

The infectious disease dynamics for many real-world systems are more complex than the SIS and SIR frameworks. For example, immunity to infection may be temporary [162], the infection may have a significant latent period in which an individual has been exposed to the pathogen but is asymptomatic and non-infectious [163] (such as with rabies [164]), asymptomatic individuals may be infectious (as with Epstein Barr virus infections [165] and COVID-19 coronavirus disease [166]) and following infection there may be a prolonged chronic stage of disease in which individuals can still transmit the infection or can revert to the infectious state (as has been suggested for African swine fever [18, 40]). Of particular relevance is the inclusion of disease-induced mortality as it may lead to a large drop in population size following an infectious outbreak and this has an impact on pathogen persistence [167]. Since disease-induced mortality leads to a non-constant population size it is also important to consider different forms of transmission, where, for example, density-dependent transmission can promote an initial infectious outbreak and frequency-dependent transmission can aid persistence of infection at low population levels [168].

In this study we develop and assess a range of infectious disease model frameworks to explore and understand how the inclusion of more complex epidemiological processes will affect the persistence of infection. In all model frameworks we include disease-induced mortality and a combination of density-dependent and frequency-dependent transmission. We extend classical infectious disease frameworks without immunity (susceptible-infected-susceptible, SIS) and with immunity (susceptible-infected-recovered/immune, SIR) to include an exposed/latent class, E and a chronically infected class, C. For this mathematical study we define E as the stage prior to full infection, I. In this exposed class, E, individuals do not incur disease-induced mortality (which individuals in the

infected class do incur) but may transmit the infection. The exposed class therefore approximates asymptomatic or presymptomatic individuals that may or may not be infectious. We examine the impact of the exposed class on pathogen persistence by comparing systems without immunity, SIS and $SEIS$, and those with immunity SIR and $SEIR$. In a similar manner we define the chronically infected class, C, as the stage that follows full infection, I. Individuals in this class may suffer disease-induced mortality and may be able to transmit the infection but at a reduced rate compared to the infected class. We examine the impact of the chronically infected class on pathogen persistence by comparing systems without immunity, SIS and $SICS$, and those with immunity, SIR and $SICR$. We estimate the persistence time of the infection numerically using a suite of stochastic continuous-time Markov chain models [169, 88] and our aim is to understand the importance of exposed/latent and chronic infection on pathogen persistence. While the definitions of exposed/latent and chronic infection we employ are common in the theoretical literature [153, 93, 8, 18] we acknowledge that their definitions may not match the precise characteristics of a specific infectious disease. Notwithstanding, our model framework allows the effect of exposed/latent and chronic infection on the mean time to extinction of an infection to be isolated and allows us to infer and discuss the impact of these processes on the persistence and management of specific infectious diseases.

4.2 Methods

We will first outline the model frameworks in the absence of immunity. For the SIS framework we describe the deterministic model framework and then the corresponding stochastic (continuous-time Markov chain) model [88, 89]. The deterministic SIS model is based on classical, compartmental infectious disease modelling frameworks [103, 93] and is represented by the following system of equations:

$$\begin{aligned}\frac{dS}{dt} &= bN(1-qN) - \beta_F S\frac{I}{N} - \beta_D SI + \gamma I - dS,\\ \frac{dI}{dt} &= \beta_F S\frac{I}{N} + \beta_D SI - (\alpha+\gamma+d)I.\end{aligned} \tag{4.1}$$

Here, S represents the susceptible population density, I the infected density and $N = S+I$ the total population density. The maximum birth rate is given by b, which is modified due to intra-specific competition through the parameter, $q = (b-d)/bK$, where K denotes the carrying capacity of the population. The natural death rate is given by d. For the infection dynamics we denote β_F to be the frequency-dependent transmission rate, β_D the density-dependent transmission coefficient, γ the recovery rate and α the disease-induced mortality incurred by infected individuals. The equivalent stochastic model is a continuous-time Markov chain [88, 89], with transition rates given in Table 4.1.

In the stochastic model of the SIS framework the susceptible class, S, and infected class, I, are integer values that represent the population number. Individual simulations can be undertaken using a Gillespie algorithm [169, 170] that describes the dynamics for a single realisation. We run 100 realisations of the stochastic model and determine the mean time to extinction of the infection, τ, (pathogen extinction occurs when no sources of infection remain in the population) and the 95% confidence interval for the mean for each distinct model framework and set of parameters. We only consider simulations in which an initial infectious outbreak occurs, which we define as a drop in the susceptible population number below 90% of the pre-infection population size prior to pathogen extinction. For all simulations we choose a carrying capacity (the population level in the absence of infection) of $K = 1000$ and use the initial conditions: $(S_0, I_0) = (995, 5)$.

Table 4.1: Possible events and their respective state transitions and transition rates for the stochastic representation of an SIS model framework. Model parameters are defined in the main text. Note, the transition rate for the birth of a susceptible is set to zero if $qN > 1$.

	State Transition	Transition Rate
Birth of susceptible	$S \to S+1$	$bN(1-qN)$
Natural death of susceptible	$S \to S-1$	dS
Infection	$S \to S-1, I \to I+1$	$\beta_F S\frac{I}{N} + \beta_D SI$
Recovery of infected	$S \to S+1, I \to I-1$	γI
Death of infected	$I \to I-1$	$(\alpha+d)I$

We choose a baseline set of parameters as defined in Table 4.2. These are chosen such that the basic reproductive number of the infection, $\mathcal{R}_0$, is greater than unity and so pathogen persistence will depend on epidemic or endemic fade-out. The $\mathcal{R}_0$ for the SIS framework and the other model frameworks considered in this study can be found in Supplementary Information (Equations C.4-C.6). We compare results for a low, medium and high level of disease-induced mortality (see Table 4.2) and undertake a sensitivity analysis on other key parameters to understand their impact on pathogen persistence. The SIS model is then extended to an $SEIS$ or $SICS$ framework with the inclusion of an exposed/latent class, E, (referred to as the exposed class for the remainder of the methods and results section) or a chronic class, C, respectively. The deterministic versions of these model frameworks are shown in Equations (4.2-4.3).

In the $SEIS$ model (Equations 4.2) susceptible individuals progress to the exposed class, E, following transmission and subsequently progress from the exposed class to the infected class at rate κ. An exposed individual does not incur disease-induced

Table 4.2: Baseline parameter values and their biological meaning.

$b = 10$	Maximum birth rate of the population.
$d = 1$	Natural death rate of the population.
$K = 1000$	Population carrying capacity in the absence of infection.
$\beta_F = 30$	Frequency-dependent transmission rate.
$\beta_D = 0.15$	Density-dependent transmission coefficient.
$\gamma = 50$	Recovery rate of infected individuals.
$\alpha = [10, 40, 80]$	Disease-induced mortality rate, with $\alpha = 10, 40, 80$ representing a low, medium and high rate respectively.
$\kappa = 80$	Rate of progression from an exposed or chronically infected state.
Exposed/latent	
$\epsilon = 0$	Proportional pathogen transmission for the exposed/latent class.
Chronic	
$\epsilon = 0, \quad c = 0.5$ $\epsilon = 0.5, \quad c = 0$	For models that include chronic infection we consider two baseline cases for the proportional transmission from chronically infected individuals, ϵ, and the proportion of disease-induced mortality incurred by chronic individuals, c.

mortality but could be infectious and transmit the pathogen at a proportion ϵ of that of an infected, I, individual. Our default (Table 4.2) is to assume $\epsilon = 0$ and we consider $0 < \epsilon < 1$ as part of a parameter sensitivity analysis. Following infection an individual progresses back to the susceptible class at rate γ. All other parameters are as described for the SIS model. The deterministic $SEIS$ model is as follows:

$$\begin{aligned}
\frac{dS}{dt} &= bN(1-qN) - \beta_F S\frac{I+\epsilon E}{N} - \beta_D S(I+\epsilon E) + \gamma I - dS,\\
\frac{dE}{dt} &= \beta_F S\frac{I+\epsilon E}{N} + \beta_D S(I+\epsilon E) - (\kappa + d)E,\\
\frac{dI}{dt} &= \kappa E - (\alpha + \gamma + d)I.
\end{aligned} \tag{4.2}$$

In the $SICS$ model (Equations 4.3) susceptible individuals progress to the infected class, I, following transmission and then progress to the chronically infected class, C, at rate γ. A chronically infected individual can progress back to the susceptible class at rate κ and may incur disease-induced mortality at a proportion, c, of that of an infected individual. In a similar manner to the $SEIS$ model above we assume that a chronically infected individual may also be infectious (at a proportion ϵ of that of an infected individual). We consider two baseline cases, one where chronically infected individuals incur disease-induced mortality but cannot transmit the infection and one where they do not incur disease-induced mortality but can transmit the infection. All other parameters are described for the SIS model. The deterministic $SICS$ model is as follows:

$$\begin{aligned}
\frac{dS}{dt} &= bN(1-qN) - \beta_F S\frac{I+\epsilon C}{N} - \beta_D S(I+\epsilon C) + \kappa C - dS,\\
\frac{dI}{dt} &= \beta_F S\frac{I+\epsilon C}{N} + \beta_D S(I+\epsilon C) - (\alpha + \gamma + d)I,\\
\frac{dC}{dt} &= \gamma I - (\kappa + d + c\alpha)C.
\end{aligned} \tag{4.3}$$

For both the $SEIS$ and $SICS$ model the exposed and chronically infected population are not infectious when $\epsilon = 0$. Note, in the limit of $\kappa \to \infty$ both models converge back to the original SIS model. The proportional level of pathogen transmission, ϵ,

of exposed and chronic individuals, the rate of progression, κ, from the exposed and chronic class and the proportional level of disease-induced mortality incurred by the chronic class, c, will be varied to understand their effect on the persistence of infection.

We adapt the methods described above to include immunity by considering SIR, $SEIR$ and $SICR$ model frameworks. In these frameworks' individuals enter a recovered and immune class R following recovery from the infected class, I, or chronically infected class, C, as appropriate. These model frameworks are detailed in full in the Supplementary Information (Equations C.1-C.3).

4.3 Results

Model simulations showing the population dynamics for the deterministic SIS model and for 100 realisations of the stochastic SIS model, for baseline parameters and low, medium and high values of disease-induced mortality are shown in Figure 4.1. Numerical solutions of the deterministic model were produced using Matlab R2019a, ode15s. For the stochastic models considered in this manuscript we developed our own code with model simulations also undertaken in Matlab R2019a. In the deterministic model the infection persists for all scenarios with a decrease in infected density as the disease-

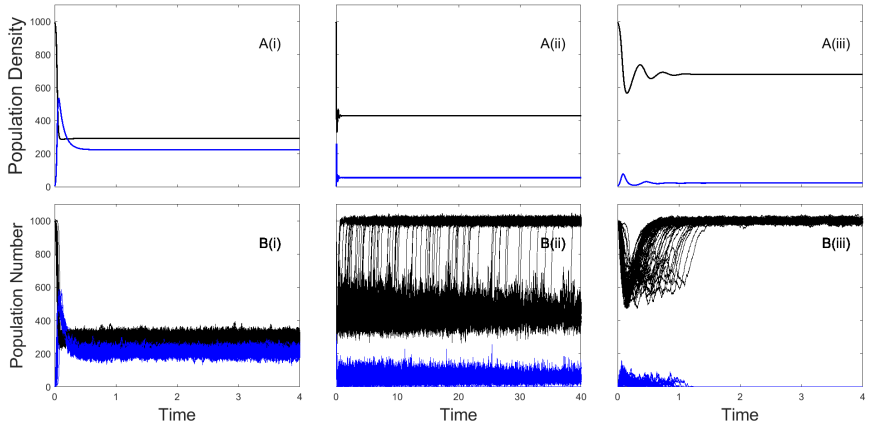

Figure 4.1: Population densities for the deterministic (Equation 4.1) SIS model framework (A) and population numbers for the stochastic (Table 4.1) SIS model framework (B) with susceptible densities/numbers (black) and infected densities/numbers (blue). For the stochastic model the results of 100 individual realisations are shown. Results are shown for three values of the disease-induced mortality rate (i) $\alpha = 10$, (ii) $\alpha = 40$ and (iii) $\alpha = 80$, representing a low, medium and high mortality rate respectively. Baseline parameter values (see Section 4.2) were used for other parameters.

induced mortality increases. For the stochastic version of the model the infection persists (for the timescale tested) in all model realisations at low levels of disease-induced mortality (Figure 4.1B(i)). At medium levels of disease-induced mortality the stochastic model typically exhibits endemic fade-out with the population settling to endemic levels prior to infection fade-out and a return to disease-free population levels (Figure 4.1B(ii)). At high levels of disease-induced mortality the stochastic model typically exhibits epidemic fade-out where the population crash and rapid turnover of infected individuals reduces the force of infection to levels that cannot support the infection (Figure 4.1B(iii)). This highlights the different possible outcomes of deterministic and stochastic frameworks and the need to consider stochastic models to determine the extinction time of infections.

4.3.1 The impact of exposed/latent infection on the mean time to pathogen extinction

Figures 4.2-4.4 explore the impact of exposed/latent infection on pathogen persistence by comparing the SIS and $SEIS$ and the SIR and $SEIR$ model frameworks. A key result is that the inclusion of an exposed class leads to a pronounced increase in the mean time to pathogen extinction. Here, exposed individuals promote pathogen persistence since they delay progression to the infected class, which in itself extends the mean time to extinction of the infection, but also reduces the severity of the population crash in the initial outbreak and thereby reduces the chance of epidemic fade-out. It is also clear that the mean time to pathogen extinction is lower in models that include recovery to immunity.

To validate the simulation method that we employ to calculate the mean time to extinction of the infection, τ, we compare our results for the SIS system with those that use continuous-time Markov chain theory on a finite set of states [171]. Details of this comparison are shown in the Supplementary Information (Section C.2) and indicate that our method of determining τ from simulations is a close fit with the Markov chain theory for the SIS framework. Note, the Markov chain theory method becomes too computationally intensive for higher dimensional models.

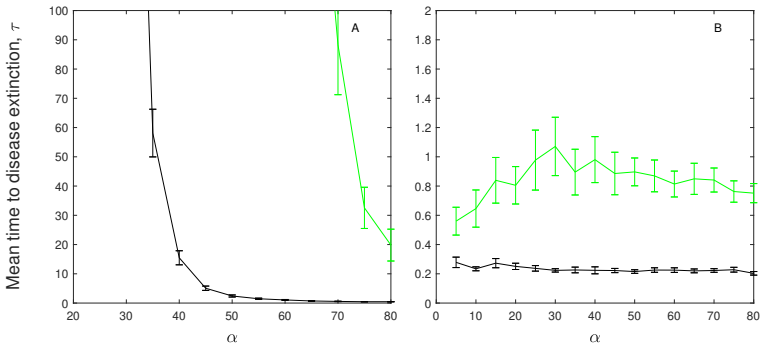

Figure 4.2: The mean time to pathogen extinction (with 95% confidence intervals) plotted against disease-induced mortality rate for (A) models without immunity: SIS (black) and $SEIS$ (green), and (B) models with immunity: SIR (black) and $SEIR$ (green). Also note the difference in vertical axis scale between A and B. When not changed in the figure baseline parameter values were used (see Table 4.2).

A parameter sensitivity analysis for the models indicates that in the absence of immunity the mean extinction time of the infection decreases as disease-induced mortality increases (Figure 4.2A). When immunity is included the mean time to extinction of the infection remains relatively constant (Figure 4.2B).

There is little change in the mean time to pathogen extinction for changes in the infection transmission terms in models without the exposed class (Figures 4.3A, B and 4.4A, B) and extinction is rapid. When an exposed class is included the mean extinction time of the infection increases as frequency-dependent and density-dependent transmission increases since this leads to an increase in exposed individuals which contribute to the persistence of the infection.

In the absence of immunity pathogen persistence is maximised at an intermediate level of the infected recovery rate, γ (Figure 4.3C). When the recovery rate is low, the time to pathogen extinction is short as there is a build-up of individuals in the infected class which increases the force of infection, leads to a large population crash and subsequent epidemic fade-out of the infection. At intermediate rates of recovery, the time spent in the infected class is reduced but is sufficient to support infection without causing a severe crash in the population, and so leads to an increase in the time to extinction of the pathogen. If the rate of recovery is increased further then the time spent in the

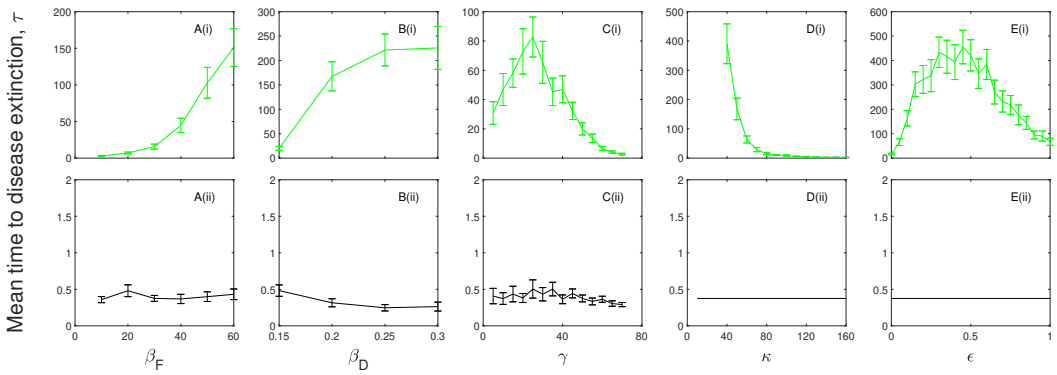

Figure 4.3: A parameter sensitivity analysis for (i) the $SEIS$ (green) and (ii) the SIS (black) model frameworks with $\alpha = 80$. The mean time to pathogen extinction (with 95% confidence intervals) is plotted against (A) the frequency-dependent transmission rate, β_F; (B) the density-dependent transmission coefficient, β_D; (C) the infected recovery rate, γ; (D) the exposed progression rate, κ; and (E) the exposed infectiousness, ϵ. When not changed in the figure baseline parameter values were used (see Table 4.2). Note, at low, $\alpha = 10$, and medium, $\alpha = 40$ levels of disease-induced mortality the mean extinction time of the infection for the $SEIS$ model exceeds our simulation time scale and so results are not shown. Results for the SIS model at $\alpha = 40$ are shown in Figures 4.5 and 4.6.

infected class is reduced to levels where infected numbers and consequently the force of infection is low leading to a reduced extinction time of the infection. When immunity is included the mean time to pathogen extinction decreases as the recovery rate increases (Figure 4.4C) since with no opportunity to progress back to a susceptible class pathogen persistence is prolonged by a low recovery rate, and thereby increased duration, in the infected class.

The mean time to extinction of the infection increases as the rate of progression from the exposed class decreases since exposed individuals do not incur additional mortality but do act as a source of future infected individuals. When the progression rate from the exposed class, κ, is high (and with $\epsilon = 0$) the length of time in the exposed class is short and the $SEIS$ and $SEIR$ models converge to SIS and SIR models respectively and therefore so do the mean extinction times (Figures 4.3D and 4.4D).

Increasing the proportional level of infectiousness of the exposed class, by increasing ϵ, increases the average time to pathogen extinction (compared to when $\epsilon = 0$)(Figures 4.3E and 4.4E) since here the exposed class provides an additional transmission route without the cost of disease-induced mortality. However, in the absence of immunity the mean extinction time of the infection is maximised at intermediate levels of ϵ (Figure

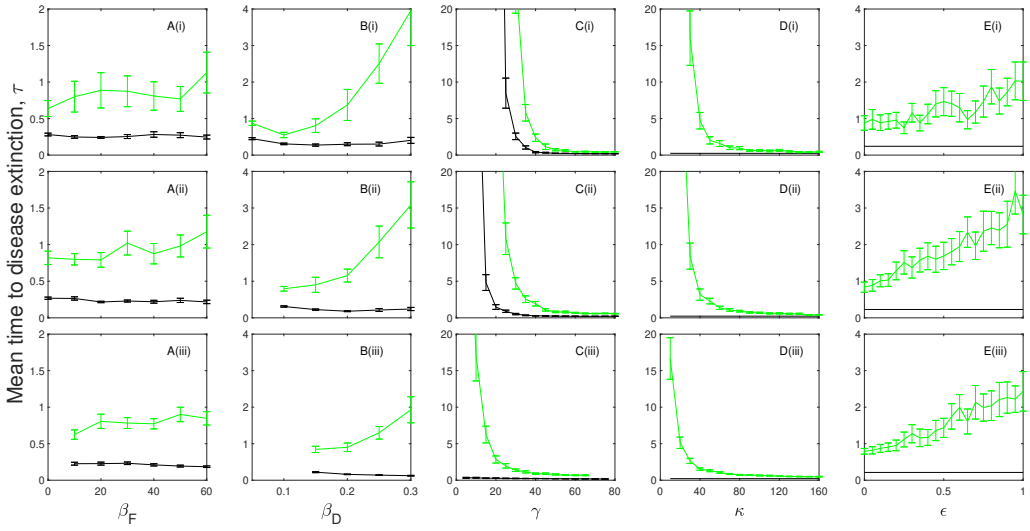

Figure 4.4: A parameter sensitivity analysis for the SIR (black) and $SEIR$ (green) model frameworks and where in (i) $\alpha = 10$, (ii) $\alpha = 40$ and (iii) $\alpha = 80$. The mean time to pathogen extinction (with 95% confidence intervals) is plotted against (A) the frequency-dependent transmission rate, β_F; (B) the density-dependent transmission coefficient, β_D; (C) the infected recovery rate, γ; (D) the exposed rate, κ; and (E) the exposed infectiousness, ϵ. When not changed in the figure baseline parameter values were used (see Table 4.2).

4.3E) as higher levels of transmission from exposed individuals increases the force of infection which reduces the pool of susceptible individuals.

4.3.2 The impact of chronic infection on the mean time to pathogen extinction

Figures 4.5-4.7 explore the impact of chronic infection on pathogen persistence by comparing the SIS and $SICS$ and the SIR and $SICR$ model frameworks. A key characteristic of chronic infection is that individuals may incur disease-induced mortality (albeit at a reduced rate compared to infected individuals) and/or may be able to transmit infection.

In the absence of immunity the mean time to pathogen extinction decreases as the proportional rate of disease-induced mortality of chronically infected individuals, c, increases (Figure 4.5A). A threshold exists for c below which the presence of a chronic class increases the mean time to extinction of the infection. When chronically infected individuals suffer high levels of disease-induced mortality they reduce the supply of susceptible individuals following recovery. When immunity is included rapid epidemic

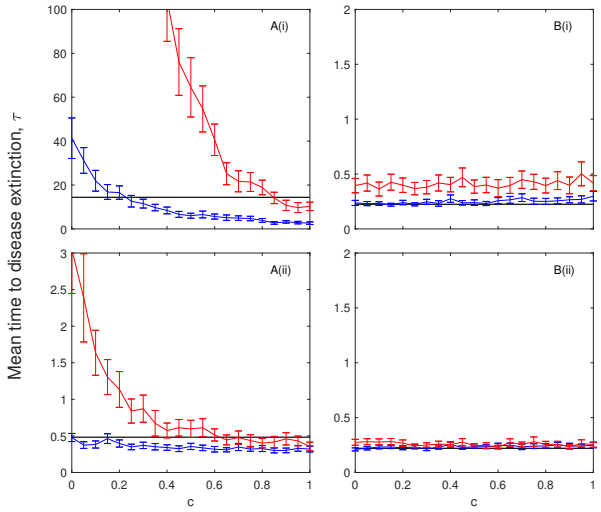

Figure 4.5: The mean time to pathogen extinction (with 95% confidence intervals) plotted against the proportion of disease-induced mortality incurred by chronically infected individuals compared to infected individuals. The results are shown for models with no immunity (A), with SIS (black), $SICS$ and $\epsilon = 0$ (blue) and $SICS$ and $\epsilon = 0.5$ (red) and for models with immunity (B), with SIR (black), $SICR$ and $\epsilon = 0$ (blue) and $SICR$ and $\epsilon = 0.5$ (red). In (i) $\alpha = 40$ and (ii) $\alpha = 80$. When not changed in the figure baseline parameter values were used (see Table 4.2). Note, at low levels of disease-induced mortality, $\alpha = 10$, the mean time to pathogen extinction for the models without immunity exceeds our simulation time scale and so results are not shown.

fade-out is seen and the mean time to extinction of the infection remains relatively constant to changes in the level of disease-induced mortality incurred by chronically infected individuals. A key result is that the characteristics of chronic infection are critical to whether the mean extinction time of the infection is increased or decreased.

We undertake a parameter sensitivity analysis for models that include a chronically infected class for the following two set-ups: (i) chronically infected individuals incur disease-induced mortality but do not transmit the infection (the blue line in Figures 4.5-4.7) and (ii) chronically infected individuals can transmit the infection but do not incur disease-induced mortality (the red line in Figures 4.5-4.7).

The mean time to extinction of the infection initially increases as frequency-dependent and density-dependent transmission increases (Figures 4.6A, B and 4.7A, B). However, further increases in transmission can reduce the mean time to pathogen extinction as the high rate of transmission leads to a more severe population crash and epidemic fade-out of the infection.

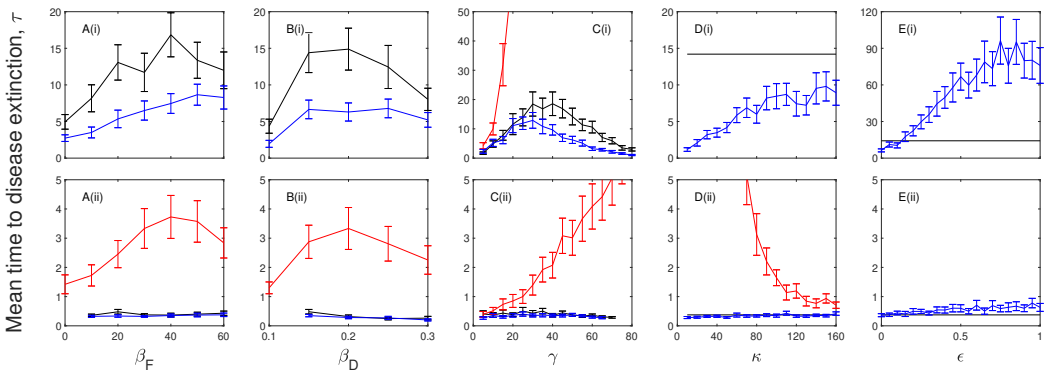

Figure 4.6: A parameter sensitivity analysis for the *SIS* (black) and *SICS* model frameworks with a chronically infected class that exhibits disease-induced mortality ($c = 0.5, \epsilon = 0$, blue) and a chronically infected class that can transmit the infection ($c = 0, \epsilon = 0.5$, red) for (i) $\alpha = 40$ and (ii) $\alpha = 80$. The mean time to pathogen extinction (with 95% confidence intervals) is plotted against (A) the frequency-dependent transmission rate, β_F; (B) the density-dependent transmission coefficient, β_D; (C) the infected recovery rate, γ; (D) the chronically infected progression rate, κ; and (E) the chronically infected infectiousness, ϵ. When not changed in the figure baseline parameter values were used (see Table 4.2). Note, at low levels of disease-induced mortality, $\alpha = 10$, the mean time to pathogen extinction exceeds our simulation time scale and so results are not shown. Red lines are not shown in figure A(i), B(i), and D(i) as here τ exceeds our simulation time scale. Red lines are not shown in E(i) and E(ii) as this scenario assumes chronic individuals are infectious.

In the absence of immunity the mean time to extinction of the infection is maximised at intermediate levels of recovery when chronic infection incurs disease-induced mortality (Figure 4.6C) in a similar manner to that described for models that include exposed infection. When chronically infected individuals transmit the infection but do not incur additional mortality an increase in the recovery rate (from the infected to chronic class) increases the mean extinction time of the infection. When immunity is included the mean time to extinction of the infection decreases as the recovery rate increases in the same way as models with exposed infection (Figure 4.7C).

In the absence of immunity and where chronically infected individuals do not transmit the infection an increase in the progression rate from the chronic class (to the susceptible class) increases the mean time to pathogen extinction (Figure 4.6D) since a more rapid transition from the chronic class (which incurs additional mortality) provides a source of susceptible individuals. In the case where chronically infected individuals can transmit the infection (but do not incur disease-induced mortality) pathogen persistence is promoted by remaining in the chronic class (Figure 4.6D). Both scenarios tend towards the *SIS* model framework as the progression rate increases. In models

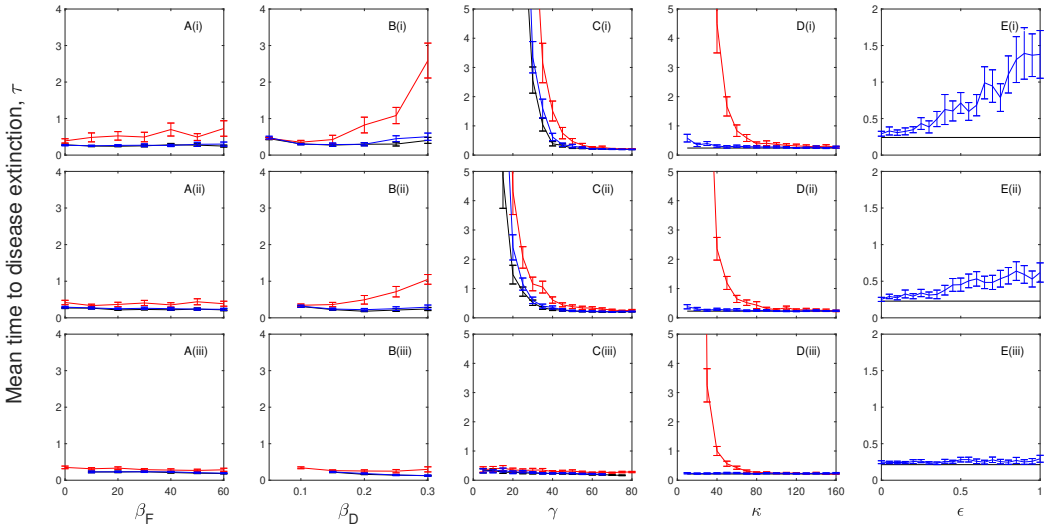

Figure 4.7: A parameter sensitivity analysis for the SIR (black) and $SICR$ model frameworks with a chronically infected class that exhibits disease-induced mortality ($c = 0.5, \epsilon = 0$, blue) and a chronically infected class that can transmit the infection ($c = 0, \epsilon = 0.5$, red) for (i) $\alpha = 10$, (ii) $\alpha = 40$ and (iii) $\alpha = 80$. The mean time to pathogen extinction (with 95% confidence intervals) is plotted against (A) the frequency-dependent transmission rate, β_F; (B) the density-dependent transmission coefficient, β_D; (C) the infected recovery rate, γ; (D) the chronically infected progression rate, κ; and (E) the chronically infected infectiousness, ϵ. When not changed in the figure baseline parameter values were used (see Table 4.2). Red lines are not shown in E(i) and E(ii) as this scenario assumes chronic individuals are infectious.

with immunity the mean time to pathogen extinction for the $SICS$ model framework without an infectious chronic class is short and shows little variation as the rate of leaving the chronic class varies (Figure 4.7D). When the chronic class can transmit the infection we see a decline in mean time to pathogen extinction as progression from the chronic class increases for the same reasons as explained for the case without immunity.

The mean time to extinction of the infection increases as the proportional rate of transmission from the chronic class increases in all scenarios (Figures 4.6E and 4.7E). Here, the additional source of infection from a class with reduced disease-induced mortality, compared to the infected class, promotes pathogen persistence.

4.4 Discussion

Both deterministic and stochastic modelling approaches are key tools for understanding the epidemiological dynamics and persistence of infectious disease. Deterministic models have advantages of analytical tractability, where for example, determining the

endemic level of infection becomes more straightforward. However, real systems are subject to random fluctuations and stochastic models developed to capture this randomness indicate that an infection can become extinct even when $\mathcal{R}_0 > 1$ [172]. In this study we examine classical infectious disease model frameworks to consider the role of exposed/latent and chronic infection in systems with and without recovery to immunity and the role of epidemiological parameters on the mean time to extinction of an infection.

Our study confirms previous findings that compare SIS and SIR frameworks and indicate that the inclusion of immunity reduces the time to extinction of the infection and therefore the likelihood of pathogen persistence [161, 162]. We also show that an increase in disease-induced mortality reduces the mean time to pathogen extinction for models that do not include immunity. Our work therefore extends previous findings for focused stochastic models that examine the impact of disease-induced mortality and infection induced reduction in fecundity in SI frameworks [167]. For models that include immunity the relationship between disease-induced mortality and mean time to pathogen extinction is less clear. For a wide range of parameters the persistence time of the infection is short and has low sensitivity to changes in disease-induced mortality. However, at lower rates of recovery from infection there is evidence of a reduction in the mean time to pathogen extinction as disease-induced mortality increases. Here, the increase in the force of infection that arises from a longer duration in the infected class is offset as the level of disease-induced mortality increases. Reduced pathogen persistence for acute disease has been shown in spatial SIR models [147] where the rapid turnover of infected individuals can lead to the loss of infection before it can be transmitted to neighbouring areas.

A key model assessment that we have undertaken in this study determines the impact of latent/exposed and chronic infection on the persistence of infection. Our model findings indicate that the mean time to pathogen extinction is increased when there is an exposed/latent period prior to infection. The extinction time of the infection is further increased if individuals in the exposed class are capable of transmission. Wildlife

diseases have been represented by models that include an exposed class [8], including those for infections that incur high levels of disease-induced mortality, such as rabies [164] and Tasmanian devil facial tumor disease [173]. Furthermore, animal tuberculosis (TB) in wild boar [63, 48, 104] has an infection process where initial infection does not cause high levels of mortality and infected individuals have low rates of transmission (similar to the exposed class in our model where exposed individuals can transmit the infection at a reduced rate). Infected wild boar progress to generalised infection in which they incur increased mortality and have high rates of transmission (similar to the infected class in our model - with a low recovery rate, γ, since individuals do not recover from TB). Under these conditions our model framework indicates that the 'exposed' class plays a significant role in pathogen persistence as it provides a future source of infected individuals. Theoretical assessments of the COVID-19 epidemic use $SEIR$ model frameworks to account for the incubation period of the virus [174, 175], and a further key aspect of COVID-19 epidemiology is that asymptomatic individuals can transmit the infection. While this latter process does not precisely fit one of our defined model frameworks, since for COVID-19 asymptomatic individuals that transmit the infection may progress directly to the immune stage, our model results do allow us to infer that infection from exposed individuals may be a key process in promoting persistence of this infection.

The impact of chronic infection on pathogen persistence depends on the characteristics of chronic infection. If chronically infected individuals incur disease-induced mortality but cannot transmit the infection then chronic infection can reduce the mean extinction time of the infection in models without immunity. Here, the chronic stage acts to delay the recovery while incurring the costs of disease-induced mortality. If chronically infected individuals can transmit the infection but incur low levels of disease-induced mortality then the mean persistence time of the infection is increased. The role of a chronic stage (named survivors in Stahl, et al. [40]) has been implicated in the persistence of African swine fever where the infection persists in the long-term even though the disease is highly virulent and leads to significant losses at the population level [18, 40]. In particular, two types of survivor are discussed [40]. Type I survivors

continue to shed the virus following infection but they are also likely to incur additional levels of mortality compared to healthy individuals. Here, our model results indicate that the balance between transmission of infection and the level of increased mortality is a key determinant of whether pathogen persistence is enhanced. Type II survivors can revert to the infectious stage from the chronic stage and could therefore be represented by a SICI model framework. A comparison between an SI and SICI framework (see Figure C.2) indicates that the chronic stage here can lead to an increase in the mean time to extinction of the infection. Therefore, our study suggests that a chronic stage of infection could aid pathogen persistence, make the infection more difficult to eradicate and could be a mechanism that promotes the observed persistence of African swine fever following an outbreak [18].

Our strategic model study has considered the importance of different epidemiological processes on the persistence of infectious disease. We have confirmed and extended the findings that indicate that pathogen persistence is reduced for infections that lead to immunity. We have also shown that a latent or chronic stage of infection can increase the persistence time of an infection which may make infectious diseases with these characteristics more difficult to manage and control.

Appendix C: Supplementary material for Chapter 4

C.1 Methodology

The deterministic model frameworks that include recovery, $SIR, SEIR$ and $SICR$ are shown in Equations (C.1-C.3). The SIR model framework is as follows:

$$\begin{aligned}
\frac{dS}{dt} &= bN(1-qN) - \beta_F S\frac{I}{N} - \beta_D SI - dS, \\
\frac{dI}{dt} &= \beta_F S\frac{I}{N} + \beta_D SI - (\alpha+\gamma+d)I, \\
\frac{dR}{dt} &= \gamma I - dR.
\end{aligned} \tag{C.1}$$

Here, S represents total susceptible population density, I the infected density and R the recovered density, with $N = S + I + R$ the total population density. The maximum birth rate is given by b, which is modified due to intra-specific competition through the parameter, $q = (b-d)/bK$, where K denotes the carrying capacity of the population. The natural death rate is given by d. For the infection dynamics we denote β_F to be the frequency-dependent transmission rate, β_D the density-dependent transmission coefficient, γ the recovery rate and α the additional death rate from the disease for infected individuals.

The SIR model can be modified to include an exposed class, E, as follows:

$$\begin{aligned}
\frac{dS}{dt} &= bN(1-qN) - \beta_F S\frac{I+\epsilon E}{N} - \beta_D S(I+\epsilon E) - dS,\\
\frac{dE}{dt} &= \beta_F S\frac{I+\epsilon E}{N} + \beta_D S(I+\epsilon E) - (\kappa+d)E,\\
\frac{dI}{dt} &= \kappa E - (\alpha+\gamma+d)I,\\
\frac{dR}{dt} &= \gamma I - dR.
\end{aligned} \tag{C.2}$$

In the $SEIR$ model infection leads to a susceptible individual entering the exposed class. Progression from the exposed class to the infected class occurs at rate κ. We also assume that individuals with the exposed form of the infection are infectious and can transmit the infection at a proportion ϵ of that of the infected class.

The SIR model can also be modified to include a chronically infected class, C, as follows:

$$\begin{aligned}
\frac{dS}{dt} &= bN(1-qN) - \beta_F S\frac{I+\epsilon C}{N} - \beta_D S(I+\epsilon C) - dS,\\
\frac{dI}{dt} &= \beta_F S\frac{I+\epsilon C}{N} + \beta_D S(I+\epsilon C) - (\alpha+\gamma+d)I,\\
\frac{dC}{dt} &= \gamma I - (\kappa+d+c\alpha)C,\\
\frac{dR}{dt} &= \kappa C - dR.
\end{aligned} \tag{C.3}$$

In the $SICR$ model individuals enter a chronically infected class following infection from which they progress to a recovered and immune class at rate κ. Chronically infected individuals may incur disease-induced mortality at a fraction, c, of that of an infected individual and are also assumed to be infectious and transmit the infection at a proportion ϵ of that of the infected class.

The stochastic versions of the $SEIR$ and $SICR$ model frameworks can be constructed following the methods outlined in Section 4.2 of the main paper.

C.1.1 Reproductive numbers

The basic reproductive number of the infection for the SIS and SIR model frameworks is shown in Equation (C.4):

$$\mathcal{R}_0 = \frac{\beta_D K + \beta_F}{\alpha + \gamma + d} \tag{C.4}$$

The basic reproductive number of the infection for the $SEIS$ and $SEIR$ model frameworks is shown in Equation (C.5):

$$\mathcal{R}_0 = \frac{\beta_D K + \beta_F}{\kappa + d} \left(\epsilon + \frac{\kappa}{\alpha + \gamma + d} \right) \tag{C.5}$$

The basic reproductive number of the infection for the $SICS$ and $SICR$ model frameworks is shown in Equation (C.6):

$$\mathcal{R}_0 = \frac{\beta_D K + \beta_F}{\alpha + \gamma + d} \left(1 + \frac{\epsilon\gamma}{\kappa + d} \right) \tag{C.6}$$

C.2 Analytical derivation of the mean time to pathogen extinction

To validate the simulation-based methods that we employ in the main paper to determine the mean time to pathogen extinction, we derive the exact time to pathogen extinction for the SIS model framework. We consider a continuous-time Markov chain on a finite state space and define all possible states, $1, \ldots, n$, of the system with the possible pathogen free states (states $1, ..., n_0$) as follows: $((S, I) = 1 : (0, 0), 2 : (1, 0), 3 : (2, 0) \ldots n_0 : (K, 0))$. We denote Q as the transition rate matrix, where each entry, q_{ij} for $i \neq j$ represents the rate of transition from state i to state j and with $q_{ii} = -\sum_{j \neq i} q_{ij}$. Then the expected time to reach the set of pathogen extinction states $1, \ldots, n_0$ from a starting state i, can be given by e_i and can be obtained by noting that $e_i = 0$ for $i = 1, 2, \ldots, n_0$ and solving the following linear system for $\{e_i : n_0 + 1 \leq i \leq n\}$:

$$\sum_{j=n_0+1}^{n} q_{ij} e_j = -1, \qquad \text{for } i = n_0 + 1, n_0 + 2, \ldots n. \tag{C.7}$$

Markov chain theory dictates that these equations have a unique solution [171], and as the states labelled $1, \dots n_0$ represent the pathogen free states, by finding e_i we find the expected time to pathogen extinction from an initial starting state i.

For our model frameworks, we use a carrying capacity, $K = 1000$, and so this gives a high number of possible states. For the SIS model framework, where the set of possible states is given by $\{S \in (0, K), I \in (0, K); S + I < K\}$, there are 501501 possible states and therefore computing the transition rate matrix Q and deriving the mean time to extinction e_i requires considerable computational effort. As we are considering a continuous Markov chain on finite space, any transition rate corresponding to a transition which requires more than one event to take place, (for example, going from one susceptible individual to three susceptible individuals) will be zero. As a result, the transition rate matrix Q can be considered sparse and this helps reduce the computational effort. We restrict the use of this method to the SIS model framework as the introduction of additional classes (such as an immune, latent or chronically infected class) greatly increase the computational effort required.

The comparison between this analytical derivation and the simulation method adopted in the main paper for calculating the mean time to pathogen extinction for the SIS

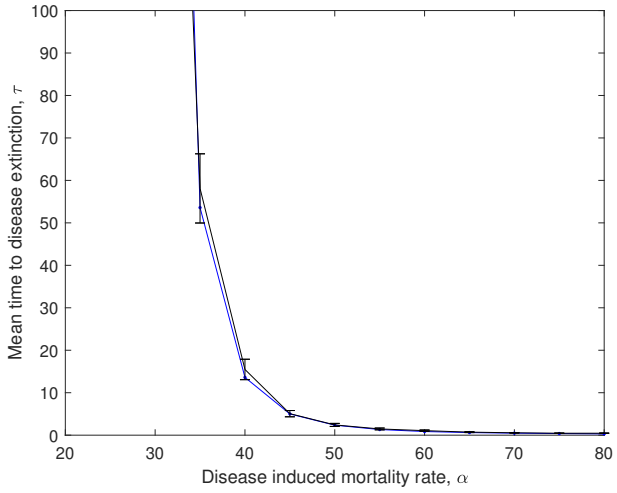

Figure C.1: The mean time to extinction of the infection in the SIS model framework against disease-induced mortality for the simulation method used in this study (black) and the exact time to pathogen extinction from analysis of a continuous-time Markov chain on a finite state space (blue).

model is shown in Figure C.1 and there is good agreement between the two methods.

C.3 An SI and SICI model framework

In the discussion of the main paper we consider the possibility of chronically infected individuals reverting back to the infected class ($SICI$) and assess how this process affects the time to pathogen extinction when compared to an SI model framework. The SI model is outlined in Equations (C.8) as follows:

$$\begin{aligned}\frac{dS}{dt} &= bN(1-qN) - \beta_F S\frac{I}{N} - \beta_D SI - dS,\\ \frac{dI}{dt} &= \beta_F S\frac{I}{N} + \beta_D SI - I(\alpha + d).\end{aligned} \tag{C.8}$$

Here, S represents total susceptible population density and I the infected density, with $N = S + I$ the total population density. The maximum birth rate is given by b, which is modified due to intra-specific competition through the parameter, $q = (b-d)/bK$, where K denotes the carrying capacity of the population. The natural death rate is given by d. For the infection dynamics we denote β_F to be the frequency-dependent transmission rate, β_D the density-dependent transmission coefficient, γ the recovery rate and α the additional death rate from the disease for infected individuals.

The SI model framework can be extended to form an $SICI$ model framework (see Equations C.9). In addition to a susceptible class, S, we assume two separate infected classes, I_1 and I_2, and a chronically infected class, C. Here, $I_T = I_1 + I_2$ denotes the total infected population density. Both infected populations can infect a susceptible individual, which then progresses to the initial infected state, I_1. An individual in this state can recover to a chronic state at rate, γ, and then progress to the secondary infected state, I_2 at rate, κ. Once in the I_2 class an individual will either die naturally or suffer disease-induced mortality at rate, α. The $SICI$ model is as follows:

$$\begin{aligned}
\frac{dS}{dt} &= bN(1-qN) - \beta_F S\frac{I_T}{N} - \beta_D S I_T - dS, \\
\frac{dI_1}{dt} &= \beta_F S\frac{I_T}{N} + \beta_D S I_T - I_1(\gamma + \alpha + d), \\
\frac{dC}{dt} &= \gamma I_1 - C(\kappa + d), \\
\frac{dI_2}{dt} &= \kappa C - I_2(\alpha_2 + d).
\end{aligned} \tag{C.9}$$

The stochastic versions of the SI and $SICI$ model frameworks can be constructed following the methods outlined in Section 4.2 of the main paper.

C.3.1 Results

A comparison of the SI and $SICI$ frameworks indicates that the mean time to pathogen extinction is increased for all levels of disease-induced mortality under the $SICI$ framework compared to an SI framework (Figure C.2).

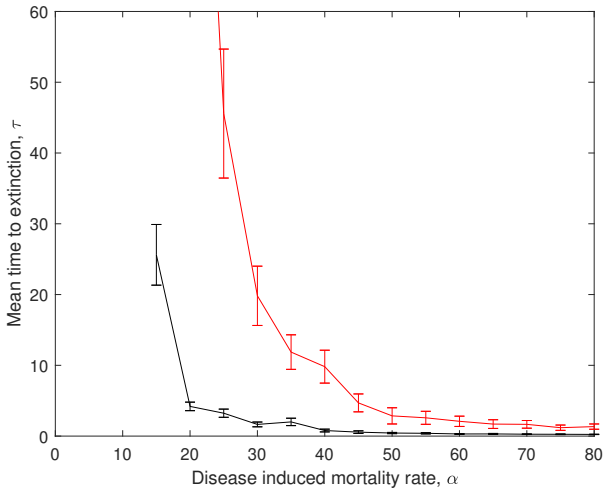

Figure C.2: The mean times to pathogen extinction (with 95% confidence intervals) plotted against the disease-induced mortality rate, α, for SI (black) and $SICI$ (red) model frameworks. Results show the mean and 95% confidence intervals for 100 realisations of each model framework. When not changed in the figure baseline parameter values were used (see Table 4.2).

Chapter 5

Tick-host demography and epidemiology

Abstract

Tick-borne diseases are a rising global public health concern due to the increasing abundance of ticks, expanding geographical range for vectors and pathogens, and emerging tick-borne infectious agents. A potential explanation for the rising impact of tick-borne disease is the increase in tick numbers which may be linked to an increase in density of the hosts on which ticks feed. In this study we extend established model frameworks to understand the link between host density and tick demography and epidemiology. Our model links the development of specific tick stages to the specific hosts on which they feed. We show that host composition and host density have an impact on tick population dynamics and that this has a consequent impact on host and tick epidemiological dynamics. A key result is that our model framework is able to capture variation in host prevalence due to changes in specific host density and therefore suggests that host composition may play a crucial role in explaining the variation in prevalence of tick-borne infection in hosts observed in the field.

5.1 Introduction

Ticks are a parasitic invertebrate, of the class *Arachnida*, that survive by feeding on the blood of warm-blooded animals [73]. There exist two main sub-classes of ticks: Ixodid ticks (hard ticks) and Argasid ticks (soft ticks) both with a structured life cycle of progression from egg to larvae to nymph and finally to adult stages that can lay

further eggs [73]. Ticks can be considered one-host, two-host or three host ticks, where once attached an individual either spends their whole life cycle on a host, two stages upon the same host (and the third on a different host) or feed on different hosts at each stage [176, 177, 178]. Progression between stages requires at least one blood meal with larvae generally feeding on small mammals, such as rabbits (*Oryctolagus cuniculus*), hares (*Lepus*) or birds; and adults generally feeding on large mammals, such as red deer (*Cervus elaphus*), wild boar (*Sus scrofa*), livestock or humans, although this can vary depending on the type of tick considered [74, 75]. The nymph stage can feed on either small or large mammals and is dependent on both host composition and the type of tick considered. The interaction between ticks and hosts means they are a vector for the transmission of infectious disease [76]. They can become infected through feeding on an infected host and then can transmit the infection by feeding on susceptible hosts at a later point in their life cycle [179, 180]. Ticks can also become infected through vertical transmission from infected adults to eggs, or by co-feeding (where a susceptible tick feeds with an infected tick on the same host) [181, 182].

Ticks transmit the largest range of diseases, including bacterial, protozoan and virus diseases [77, 79], of arthropod vectors at the global scale and are among the most important vectors of diseases affecting livestock and humans [78, 183]. They can cause severe toxic conditions such as paralysis and toxicosis, and along with their infections, have coevolved with wildlife hosts which act as reservoirs for the ticks and tick-borne infections [78]. Tick-borne diseases are an increasing global public health concern due to the increasing abundance of ticks, expanding geographical range for vectors and pathogens, and emerging tick-borne infectious agents [184, 7, 2, 185] as well as an increase in antimicrobial resistance among bacterial pathogens [80, 79]. There is evidence that this increased threat is linked to climate change that has made environmental conditions more favourable to ticks [186, 187, 188, 189, 2, 7, 190, 191, 192]. It has also been suggested that increases in the abundance and range of wildlife reservoir hosts may play an important role in the increased risk of spillover of tick-borne disease to humans and wildlife [7, 81, 185]. Further investigations into the causes of the increased risk of tick-borne disease are required if we are to control and manage these infections.

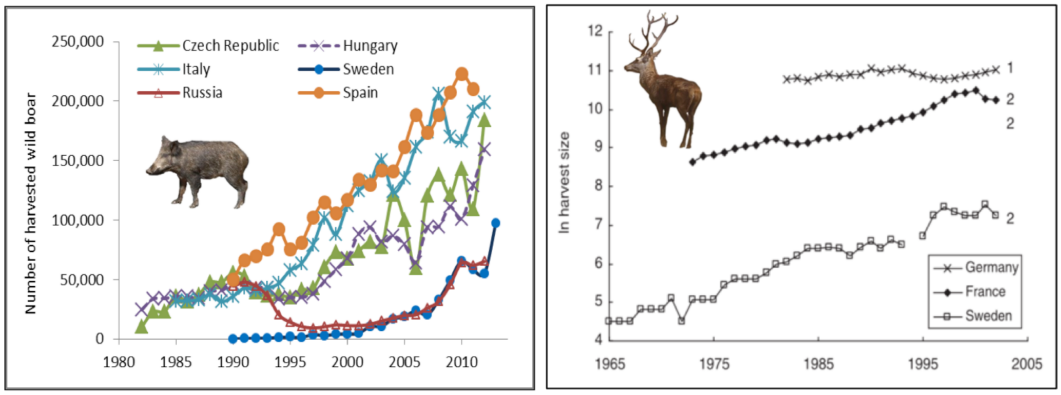

Figure 5.1: Increasing trends for wild boar (left) and red deer (right) population abundance. Sources: [22, 23].

A potential explanation for the increasing impact of tick-borne disease is the increase in tick numbers [185, 193]. However, there is considerable variation in disease incidence at a regional level which may be affected by the abundance and competence of specific vertebrae hosts and we know little about regional host compositions [185]. Some studies indicate a direct link between host diversity and disease risk [194, 195] and some indicate that increased host biodiversity could lead to increased parasite diversity and exposure [2]. There is evidence there has been a widespread increase in the density of wild ungulates across Europe [21, 22, 23, 24] (see Figure 5.1). Since these are key hosts for ticks this could have an impact on tick demography with a consequent impact on the prevalence and risk of zoonotic transmission of tick-borne infectious disease. However, ticks require different hosts to complete their development and so without a commensurate increase in other hosts, such as small mammals, which are key hosts for larval tick stages, there may be a bottleneck in tick development that limits tick density increases [196]. The aim of this chapter is to assess the impact of increasing host density on tick demography and infection prevalence. A key novel extension will be to consider different host classes for different tick stages and to explore if variation in the density of different host classes can explain the observed variation in tick disease incidence.

Mathematical models have been used to explore and understand the epidemiological dynamics of host-tick interactions and the persistence of tick-borne diseases [197, 198,

82, 83, 84]. Switkes et al. (2016) [84] developed a model for Crimean-Congo haemorrhagic fever virus (CCHFv) that considered a single tick class (all tick stages were grouped into one class) and that considered two large mammal hosts (cattle and humans). They explored thresholds for disease persistence, including the reproductive number of the virus, as well as the progression of the disease under a hypothetical outbreak. Tick-human transmission was identified as the main cause for the spread of CCHFv in humans. This model considered a constant tick population size, with no link between host density and tick density. Lou and Wu (2014) [197] developed a model examining different methods of tick-host attachment terms and their implications on Lyme disease. A tick stage-structured model was used for larvae, nymph and adult ticks, with progression to the subsequent stage depending upon either a density-dependent attachment, frequency-dependent attachment or a Holling type-II attachment term. In the density-dependent and Holling type-II scenario the model predicts a reduction in host density could either reduce or increase infection risk, whilst in the frequency-dependent model scenario a reduction in host density will always reduce infection risk. Norman et al. 1999 [82] developed a model to understand the persistence of the Louping-ill virus in grouse which was then extended and generalised by Rosá et al. (2003) [85]. For both studies a tick stage-structured model was used where all stages could feed on either a viraemic or non-viraemic host and tick birth rate was linked to host density but was limited through self-regulation. Results showed that non-viraemic hosts could either amplify the tick population and assist in virus persistence or dilute the infection and cause it to die out. A threshold density for the viraemic host was also found, where for low viraemic host density the virus would die out. Although this work considered the link between ticks and multiple hosts on tick density it did not consider the link between the tick stages and their respective hosts and ticks were limited by self-regulation rather than host density. Notwithstanding, it does highlight that the link between host and tick density can be critical to explaining the epidemiology of tick-borne infections.

Rosá and Pugliese (2007) [83] developed a model framework to explore the effect of tick population dynamics and host density on the persistence of tick-borne infections. Tick age-structure and two different hosts, small rodents and large mammals, are included,

with different tick stages feeding on different hosts. The link between tick density and host density was included either through density-dependent birth or through density-dependent moulting. Unlike previous models, a dynamic regulation of tick density based on host density was explored. This was originally incorporated into the birth function but was also suggested for the moulting term to represent how high tick density per host may lead to hosts developing immunity that limits moulting success [199, 200]. They found that the effect that host densities have on tick-borne disease can depend strongly on how the tick population is regulated and that the dilution effect of an infection for a high density of competent hosts occurred only if tick density is independent of host density. Some drawbacks of this framework were that tick reproduction and development depended on host health that was averaged across all hosts, rather than considering the health of specific hosts separately and linking the development of tick stages to the health of their relevant hosts. Furthermore, the density-dependent functions used a negative exponential form which unrealistically led to a decrease in the production of larvae as tick density increased. This was improved upon in Pugliese and Rosá (2008) [86], where the density-dependent functions were represented by a Holling-type II form but here regulation through host density was no longer examined.

In this chapter we seek to extend established model frameworks to understand the link between host density and tick demography and epidemiology. We begin by considering an extension to Switkes et al. (2016) [84], that uses a single tick stage to explore a direct link between tick and host density. We then use a modification of the frameworks of Rosá and Pugliese (2007) [83] and Pugliese and Rosá (2008) [86] that considers multiple tick stages feeding on different hosts, to explore the dynamic regulatory link between tick density and host density (as in Rosá and Pugliese, 2007) represented by a Holling type-II functional response (as in Pugliese and Rosá, 2008). We then use the insights from this analysis to develop a new model that links tick development to the health of the specific host on which the different tick stages feed. Our aim is to understand the impact of host density and host composition on the density of ticks and the persistence, prevalence and risk of transmission of tick-borne infections.

5.2 Mathematical models of tick-host demography and epidemiology

5.2.1 An extension of the model of Switkes et al. (2016)

The model of Switkes et al. (2016) [84] considers a general framework of tick-host interactions with a focus on the epidemiological dynamics of Crimean-Congo haemorrhagic fever virus for a host, subscript H, and a single class of ticks, subscript V. The host population is split into three classes reflecting the infection status: susceptible S, infected I and recovered R. The tick population is assumed to either be susceptible S, or infected I. The total densities of both ticks and hosts are considered constant. We modify their framework to consider changes in host density and link tick reproduction to host density. The model framework is detailed below:

$$\begin{aligned}
\frac{dS_H}{dt} &= (a_H - q_H H)H - \beta_{HV}\frac{S_H}{H}I_V - b_H S_H,\\
\frac{dI_H}{dt} &= \beta_{HV}\frac{S_H}{H}I_V - \gamma_H I_H - b_H I_H,\\
\frac{dR_H}{dt} &= \gamma_H I_H - b_H R_H,\\
\frac{dS_V}{dt} &= (a_V - q_V(H)V)(V - pI_V) - \beta_{VV}\frac{S_V}{V}I_V - \beta_{VH}\frac{I_H}{H}S_V - b_V S_V,\\
\frac{dI_V}{dt} &= (a_V - q_V(H)V)pI_V + \beta_{VV}\frac{S_V}{V}I_V + \beta_{VH}\frac{I_H}{H}S_V - b_V I_V.
\end{aligned} \tag{5.1}$$

Here, H and V denote the total host and tick density, respectively. The maximum birth rates of hosts and ticks are given by a_H and a_V, with natural death rates given by b_H and b_V, respectively. The hosts susceptibility to crowding is given by $q_H = (a_H - b_H)/K_H$, where K_H denotes the carrying capacity of hosts, with the ticks susceptibility to crowding $q_V(H) = (a_V - b_V)/(nH)$ dependent on host density, H, and the average number of ticks that a host can support, n.

Ticks can transmit the virus to hosts through frequency-dependent transmission at rate β_{HV}, with host-tick transmission occurring at rate β_{VH}. Tick-tick transmission can occur through non-systemic transmission (co-feeding) at rate β_{VV} or through vertical transmission, with a proportion p of infected ticks transmitting the virus to offspring.

Table 5.1: Baseline parameter values for the model extension to Switkes et al. (2016) and their biological meaning.

$a_H = \log(4)$	Maximum birth rate of hosts
$a_V = 150$	Maximum birth rate of ticks
$b_H = 1/7$	Natural death rate of hosts
$b_V = 1$	Natural death rate of ticks
$q_H = (a_H - b_H)/K_H$	Susceptibility to crowding of hosts
$q_V = (a_V - b_V)/(nH)$	Susceptibility to crowding of ticks
$\beta_{HV} = 0.0112$	Tick-host transmission coefficient
$\beta_{VH} = 0.56$	Host-tick transmission coefficient
$\beta_{VV} = 0.00112$	Non-systemic transmission coefficient (co-feeding)
$p = 0.1$	Proportion of infected offspring from infected individuals
$\gamma_H = 0.4$	Recovery rate of infected hosts
$a_S = 1/50$	Birth rate of humans
$\beta_{VS} = 0.00112$	Tick-human transmission coefficient
$\gamma_S = 0.4$	Recovery rate of infected humans

Hosts can recover from the infection at rate γ_H.

This model can be extended to include a human population (see Equations 5.2) to examine the significance of an increase in host and tick density on the risk of infection to humans. A human individual can be considered susceptible, S, infected I or recovered R. This model extension is detailed below:

$$\begin{aligned} \frac{dS_S}{dt} &= a_S N - \beta_{VS}\frac{S_S}{N} I_V - a_S S_S, \\ \frac{dI_S}{dt} &= \beta_{VS}\frac{S_S}{N} I_V - \gamma_S I_S - a_S I_S, \\ \frac{dR_S}{dt} &= \gamma_S I_S - a_S R_S. \end{aligned} \tag{5.2}$$

Here, $N = S_S + I_S + R_S$ denotes the total human population and a_S the birth and natural death rate, with total human density assumed to be constant. Humans can become infected at rate β_{VS} through infected tick contact and can recover at rate γ_S. Infection through contact with livestock/other hosts is assumed negligible [84].

Parameter values for the maximum birth rate and natural death rate for hosts were

taken from Díez-Delgado et al. (2018) [63]. The natural death rate for ticks is taken to be $b_V = 1$, to represent an average lifetime of one year, with the maximum birth rate of $a_V = 150$. The transmission coefficients and recovery rates are then approximated so that endemic results match with the prevalence of CCHFv found in cattle/goats ($\sim 20\%$) [201] and in ticks ($2-7\%$) [202]. The birth rate/natural death rate of humans is given to be $a_S = 1/50$ to represent an average lifespan of 50 years and the tick-human transmission coefficient is taken to be a tenth of the tick-host transmission coefficient to represent a reduced contact rate between ticks and humans. The recovery rate of humans is given to be the same as in hosts. All model parameter values are given in Table 5.1.

Results for the modified model of Switkes et al. (2016)

Varying the number of ticks that a host can support indicates that there is a threshold below which the infection cannot persist (see Figure 5.2). Here, as n is decreased the density of ticks is reduced to a point where the infection cannot be sustained. However, above this threshold the density of infected ticks increases resulting in the increase of both host and tick prevalence as n increases.

Increasing the host carrying capacity (and therefore density) of the host increases all tick and host classes linearly, including the infected classes (see Figure 5.3). Due to the frequency-dependent nature of transmission this means the prevalence of infection

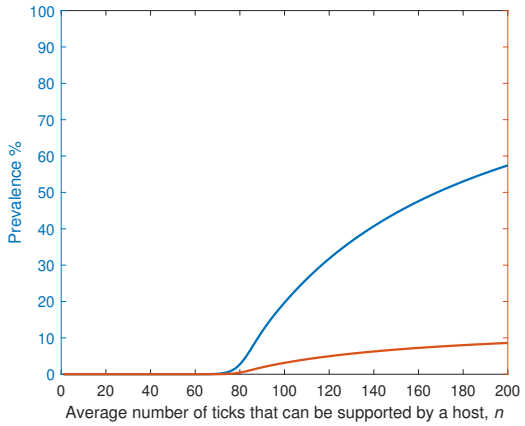

Figure 5.2: Prevalence levels (%) for hosts (blue) and ticks (orange) against the number of ticks that can be supported by a host, n. Other parameters are as seen in Table 5.1.

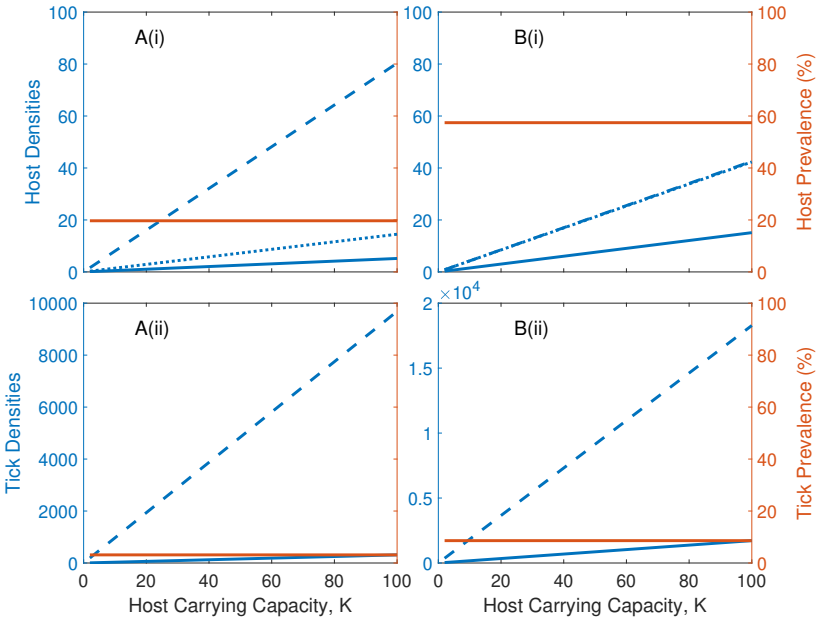

Figure 5.3: Host and tick population densities (blue) and host and tick prevalence levels (orange) for different levels of host carrying capacity with a tick burden of (A) $n = 100$ ticks per host and (B) $n = 200$ ticks per host. Densities for (i) hosts and (ii) ticks are split into their different classes with susceptible (dashed), infected (solid) and recovered (dotted). When not varied in the figure parameters were as in Table 5.1.

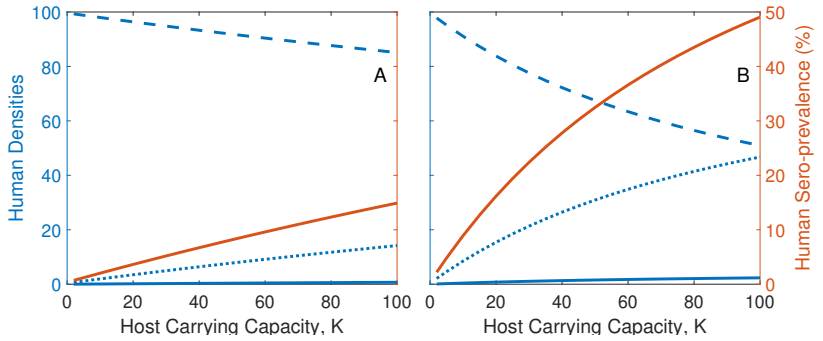

Figure 5.4: Human population densities (blue) and seroprevalence (orange) for different levels of host carrying capacity with a tick burden of (A) $n = 100$ ticks per host and (B) $n = 200$ ticks per host. The population densities are split into the different classes with susceptible (dashed), infected (solid) and recovered (dotted). When not varied in the figure parameters were as in Table 5.1.

in ticks and hosts remains constant as host density increases. Whilst increasing the host population density has little effect on the prevalence of the infection in ticks or hosts, it does increase the density of infected ticks (see Figure 5.3). As a result, this increases the risk of transmission to a human population, increasing both the infected and recovered densities and the prevalence of infection in humans (see Figure 5.4). This highlights the importance of determining prevalence and density estimates for natural systems to be able to assess the risk of spillover to other hosts. Nevertheless, this model

could not capture variation in disease prevalence in ticks and hosts for changes in host density.

5.2.2 An extension of the model of Rosá and Pugliese (2007)

We extend the model of Rosá and Pugliese (2007) [83] by adapting the terms that link tick birth and moulting to host density to be Holling type-II function forms, as seen in Pugliese and Rosá (2008) [86]. This allows for the inclusion of dynamic regulation of the tick population through host density. The model includes three stages of tick development: larvae, L; nymph, N; and adult, A, which are each further classified into a questing class, subscript Q, and a feeding class, subscript F, with total tick density given by T. Larvae are assumed to only feed on small mammals, H_S, with adults solely feeding on ungulates, H_U. Nymphs can feed on either host population. The model is detailed below:

$$\begin{aligned}
\frac{dL_Q}{dt} &= \sigma_A a_T(T,H)A_F - \beta_1 H_S L_Q - b_L L_Q,\\
\frac{dL_F}{dt} &= \beta_1 H_S L_Q - \sigma_L L_F,\\
\frac{dN_Q}{dt} &= \sigma_L m_L(T,H)L_F - \beta_2 H_S N_Q - \beta_3 H_U N_Q - b_N N_Q,\\
\frac{dN_F}{dt} &= \beta_2 H_S N_Q + \beta_3 H_U N_Q - \sigma_N N_F,\\
\frac{dA_Q}{dt} &= \sigma_N m_N(T,H)N_F - \beta_4 H_U A_Q - b_A A_Q,\\
\frac{dA_F}{dt} &= \beta_4 H_U A_Q - \sigma_A A_F.
\end{aligned} \tag{5.3}$$

Here, the natural death rate of questing ticks is given by b_L, b_N and b_A for questing larvae, nymph and adults, respectively, while the death of feeding ticks is assumed to be negligible [83]. Ticks attach to respective hosts for feeding at rates $\beta_1, \beta_2, \beta_3$ and β_4, for larvae, nymphs onto small mammals, nymphs onto ungulates and adults, respectively, and detach at rates σ_L, σ_N and σ_A for larvae, nymphs and adults, respectively. The birth rate, $a_T(T,H)$ and successful moulting rates, $m_L(T,H)$ and $m_N(T,H)$ (for larvae and nymphs, respectively) are dependent on total host and tick density and given by Equations (5.4-5.5). The small mammal densities H_S, and ungulate densities H_U, can

be varied to assess the relationship between tick and host density.

$$a_T(T,H) = r_T \frac{1}{1+\frac{s_T T}{uH_S+vH_U}}, \tag{5.4}$$

$$m_L(T,H) = r_L \frac{1}{1+\frac{s_L T}{uH_S+vH_U}}, \qquad m_N(T,H) = r_N \frac{1}{1+\frac{s_N T}{uH_S+vH_U}}. \tag{5.5}$$

In these expressions, the maximum birth rate is given by r_T, with maximum moulting success rates r_L and r_N for larvae and nymphs, respectively. The coefficients s_T, s_L and s_N measure the strength of the density dependence, with u and v scalings for density dependence of the particular host. All parameter values for this model were as used in Rosá and Pugliese (2007) [83].

Results for the extension to Rosá and Pugliese (2007)

We explore the effect of an increase in ungulate density and small mammal density on the tick population demography (see Figure 5.5). The density of feeding ticks increases with an increase in both ungulate and small mammal density. The density of questing larvae increases with ungulate density but decrease and tend towards a constant level for an increase in small mammal density. The density of questing nymphs and adults increase with small mammal density but decrease and tend towards a constant level for an increase in ungulate density. We now attempt to explain these trends in tick density. An increase in small mammal density increases the rate of attachment of larvae more quickly than the increase in reproduction and therefore decreases the density of questing larvae. An increase in ungulate host density increases the density of questing larvae as this increases the successful rate of reproduction with no effect on the rate of attachment. A similar effect is seen in the questing nymph and adult population where an increase in ungulate host density leads to a reduction in the density of questing adults. However, the questing nymph density saturates with an increase in small mammal density as questing nymphs can attach to either host type and the regulatory moulting progression from feeding larvae is dependent on both host densities. The density of feeding larvae increases with small mammal density as the rate of attachment increases, and increases with ungulate density as the density of questing

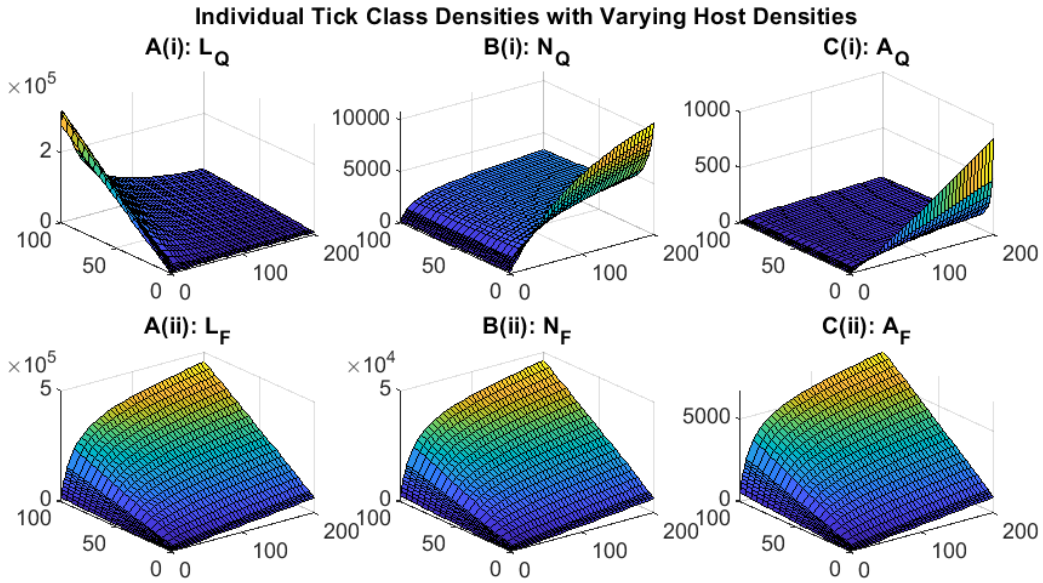

Figure 5.5: Tick population densities (vertical axis) for a varying ungulate density (from 0 to 100) and varying small mammal density (from 0 to 200) under the extended Rosá and Pugliese model framework. Steady state densities were plotted for (A) larvae, (B) nymphs and (C) adults, for both (i) questing ticks and (ii) feeding ticks. Parameter values are: $a_T = 2000, b_L = 0.0365, b_N = 0.015, b_A = 0.00625, \sigma_A = 0.12, \sigma_L = 0.28, \sigma_N = 0.22, \beta_1 = 0.015, \beta_2 = 0.0005, \beta_3 = 0.03, \beta_4 = 0.13, r_L = 1, r_N = 1, s_T = 0.001, s_L = s_N = s_T, u = 0.04, v = 0.4$ (taken from Rosá and Pugliese, 2007).

larvae increases. Similarly, the density of feeding adult ticks increases with ungulate density as the rate of attachment increases, and increases with small mammal density as the density of questing adults increases. The density of feeding nymphs increases with both host densities, as the rate of attachment increases with these densities.

5.3 A new model linking tick density to host density

The model extensions of Switkes et al. (2016) and Rosá and Pugliese (2007) provide useful insights into the modelling of tick-borne diseases and tick-host dynamics. However, these models still contain drawbacks in their approach. For the modified model of Swtikes et al. (2016) the simplicity of the model cannot provide useful information on the tick-host demographics or on the influence of host composition on the tick dynamics. In Rosá and Pugliese (2007) the regulatory dynamics of each tick development phase is independent of the specific hosts upon which the tick stages feed. Therefore, we develop a new model formulation, based on the framework of Rosá and Pugliese (2007) and our extension (Equations 5.3-5.5), that links the development of tick stages to the health of

the specific hosts on which they feed. The population regulation of ticks arises through host immunity [184, 203] with both small and large mammal hosts acquiring resistance to tick feeding as a result of repeated infestation [184, 199, 83, 200]. Several effects of acquired resistance in hosts have been observed, including reduced engorgement weight of ticks, inhibition to feeding and blocked moulting [184, 199, 200] and reduced tick burden [204, 205]. Here, we develop a model that accounts for acquired host immunity by considering the moulting success of ticks after attaching to hosts. We extend the approach of Rosá and Pugliese (2007) who argue that a model that considers individual tick loads and immune histories would be too complex and instead assumes host immunity depends on the instantaneous average tick load. We differ from Rosá and Pugliese (2007) in that we consider the effect of the immune status of small mammal hosts and ungulate hosts separately such that they impact different stages of tick development.

5.3.1 Tick-host model with host specific density dependence

We outline a tick-host model in which the moulting success of different tick stages depends on the specific hosts on which they feed. The model considers the three main stages of tick development (excluding the egg stage): larvae, L; nymph, N; and adult, A and considers a questing, subscript Q, and feeding, subscript F, tick class for each tick stage. For the feeding nymph class, it is useful to distinguish those that feed on small mammals N_{FS}, and those that feeds on ungulates, N_{FU}. The model also considers the density of small mammals, H_s and ungulates, H_u. The model is detailed below:

$$
\begin{aligned}
\frac{dL_Q}{dt} &= \sigma_A a_T(N_{FU}, A_F, H_U)A_F - \beta_1 H_S L_Q - b_L L_Q,\\
\frac{dL_F}{dt} &= \beta_1 H_S L_Q - \sigma_L L_F,\\
\frac{dN_Q}{dt} &= \sigma_L m_L(L_F, N_{FS}, H_S)L_F - \beta_2 H_S N_Q - \beta_3 H_U N_Q - b_N N_Q,\\
\frac{dN_{FS}}{dt} &= \beta_2 H_S N_Q - \sigma_N N_{FS},\\
\frac{dN_{FU}}{dt} &= \beta_3 H_U N_Q - \sigma_N N_{FU},\\
\frac{dA_Q}{dt} &= \sigma_N(m_{NS}(L_F, N_{FS}, H_S)N_{FS} + m_{NU}(N_{FU}, A_F, H_U)N_{FU}) - \beta_4 H_U A_Q - b_A A_Q,\\
\frac{dA_F}{dt} &= \beta_4 H_U A_Q - \sigma_A A_F.
\end{aligned}
\tag{5.6}
$$

Table 5.2: Baseline parameter values for the tick-host model with hot specific density dependence.

$a_T = 2000$	Maximum birth rate per adult tick.
$b_L = 0.0365$	Natural death rate of questing larvae.
$b_N = 0.015$	Natural death rate of questing nymph.
$b_A = 0.00625$	Natural death rate of questing adults.
$\sigma_L = 0.28$	Average rate of feeding for larvae.
$\sigma_N = 0.22$	Average rate of feeding for nymphs.
$\sigma_A = 0.12$	Average rate of feeding for adults.
$\beta_1 = 0.015$	Attachment coefficient for larvae onto small mammals.
$\beta_2 = 0.0005$	Attachment coefficient for nymph onto small mammals.
$\beta_3 = 0.03$	Attachment coefficient for nymph onto ungulates.
$\beta_4 = 0.13$	Attachment coefficient for larvae onto ungulates.
$r_L = r_N = 1$	Maximum rate of success for moulting larvae and nymphs.
$s_{NS} = s_L = 0.025$	Coefficients for the strength of the small mammal host density dependence.
$s_{NU} = s_T = 0.0025$	Coefficients for the strength of the ungulate host density dependence.

Here, b_L, b_N and b_A represent the natural death rates of larvae, nymphs and adults, respectively. The attachment rates are given by $\beta_1, \beta_2, \beta_3$ and β_4 and ticks detach from hosts at rates σ_L, σ_N and σ_A (and the reciprocal of these rates represent the average feeding times of the different tick stages). We assume that moulting success and reproduction (both of which require successful feeding) depend on the specific host on which the tick stages feed and are density-dependent functions of relative density of the number of feeding ticks on specific hosts and the hosts themselves (see Equations 5.7).

$$\begin{aligned}
a_T(N_{FU}, A_F, H_U) &= r_T \frac{1}{1 + \frac{s_T(N_{FU}+A_F)}{H_U}}, \\
m_L(L_F, N_{FS}, H_S) &= r_L \frac{1}{1 + \frac{s_L(L_F+N_{FS})}{H_S}}, \\
m_{NS}(L_F, N_{FS}, H_S) &= r_{NS} \frac{1}{1 + \frac{s_{NS}(L_F+N_{FS})}{H_S}}, \\
m_{NU}(N_{FU}, A_F, H_U) &= r_{NU} \frac{1}{1 + \frac{s_{NU}(N_{FU}+A_F)}{H_U}}.
\end{aligned} \tag{5.7}$$

Here, r_T represents the maximum birth rate with r_L, r_{NS} and r_{NU} the maximum moult-

ing success rates of each respective class. The coefficients s_T, s_L, s_{NS} and s_{NU} measure the respective strength of the density dependence. Where possible the model parameters took values as seen in Section 5.2.2, so that a direct comparison between the two model frameworks could be seen. As the density-dependent moulting term is now specific to a particular host, the scalings, u and v from Equations (5.4-5.5), are absorbed within the coefficients s_T, s_L, s_{NS} and s_{NU}. The parameter values are detailed in Table 5.2.

The impact of host density on tick density for the tick-host model with host specific density dependence

We vary the density of small mammals and ungulates and examine the impact on feeding and questing ticks under the tick-host model with host specific density dependence (see Figure 5.6). The model results exhibit similar dynamics to those seen for the model extension in Section 5.2.2, particularly in the questing class of ticks. However, the density of feeding larvae and adults exhibit a stronger saturation as the densities of either host is increased, stemming from the density dependence acting on specific hosts. The density of feeding nymphs also exhibit saturation with an increase in ungulate density,

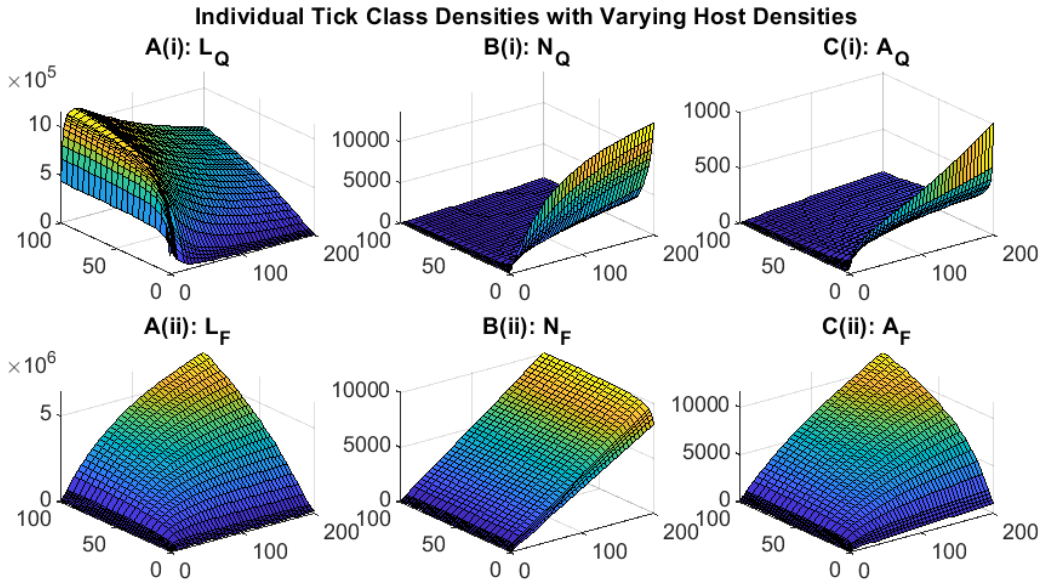

Figure 5.6: Tick population densities (vertical axis) for a varying ungulate density (from 0 to 100) and varying small mammal density (from 0 to 200) under the tick-host model framework with host specific density dependence (Equations 5.6-5.7). Steady state densities were plotted for (A) larvae, (B) nymphs and (C) adults, for both (i) questing ticks and (ii) feeding ticks. When not varied in the figure parameter values are as in Table 5.2.

although not with an increase in small mammal density. Here, the feeding larvae density saturates as the ungulate density increases, meaning the questing nymph population now decreases with an increase in ungulate population, as the rate of attachment (from questing nymph to feeding nymph) outweighs the incoming rate of moulting nymphs. This decline in questing nymph density coupled with the increased rate of attachment means the total feeding nymph class varies little with ungulate density. For a fixed ungulate density, an increase in small mammal density increases the density of questing nymphs due to the increase in successfully moulted larvae. The increase in the attachment rate of questing nymphs then allow for an increase in the density of feeding nymphs.

5.3.2 Model selection

We examine and compare results from the model frameworks used in Section 5.2.2 and 5.3.1 in more detail. We explore the effect of an increase in small mammal density with fixed ungulate density (and vice versa) on the density of feeding larvae and adults for each model framework. We see that the original extension of Rosá and Pugliese, where moulting depends on combined host density, gives a linearly increasing relationship between the tick densities and the host densities whilst the tick-host model with host specific density dependence exhibits saturating behaviour as one host type increases for a fixed density of the other host (Figure 5.7). We believe this saturation behaviour is more representative of real systems where a limit in a specific host type would restrict overall tick density [196]. We therefore believe that our modified model represents a key trend in tick-host population dynamics that has been absent from previous studies.

5.4 Epidemiological dynamics

In this section we extend our model of host-tick dynamics (Equations 5.6-5.7) to include a representation of tick-borne infectious disease. This will extend previous studies in which mathematical models have been used to explore and understand the epidemiological dynamics and persistence of tick-borne disease [196, 206, 207, 82, 85, 84]. Previous studies have determined thresholds for disease persistence [208, 209, 210] and explored

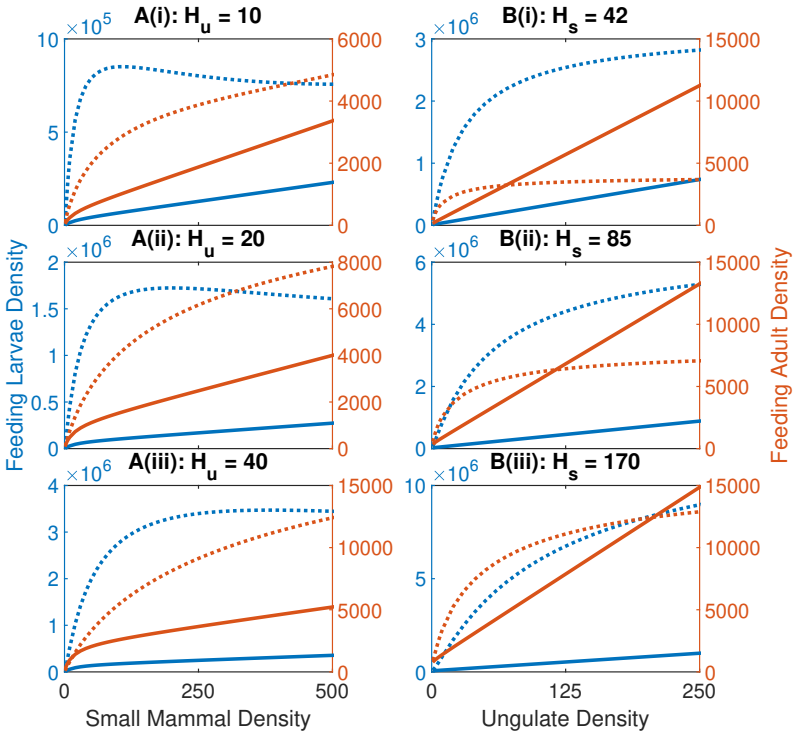

Figure 5.7: Tick population densities for (A) a fixed ungulate density and varying small mammal density and (B) a fixed small mammal density and varying ungulate density. Densities are shown for feeding larvae (blue) and feeding adults (orange) under different model frameworks with the solid line representing the extension of Rosá and Pugliese (Section 5.2.2) and the dotted line representing the tick-host model with host specific density dependence (Section 5.3.1). This is done for different fixed values of host density with (i) $H_U = 10$ or $H_S = 42$, (ii) $H_U = 20$ or $H_S = 85$ and (iii) $H_U = 40$ or $H_S = 170$. When not varied in the figures the parameters are as described for each model framework (see Figure 5.5 and Table 5.2).

how different host types [211, 82, 83, 85, 84] and seasonality [212, 198, 213, 214, 215] will affect the epidemiological dynamics. Models have shown that increases in host density or host diversity can either have a diluting effect or an amplifying effect on the persistence of tick-borne diseases [216, 217, 82, 85]. We extend the tick-host model outlined in Section 5.3.1, in which tick progression between life stages is a density-dependent function of the host stage on which the tick feeds, to explore the impact of host-tick population dynamics on disease persistence and prevalence. This will allow us to assess how changes in host composition for different tick life stages can impact on the prevalence and risk of spillover of infectious disease to tick hosts. Our model will include the key transmission routes for tick disease which include tick to host and host to tick direct transmission, a non-systemic (co-feeding) transmission route and vertical transmission from parent to offspring [181, 218, 219]. Although important in some circumstances [82, 85], non-viraemic hosts are omitted and we assume all hosts can become infected

and infectious. The general model framework we present can be adapted to explore the epidemiological dynamics of many different tick-borne disease systems.

In the extension to the model (Equation 5.6) each tick class and type of host are split into a susceptible class (additional subscript s) or an infected class (additional subscript i), with hosts able to recover from the infection to form a recovered class (additional subscript r). The full model is detailed in Equations (5.8-5.10):

$$
\begin{aligned}
\frac{dL_{Qs}}{dt} &= a_T\sigma_A\left(A_{Fs}+(1-\rho)A_{Fi}\right)-\beta_1 H_S L_{Qs}-b_L L_{Qs},\\
\frac{dL_{Qi}}{dt} &= a_T\sigma_A\rho A_{Fi}-\beta_1 H_S L_{Qi}-b_L L_{Qi},\\
\frac{dL_{Fs}}{dt} &= \beta_1\left(H_S-p^L H_{Si}\right)L_{Qs}-\theta_{TT}\frac{I_{TS}}{T_{TS}}L_{Fs}-\sigma_L L_{Fs},\\
\frac{dL_{Fi}}{dt} &= \beta_1 H_S L_{Qi}+p^L\beta_1 H_{Si}L_{Qs}+\theta_{TT}\frac{I_{TS}}{T_{TS}}L_{Fs}-\sigma_L L_{Fi},\\
\frac{dN_{Qs}}{dt} &= m_L\sigma_L L_{Fs}-\beta_2 H_S N_{Qs}-\beta_3 H_U N_{Qs}-b_N N_{Qs},\\
\frac{dN_{Qi}}{dt} &= m_L\sigma_L L_{Fi}-\beta_2 H_S N_{Qi}-\beta_3 H_U N_{Qi}-b_N N_{Qi},\\
\frac{dN_{FSs}}{dt} &= \beta_2\left(H_S-p^{N_1}H_{Si}\right)N_{Qs}-\theta_{TT}\frac{I_{TS}}{T_{TS}}N_{FSs}-\sigma_N N_{FSs},\\
\frac{dN_{FSi}}{dt} &= \beta_2 H_S N_{Qi}+p^{N_1}\beta_2 H_{Si}N_{Qs}+\theta_{TT}\frac{I_{TS}}{T_{TS}}N_{FSs}-\sigma_N N_{FSi},\\
\frac{dN_{FUs}}{dt} &= \beta_3\left(H_U-p^{N_2}H_{Ui}\right)N_{Qs}-\theta_{TT}\frac{I_{TU}}{T_{TU}}N_{FUs}-\sigma_N N_{FUs},\\
\frac{dN_{FUi}}{dt} &= \beta_3 H_U N_{Qi}+p^{N_2}\beta_3 H_{Ui}N_{Qs}+\theta_{TT}\frac{I_{TU}}{T_{TU}}N_{FUs}-\sigma_N N_{FUi},\\
\frac{dA_{Qs}}{dt} &= \sigma_N\left(m_{NS}N_{FSs}+m_{NU}N_{FUs}\right)-\beta_4 H_U A_{QS}-b_A A_{Qs},\\
\frac{dA_{Qi}}{dt} &= \sigma_N\left(m_{NS}N_{FSi}+m_{NU}N_{FUi}\right)-\beta_4 H_U A_{Qi}-b_A A_{Qi},\\
\frac{dA_{Fs}}{dt} &= \beta_4\left(H_U-p^A H_{Ui}\right)A_{Qs}-\theta_{TT}\frac{I_{TU}}{T_{TU}}A_{Fs}-\sigma_A A_{Fs},\\
\frac{dA_{Fi}}{dt} &= \beta_4 H_U A_{Qi}+p^A\beta_4 H_{Ui}A_{Qs}+\theta_{TT}\frac{I_{TU}}{T_{TU}}A_{Fs}-\sigma_A A_{Fi}.
\end{aligned}
\tag{5.8}
$$

$$
\begin{aligned}
\frac{dH_{Ss}}{dt} &= a_S H_S\left(1-q_S H_S\right)-\left(q^L\beta_1 L_{Qi}+q^{N1}\beta_2 N_{Qi}\right)H_{Ss}-b_S H_{Ss},\\
\frac{dH_{Si}}{dt} &= \left(q^L\beta_1 L_{Qi}+q^{N1}\beta_2 N_{Qi}\right)H_{Ss}-\gamma_S H_{Si}-b_S H_{Si},
\end{aligned}
\tag{5.9}
$$

$$\frac{dH_{Sr}}{dt} = \gamma_S H_{Si} - b_S H_{Sr}.$$

$$\begin{aligned}
\frac{dH_{Us}}{dt} &= a_U H_U \left(1 - q_U H_U\right) - \left(q^{N2}\beta_3 N_{Qi} + q^A \beta_4 A_{Qi}\right) H_{Us} - b_U H_{Us}, \\
\frac{dH_{Ui}}{dt} &= \left(q^{N2}\beta_3 N_{Qi} + q^A \beta_4 A_{Qi}\right) H_{Us} - \gamma_U H_{Ui} - b_U H_{Ui}, \\
\frac{dH_{Ur}}{dt} &= \gamma_U H_{Ui} - b_U H_{Ur}.
\end{aligned} \tag{5.10}$$

Here, $H_S = H_{Ss} + H_{Si} + H_{Sr}$ and $H_U = H_{Us} + H_{Ui} + H_{Ur}$ denote the total population density of small mammals and ungulates, respectively, $I_{TS} = L_{Fi} + N_{FSi}$ and $I_{TU} = N_{FUi} + A_{Fi}$ represent the total infected ticks feeding on small mammals and ungulates, respectively, and $T_{TS} = L_{Fs} + L_{Fi} + N_{FSs} + N_{FSi}$ and $T_{TU} = N_{FUs} + N_{FUi} + A_{Fs} + A_{Fi}$ represent the total ticks feeding on small mammals and ungulates, respectively. We assume four methods of transmission: host to tick, tick to host, vertical transmission and non-systemic transmission (co-feeding). The first three transmission routes are as described in Rosá and Pugliese (2007) [83] with host-tick transmission coefficients p^L, p^{N1}, p^{N2} and p^A for each respective class of tick; tick to host transmission coefficients q^L, q^{N1}, q^{N2} and q^A for each respective class of tick and for vertical transmission a proportion ρ of larvae reproduced from feeding infected adult ticks remain infected. Ticks acquire infection through non-systemic transmission (co-feeding ticks) during feeding with transmission coefficient θ_{TT} and at a rate dependent on the ratio between infected

Table 5.3: Baseline parameter values for the model including infection and their biological meaning.

$p^L = p^{N1} = p^{N2} = p^A = 0.2$	Infected host to tick transmission coefficient.
$q^L = q^{N1} = 0.000005$	Infected tick to small mammal transmission coefficient.
$q^{N2} = q^A = 0.0001$	Infected tick to ungulate host transmission coefficient.
$\rho = 0.2$	Vertical transmission proportion.
$\theta_{TT} = 0.1$	Non-systemic transmission coefficient (co-feeding).
$\gamma_S = 0.01$	Recovery rate of infected small mammal hosts.
$\gamma_U = 0.01$	Recovery rate of infected ungulate hosts.
$a_S = 0.1$	Maximum birth rate of small mammal hosts.
$a_U = 0.05$	Maximum birth rate of ungulate hosts.
$b_S = 1/1825$	Natural death rate of small mammal hosts.
$b_U = 1/5475$	Natural death rate of ungulate hosts.

ticks and total ticks feeding on a specific host.

We choose parameter values (see Table 5.3) such that infection persists in all hosts and ticks and so that the seroprevalence in both host types was approximately 30% for baseline parameter values, which has been seen in field situations for tick-borne infections [201] (see Figure 5.11). These parameter values are not intended to represent a specific tick-host disease but rather highlight the trends in the epidemiological dynamics as host dynamics change.

5.4.1 Results for the model with infection

We vary the small mammal and ungulate host density to determine their effect on the epidemiological dynamics and disease prevalence (see Figure 5.8, 5.9 and 5.10). We define the prevalence in ticks as the infected density divided by the total density and the seroprevalence in hosts as the infected and recovered density divided by total density. An increase in the density of ungulate hosts leads to an increase in seroprevalence in small mammal hosts, which saturates at high ungulate densities, and a decrease in the seroprevalence in ungulate hosts (Figure 5.8). Similarly, an increase in density for small mammals leads to an increase in seroprevalence in ungulate hosts, which saturates at high small mammal densities, and a decrease in the seroprevalence in small mammals. Here, the increase in ungulate host density results in the overburden of ticks on small mammals, therefore increasing the small mammal prevalence, while the increase in small mammal density shifts the overburden onto ungulate hosts, therefore increasing the prevalence in ungulate hosts. For the tick infection dynamics an increase in ungulate host density increases the prevalence for all tick stages up to a host density where the prevalence then saturates. An initial increase in small mammal density from low levels increases the prevalence in ticks, but this then decreases and tends to a constant level for further increases in small mammal density. A key result is that our model framework can capture variation in host seroprevalence due to changes in host composition. In particular, changes to small mammal and ungulate density can lead to a wide range of seroprevalence levels for ungulate hosts in the model (Figure 5.8) and may therefore be able to explain the variation in prevalence observed in the field [185].

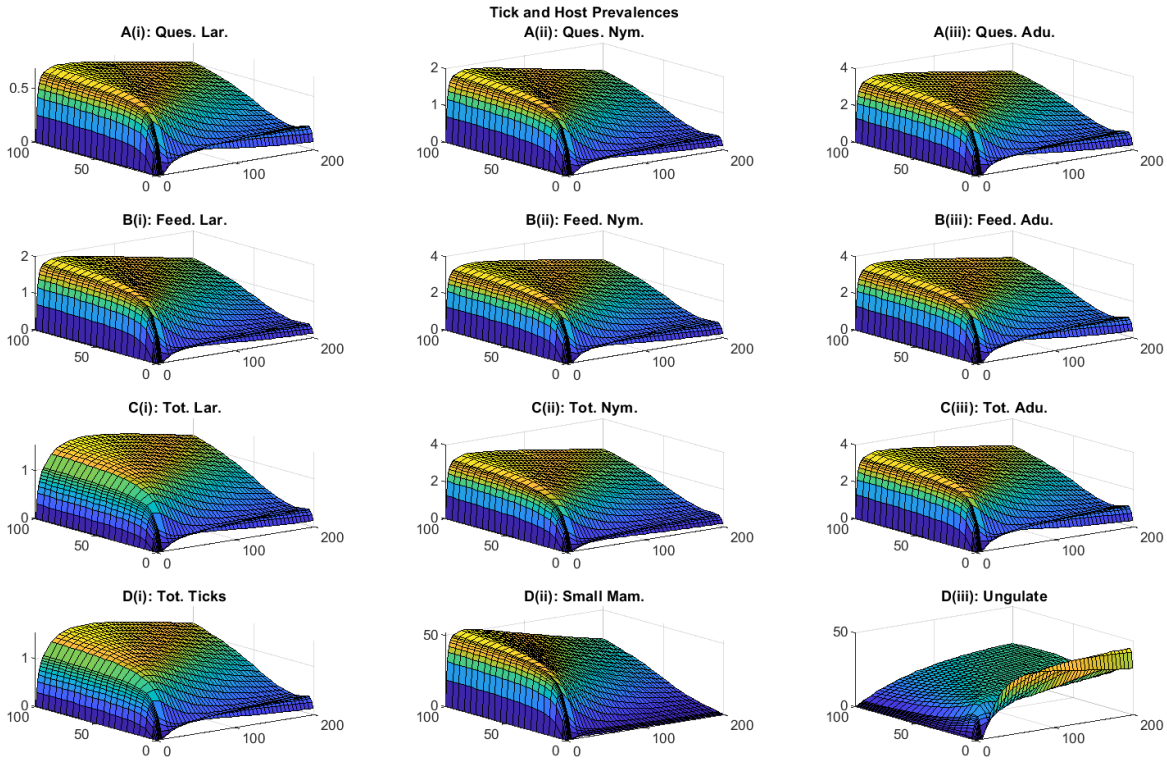

Figure 5.8: Steady state prevalence and seroprevalence (%) levels for ticks and hosts when varying the ungulate host density (from 0 to 100) and small mammal host density (from 0 to 200) under the model framework with infection seen in Section 5.4. The prevalence levels are shown for (A) questing ticks, (B) feeding ticks and (C) total ticks of a given stage with (D) showing (i) total tick prevalence, (ii) small mammal host seroprevalence and (iii) ungulate host seroprevalence. In plots (A-C) the prevalence levels of the (i) larvae, (ii) nymph and (iii) adult stage of tick are shown. When not varied in the figure parameters are as in Table 5.2 and 5.3.

When fixing the ungulate host density and increasing the small mammal density we see an initial increase in the questing larvae density (see Figure 5.6) which results in an initial increase in the infected questing larvae density and questing larvae prevalence (see Figures 5.9 and 5.10). Further increase in small mammal density then decreases the questing larvae class and consequentially the infected questing larvae class. This therefore decreases the prevalence in small mammal hosts as there are less infected questing larvae and more small mammals. Upon further increases in small mammal density the prevalence in small mammals decreases to a constant level. Here, the decrease in infected ticks feeding on small mammals (questing larvae and nymphs) is stronger than the respective increase in small mammal density meaning the transmission of infection to infected small mammal hosts decreases. The decrease in infected questing larvae balances the increase in small mammal density leading to a constant transmission of

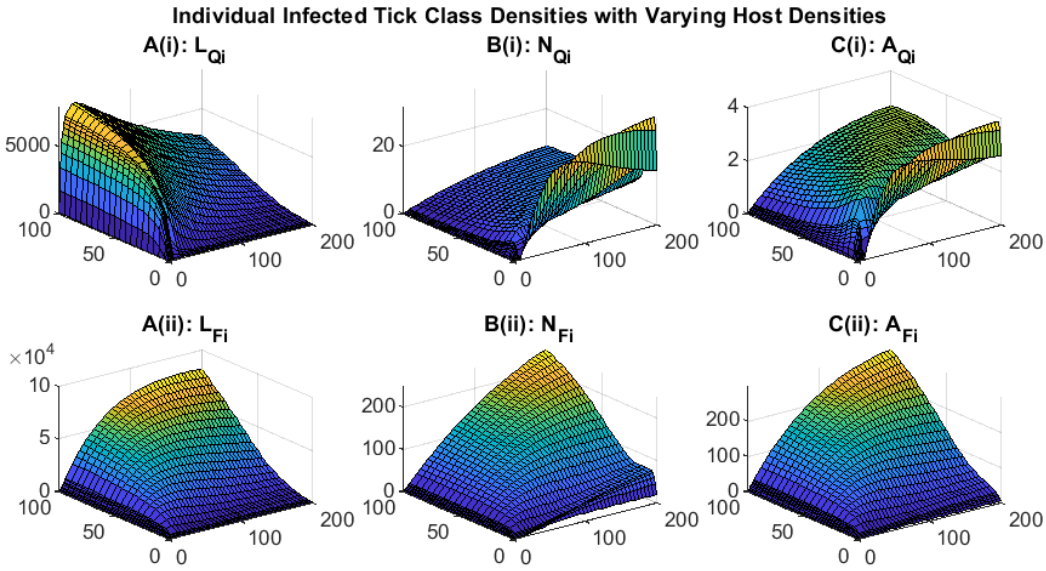

Figure 5.9: Steady state densities for the infected stages of tick when varying the ungulate host density (from 0 to 100) and small mammal host density (from 0 to 200) under the model framework with infection seen in Section 5.4. Densities are shown for (A) the questing class of ticks and (B) the feeding class of ticks and for the (i) larvae, (ii) nymph and (iii) adult stage of tick. When not varied in the figure parameters are as in Table 5.2 and 5.3.

infection and therefore prevalence and density of infected small mammals (see Figures 5.8 and 5.10). As in the model without infection, an increase in small mammal density increases the rate of attachment for questing larvae, therefore increasing the density of infected feeding larvae. Further increase in small mammal density results in the saturation of the feeding larvae density (see Figure 5.6), which would mean a saturation in infected larvae. However, with the density of infected small mammals reducing to constant levels at high small mammal density, the transmission from infected hosts to susceptible questing larvae ($p^L\beta_1 H_{Si} L_{Qs}$) decreases with an increase in small mammal density (the susceptible questing larvae density decreases with an increase in small mammal density). Therefore, the infected feeding larvae density decreases with a further increase in small mammal density before settling to a constant level. As the density of infected feeding larvae exhibits similar behaviour to the total feeding larvae class in the model without infection (see Figure 5.6) but with a decrease to constant levels, the infected questing nymph density also experiences similar behaviour to the total nymph density seen in the model without infection but also with a decrease in density to constant levels upon further increases in small mammal density. This effect is seen for all subsequent classes when small mammal density is further increased. As

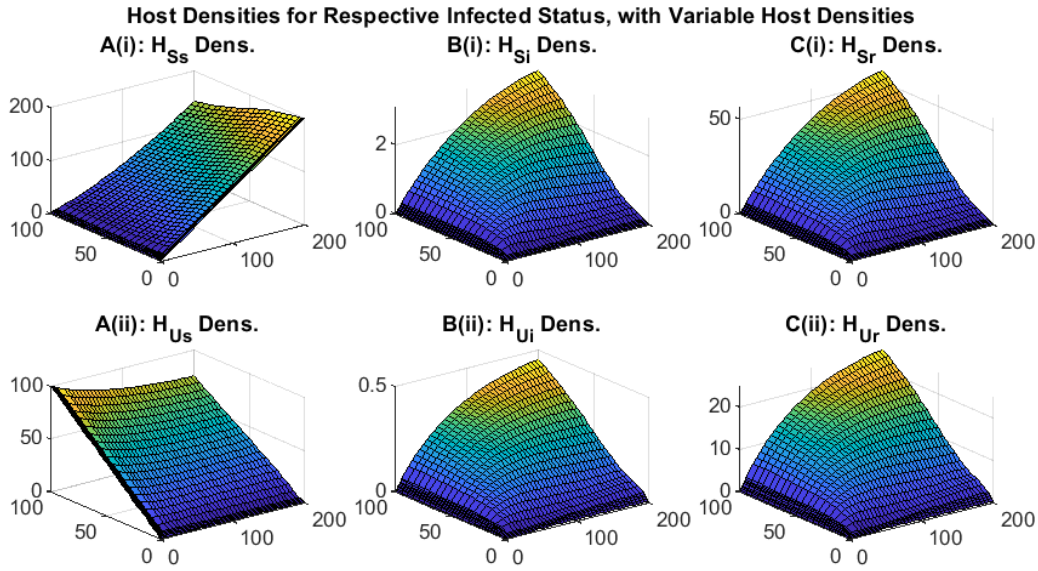

Figure 5.10: Steady state densities for the different classes of hosts when varying the ungulate host density (from 0 to 100) and small mammal host density (from 0 to 200) under the model framework with infection seen in Section 5.4. Densities are shown for (A) small mammal hosts and (B) ungulate hosts and for the different infection status' of (i) susceptible, (ii) infected and (iii) recovered. When not varied in the figure parameters are as in Table 5.2 and 5.3.

this is seen for both infected questing nymphs and infected questing adults, the infected and recovered ungulate host densities also experience this decrease to constant levels albeit much less noticeable. This explains the decrease in seroprevalence for ungulate hosts for fixed ungulate density and an increase in small mammal density.

When fixing the small mammal host density and increasing the ungulate host density the total questing larvae density, and therefore infected questing larvae density, increases and saturates at high ungulate densities (see Figure 5.9). This results in the increase in density of infected small mammal hosts and therefore their prevalence (as the total small mammal density is assumed constant) (see Figures 5.8 and 5.10). The increase in density of questing larvae means an increase in density of feeding larvae and therefore infected feeding larvae density which saturates at high ungulate density as the density of infected small mammal hosts also saturates here. Here, the density of infected feeding larvae does not decrease to constant levels as the transmission of infection does not decrease with a saturation of infected small mammals. As the trends seen for infected feeding larvae are similar to those seen in the model without infection (see Figure 5.6) when increasing ungulate density, the subsequent infected classes also

exhibit similar behaviour to the model simulations without infection. The decrease to constant levels in infected questing nymph and adult density means that the density of infected ungulate hosts saturate at high densities of total ungulate hosts. Unlike the behaviour seen for small mammals, the infected density of ungulates does not decrease to constant levels with further increases in ungulate host density. Here, the density of nymph and adult ticks are much smaller than the density of larvae, meaning the decrease in density of nymphs and adults as the density of ungulates is increased does not outweigh the increase in ungulate density. Therefore, the progression from susceptible ungulate host to infected ungulate host does not decrease as the density of ungulate hosts increase. Consequentially, the density of infected ticks does not decrease to constant levels with a further increase in ungulate host density. With low densities of small mammal hosts the transmission from hosts to the nymph stage of ticks is limited to the over abundant ungulate hosts and so the infected feeding nymph density saturates quickly as ungulate density increases. For higher fixed small mammal densities, the transmission from hosts to the nymph stage is less limited to ungulate hosts, as they are not as abundant in comparison to small mammal hosts. As a result, the saturating effect in infected ungulate hosts, infected feeding nymphs and infected feeding adults is slower and requires a greater increase in ungulate hosts.

5.5 Discussion

In this chapter we have modified and extended previous established model studies to further examine the relationship between tick and host density and the implication for tick-borne infections. By comparing different model formulations that link tick density to host density we show that the relationship between ticks and hosts can have a significant impact on the population dynamics. Lou et al. (2014) [197] compared three different host seeking behaviours: frequency-dependent, density-dependent and Holling type-II model forms to explore their implications on tick-borne disease persistence and control. They determined that a decrease in rodent density under a frequency-dependent model would have negative consequences on containing the disease but that reducing or increasing the density of rodent hosts in the other two model

frameworks can have more complex effects. In our model where tick density was limited through birth, which was dependent on tick burden and host density, the relationship between host density and tick density was linear (Section 5.2.1). Rosá and Pugliese (2007) [83] considered different tick stages which fed on different hosts and showed that when the density of ticks is dependent upon host density but independent of host type, tick density will continue to increase for an increase in density of one host type and fixed density in the other. However, our new model form (Section 5.3) in which the density of ticks is dependent upon host density and the development stages of ticks are dependent upon a specific host type then saturation of tick density can occur due to restrictions caused by a fixed host type when the other host increases in density. This confirms the findings of Cobbold et al. (2015) [196], which examined strategies to manage tick density (but did not consider infectious disease) and had a similar density-dependent link between ticks and specific hosts as our proposed model (Section 5.3). A key finding of our model study is that tick density can saturate due to restrictions in a specific host type, therefore showing that host composition is an important driver of tick density and should be considered in tick-host models.

Our results highlighting how tick development linked to specific host density can impact the host tick population dynamics will also have important consequences for the epidemiological dynamics of tick-borne infections. We show that increases in the density of specific hosts can lead to an initial increase in disease prevalence in ticks and hosts but that disease prevalence can decrease at higher host levels. Norman et al. (1999) [82] focused on determining the host density thresholds that would support tick-borne infection but also showed, similar to our findings, that a change in host carrying capacity can have both amplification and dilution effects on pathogen prevalence. In general, our model study shows that increases in ungulate host density increase the prevalence of infection in small mammals and the density of infected questing larvae. Increases in small mammal host density increase the prevalence of infection in ungulates and the density of infected questing nymphs and adults. Hence, different regional host compositions could have differing impacts on the risk of tick-borne infection to wildlife species, livestock and humans. While we assume the larval tick stages feed exclusively

on smaller hosts and adults on larger hosts, we recognise that ticks are opportunistic feeders and will feed on any host [196, 203]. However, larvae tend not to bite humans [220, 221] and nymph and adult stages can be considered to be the main threat for the spreading of infection within humans in Europe and the United States [220, 222, 223]. Therefore, high densities of infected questing nymphs and adults present the greatest risk of infection spillover in humans which, from our model simulations, corresponds to host compositions with high small mammal densities and low ungulate host densities.

Our model study highlights how different host densities and host compositions can drive variation in the prevalence and risk of tick-borne disease. This could help to understand and explain the variance in infection levels seen for different tick-borne disease, such as Lyme disease in the UK for humans [224] and for cattle and sheep [225], for overall tick-borne pathogen prevalence in Europe (where pathogens include *Borrelia miyamotoi*, *Rickettsia* spp. and *Babesia* spp.) [226], overall tick-borne pathogen prevalence in China (where pathogens include *Anaplasma phagocytophilum*, *Borrelia burgdorferi sensu stricto* and *Borrelia garinii*) [227] or for tick-borne infection (*Borrelia* spp., *Rickettsia* spp., and *Anaplasma* spp.) in small mammals in Mongolia [228]. This study suggests regions of higher disease incidence in humans or livestock could be due to high population levels of small mammals and limited ungulate hosts. As well as increased densities in questing nymphs and adults, the limitation in ungulate hosts means these tick stages would be more likely to find alternative forms of hosts, which would include humans or livestock. Meanwhile, differing ungulate host density levels could explain the trends in tick-borne infection seen in small mammals where high ungulate densities could lead to an increased incidence of infection in small mammals.

A tick-borne infection which is of current importance is Crimean-Congo haemorrhagic fever virus which causes severe disease in humans and has an increasing incidence at the global scale [229, 230]. In wildlife systems the seroprevalence of CCHFv virus shows significant variation across the different regions of Spain (see Figure 5.11). We acknowledge that climate variability, different environmental factors or habitats could impact the abundance of ticks and prevalence of tick-borne disease [204, 231, 232, 233,

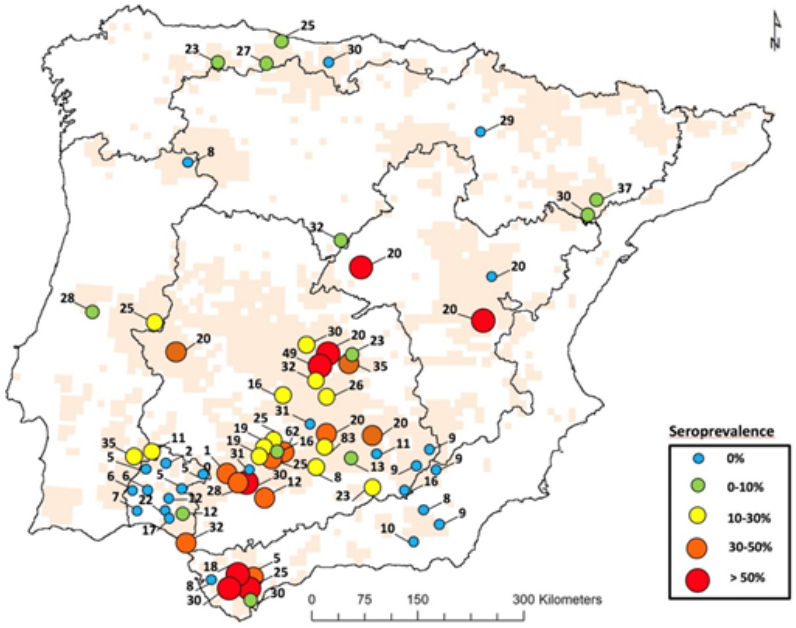

Figure 5.11: Seroprevalence (%) levels of Crimean Congo Haemorrhagic fever virus (CCHFv) in deer across regions in Spain. This figure has been provided by IREC, Spain.

234, 235]. However, densities of hosts can also be linked to environmental conditions and habitats [236, 237, 233, 235] and our model study indicates that host composition could have a strong impact on the seroprevalence of infection across different hosts of ticks. As part of a future research study, we hope that our general model framework can be adapted to represent the CCHFv system in Spain and used to explore whether specific host density and host composition can explain the variance in prevalence in CCHFv. We hope that this research could be used to manage hosts and therefore tick densities to reduce the risk of zoonotic spread of tick-borne disease to humans and livestock.

Chapter 6

Conclusion

Each chapter in this thesis is a distinct piece of work, the majority of which have been published, and each chapter contains a detailed discussion. Therefore, this conclusion briefly summarises the key methods used in each chapter and the key findings from each piece of work. It also highlights the wider significance of the work and discusses it with reference to current developments for the specific epidemiological systems we consider in this thesis.

This thesis has demonstrated how mathematical models can be used to explore and understand the dynamics of a range of biological and epidemiological systems. We have used ODE frameworks to explore the key routes of transmission that promote the persistence of the highly virulent African swine fever infection. The model also allowed us to test control strategies that could limit ASF outbreaks and its persistence. The modelling techniques were extended to consider the impact of an ASF outbreak on endemic tuberculosis in wild boar. The generality of the model framework meant that the results could add new perspective on the coexistence of multiple pathogens. The work exploring the persistence of ASF motivated a general model study to explore how the epidemiological characteristics of a disease would impact the mean pathogen extinction time and required the use of suite of stochastic continuous-time Markov chain models. The final research chapter of this thesis considered how ungulates contribute to tick-borne infections. We developed a model framework that expanded on previously studied models to incorporate the regulation of tick density based on the density of

the specific hosts on which different tick stages feed. Our new model framework was extended to include tick-borne infection to examine how host density and composition could account for variation of tick-borne prevalence and incidence levels.

6.1 Contribution and significance

Our model study exploring the persistence of African swine fever highlighted how the severity of an infectious outbreak depended on density-dependent infection transmission but that the long-term persistence of infection required a contribution from a slowly decaying environmental source of infection (infected carcasses) and from a survivor class that may be subject to reinfection. While the survivor class had been observed in the field there was limited information on the role and significance of this class of wild boar individuals, which survive the initial wave of infection [40]. Our model study suggested that individuals which survived the initial infection and could revert to an infected status at a later stage were key for the persistence of ASF. Our model was also used to test the impact of supplementary feeding and control measures, such as culling and the removal of carcasses, on ASF prevalence. We found that a combination of these control measures and their early implementation led to a reduction in ASF prevalence and to its potential eradication. We also highlighted how supplemented feeding boosted host density and led to a more severe outbreak and enhanced persistence of ASF.

Our work has been included in key European Food Safety Authority (EFSA) reports that aim to outline the key epidemiological properties of ASF and the methods to monitor and control ASF [238, 239]. Our study was used to highlight the possible interference of wild boar feeding with ASF control, due to higher underlying wild boar densities and longer breeding seasons associated with supplemented feeding, suggesting this should be examined in the field [238]. It also contributed to the debate on the persistence of ASF and the role of asymptomatic spread and virus shedding [239]. In addition to our contribution to EFSA reports our work has also been used to explain the role of wild boar in the spread of ASF in China [240], South Korea [241, 242], Japan [243, 244], Poland [245] and other countries. Our findings have been used to highlight

potential methods to control ASF outbreaks [241, 240] and how the removal of infected carcasses can reduce the severity and duration of an ASF outbreak [242]. Our work has also been used to highlight how a potential ASF outbreak in wild boar populations could lead to a devastating decrease in population abundance in some regions of Japan [243].

The ASF situation has developed further since our work exploring its persistence, with the European affected countries now including Belarus, Belgium, Bulgaria, Estonia, Germany, Greece, Hungary, Latvia, Lithuania, Moldova, Poland, Romania, Russia, Serbia, Slovakia, and Ukraine [238, 246]. For countries such as Bulgaria and Hungary the epidemic has expanded, with stagnation being seen in Latvia and Lithuania [238]. In Estonia ASF is experiencing infection fade-out, whilst Belgium and Greece have successfully controlled the infection [238]. Wild boar have been identified as one of the main catalysts in the spread of ASF as well as posing a risk to backyard farms, with higher wild boar densities increasing the risk of infection spread to domestic pigs [238, 247]. Three other factors have been identified as topics of interest in understanding the spread and control of ASF. These include the seasonality of ASF, the survival of the infection in wild boar carcasses and the role of vectors, including stable flies, in the transmission of ASF [246, 247]. Summer peaks in ASF outbreaks have been observed in domestic pig populations, whilst cases in wild boar decline in the summer but increase in the winter months [248, 249, 238, 239, 247]. It is speculated that the cases in wild boar increase in winter months due to the prolonged survival time of infection in carcasses during winter months [238], which correlates well with our model study findings relating to wild boar carcasses.

ASF is considered endemic in many African countries but is not currently present in South America [250]. In Asia, the infection was introduced in 2018, spreading from Russia into the north-east area of China [251, 252]. It has since spread through China and into Cambodia, Hong Kong, India, Indonesia, Laos, Mongolia, Myanmar, North Korea, Papua New Guinea, the Philippines, South Korea, Timor-Leste, and Vietnam [253, 241, 251, 254]. Cambodia, Mongolia, Myanmar, and Hong Kong have no fur-

ther reports on ASF outbreaks, indicating the control or eradication of ASF here [251]. Many countries, such as Kazakhstan, are currently free from ASF [254]. However, it is recommended that these countries develop strong biosecurity practices to prevent future ASF outbreaks [254, 252]. Contrary to the situation in Europe, there is no visible link for the transmission of ASF from wild boar to domestic pigs in China [252]. Instead, supplemented feeding has been identified as one of the main risk factors in the persistence and spread of ASF with ticks also suggested as a cause for ASF transmission and spread [252]. Future work could examine the role of vectors on the spread of ASF in wild boar, both within wild boar populations and to domestic pig populations. Our strategic model would provide a sound framework to test the importance of vector transmission.

The work exploring the effect of introducing an emerging disease, ASF, to an endemic infection, tuberculosis, adds new context to the coexistence of multiple pathogens. Previous studies have shown that when only density-dependent transmission is used the pathogen with the highest basic reproductive number will out-compete the other pathogen, and that disease-induced mortality can suppress the density of hosts such that only one pathogen can be maintained [10, 142]. Our work shows that when you include both density-dependent and frequency-dependent forms of transmission the corresponding contribution to the pathogens reproductive number from frequency-dependent transmission may not drop below unity as the density of hosts decreases. This would therefore allow multiple pathogens to be maintained provided the transmission coefficients are sufficiently high. When modelling the interaction between TB and ASF, we find that the introduction of ASF into the TB wild boar system leads to a significant drop in density for infected TB individuals and in the prevalence of TB. While an ASF outbreak may be devastating for wild boar population levels, its impact on TB epidemiology may provide a window of opportunity to control TB in one of the main reservoir populations (wild boar) across Europe.

Our work exploring the role of individuals chronically infected with ASF on disease persistence motivated a more general study that investigated how the characteristics of

infection would affect the mean time to extinction of a pathogen. Here, we considered a stochastic model framework to explore the role of exposed and chronically infected individuals in extensions of classical SIS and SIR models. We showed that an exposed class would generally extend the time to disease extinction and thereby make the infection more difficult to eradicate. Chronically infected individuals either increase or decrease pathogen persistence depending on the specific parameter values. The correct parametrisation of such models and the inclusion of multiple transmission pathways has been shown to be key to understand control strategies for infectious disease systems [255]. Our study has implications for understanding and controlling specific infectious disease in wildlife and humans where the epidemiological characteristics may include exposed or chronic infection.

In this thesis we also examined how ungulate density may impact tick-borne infections. We extended previous model frameworks [83, 84], to develop a model which adds new perspective on the dynamics between ticks and hosts, by having a dynamic regulation of ticks where progression from each tick developmental stage is dependent on the density of the specific hosts upon which they are most likely to feed. This allowed us to explore a key question of how host density and host composition would affect tick density and the prevalence and persistence of tick-borne infection. The model results predict that large densities of ungulate hosts would produce more questing larvae ticks while large densities of small mammals would produce more questing nymphs and adults and this has implications for infection transmission. A key finding is that high small mammal densities pose an increased risk of infection to humans, as this drives an increase in infected questing nymphs and adults which are then more likely to feed on human hosts.

The infection model framework can be applied to specific systems of infection providing a greater understanding of the epidemiological dynamics of tick-borne diseases at a wildlife interface. Through collaboration with field biologists and infectious disease experts in Spain, future work will parametrise our general model framework to be representative of the Crimean-Congo Haemorrhagic fever virus system in Spain. Using this model, we aim to capture and explain the variance in CCHFv prevalence seen across

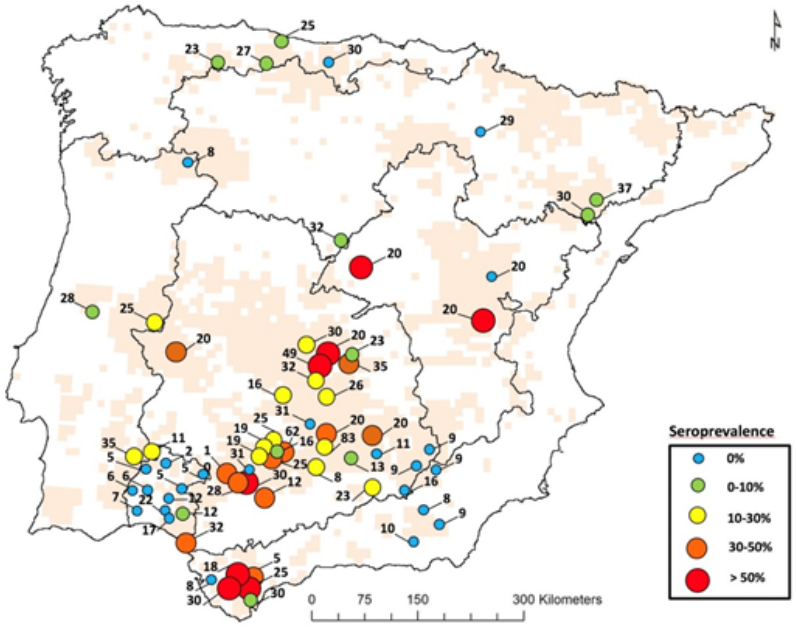

Figure 6.1: Seroprevalence (%) levels of Crimean-Congo Haemorrhagic fever virus (CCHFv) in deer across regions in Spain. This figure has been provided by IREC, Spain.

the country (see Figure 6.1). We will assess whether host density, host composition and host health (correlated with the average tick burden of hosts) can account for the variation in prevalence in ungulate hosts observed in Spain. This information can then be used to suggest how different environments can influence the infection incidence of CCHFv in humans, inform policy and develop management strategies on how to reduce the impact of this tick-borne infection.

Our knowledge and understanding of wildlife diseases is limited resulting in a scarcity of data available to help model the relevant epidemiological systems [8]. This presented a challenge for the models developed in this thesis. For African swine fever this arose from the limited information with regards to transmission routes, and what could contribute to the spread of ASF [100, 246, 247]. When modelling tick-host interactions, it can be hard to determine how successful a tick can be in attaching onto hosts, or in progressing from feeding to questing tick whilst under field conditions [199, 203, 83, 200]. With these further pieces of information, the modelling of the relevant systems could become clearer and be more accurate in predicting the future spread of disease or in understanding tick-host interactions.

In summary, we believe the work in this thesis has highlighted how mathematical models are important tools for understanding epidemiological dynamics in wildlife systems. They are particularly important as the data available for many wildlife diseases can be limited [8]. Mathematical models can be used to develop and test management strategies that can be implemented in the field to control infectious disease and our model frameworks have had an impact on the management of key, current, endemic and emerging diseases in wildlife systems.

Bibliography

[1] A.K. Wiethoelter, D. Beltrán-Alcrudo, R. Kock, and S.M. Mor. Global trends in infectious diseases at the wildlife-livestock interface. *Proc. Natl. Acad. Sci. U.S.A.*, 112(31):9662–9667, 2015.

[2] K. Jones, N.G. Patel, M.A. Levy, A. Storeygard, D. Balk, J.L. Gittleman, and P. Daszak. Global trends in emerging infectious diseases. *Nature*, 451(7181):990–993, 2008.

[3] M.B. Joseph, J.R. Mihaljevic, A.L. Arellano, J.G. Kueneman, D.L. Preston, P.C. Cross, and P.T. Johnson. Taming wildlife disease: bridging the gap between science and management. *Journal of Applied Ecology*, 50(3):702–712, 2013.

[4] C. Gortázar, I. Díez-Delgado, J.A. Barasona, J. Vicente, J. de la Fuente, and M. Boadella. The wild side of disease control at the wildlife-livestock-human interface: a review. *Frontiers in Veterinary Science*, 1:27, 2015.

[5] R. Coker, J. Rushton, S. Mounier-Jack, E. Karimuribo, P. Lutumba, D. Kambarage, D.U. Pfeiffer, K. Stärk, and M. Rweyemamu. Towards a conceptual framework to support one-health research for policy on emerging zoonoses. *Lancet Infect. Dis.*, 11:326–331, 2011.

[6] N.E. Trimmel and C. Walzer. Infectious wildlife diseases in Austria—a literature review from 1980 until 2017. *Frontiers in Veterinary Science*, 7:3, 2020.

[7] C. Gortázar, L.A. Reperant, T. Kuiken, J. de la Fuente, M. Boadella, B. Martínez-Lopez, F. Ruiz-Fons, A. Estrada-Peña, C. Drosten, G. Medley, R. Ostfeld, T. Peterson, K.C. VerCauteren, C. Menge, M. Artois, C. Schultsz, R. Delahay, J. Serra-Cobo, R. Poulin, F. Keck, A.A. Aguirre, H. Henttonen, A.P. Dobson, S. Kutz,

J. Lubroth, and A. Mysterud. Crossing the interspecies barrier: Opening the door to zoonotic pathogens. *PLOS Pathogens*, 10(7):e1004296, 2014.

[8] H.A. McCallum. Models for managing wildlife disease. *Parasitology*, 143(7):805–820, 2016.

[9] R. Ross and H.P. Hudson. An application of the theory of probabilities to the study of a priori pathometry - Part II. *Proc. R. Soc. Lond.*, 93(650):212–225, 1917.

[10] R.M. Anderson and R.M. May. Population biology of infectious diseases. *Nature*, 280:361–367, 1979.

[11] D.L. DeAngelis and V. Grimm. Individual-based models in ecology after four decades. *F1000Prime Reports*, 6(39):6, 2014.

[12] S.F. Railsback and V. Grimm. *Agent-Based and Individual-Based Modeling: A Practical Introduction, Second Edition*. Princeton University Press, 2019.

[13] L. Willem, F. Verelst, J. Bilcke, N. Hens, and P. Beutels. Lessons from a decade of individual-based models for infectious disease transmission: a systematic review (2006-2015). *BMC Infectious Diseases*, 17(612):16, 2017.

[14] A. Endo, E. van Leeuwen, and M. Baguelin. Introduction to particle Markov-chain Monte Carlo for disease dynamics modellers. *Epidemics*, 29:100363, 2019.

[15] S. Funk, A. Camacho, A.J. Kucharski, R.M. Eggo, and W.J. Edmunds. Real-time forecasting of infectious disease dynamics with a stochastic semi-mechanistic model. *Epidemics*, 22:56–61, 2018.

[16] T. Toni, D. Welch, N. Strelkowa, A. Ipsen, and M.P.H. Stumpf. Approximate Bayesian computation scheme for parameter inference and model selection in dynamical systems. *J. R. Soc. Interface*, 6:187–202, 2009.

[17] H. McCallum. Disease and the dynamics of extinction. *Philosophical Transactions of the Royal Society B*, 367:2828–2839, 2012.

[18] X. O'Neill, A. White, F. Ruiz-Fons, and C. Gortázar. Modelling the transmission and persistence of African swine fever in wild boar in contrasting European scenarios. *Scientific Reports*, 10(5895):10, 2020.

[19] C. Probst, A. Globig, B. Knoll, F.J. Conraths, and K. Depner. Behaviour of free ranging wild boar towards their dead fellows: potential implications for the transmission of African swine fever. *Royal Society Open Science*, 4(5), 2017.

[20] N.C. Grassly and C. Fraser. Mathematical models of infectious disease transmission. *Nat. Rev. Microbiol.*, 6:477–487, 2008.

[21] M. Apollonio, R. Andersen, and R. Putman. European ungulates and their management in the 21st century. Cambridge University Press. *Mammalian Biology*, 75(5):474, 2010.

[22] G. Massei, J. Kindberg, A. Licoppe, D. Gačić, N. Šprem, J. Kamler, E. Baubet, U. Hohmann, A. Monaco, J. Ozoliņš, S. Cellina, T. Podgórski, C. Fonseca, N. Markov, B. Pokorny, C. Rosell, and A. Náhlik. Wild boar populations up, numbers of hunters down? A review of trends and implications for Europe. *Pest Management Science*, 71(4):492–500, 2015.

[23] J.M. Milner, C. Bonefant, A. Mysterud, J.M. Gaillard, S. Csányi, and N.C. Stenseth. Temporal and spatial development of red deer harvesting in Europe: biological and cultural factors. *Journal of Applied Ecology*, 43(4):721–734, 2006.

[24] A.M. Valente, P. Acevedo, A.M. Figueiredo, C. Fonseca, and R.T. Torres. Overabundant wild ungulate populations in Europe: management with consideration of socio-ecological consequences. *Mammal Review*, 50:353–366, 2020.

[25] P. Cwynar, J. Stojkov, and K. Wlazlak. African swine fever status in Europe. *Viruses*, 11(4):310–327, 2019.

[26] C. Jurado, E. Fernández-Carrión, L. Mur, S. Rolesu, A. Laddomada, and J.M. Sánchez-Vizcaíno. Why is African swine fever still present in Sardinia? *Transboundary and Emerging Diseases*, 65(2):557–566, 2018.

[27] A. Laddomada, S. Rolesu, F. Loi, S. Cappai, A. Oggiano, M.P. Madrau, M.L. Sanna, G. Pilo, E. Bandino, D. Brundu, S. Cherchi, S. Masala, D. Marongiu, G. Bitti, P. Desini, V. Floris, L. Mundula, G. Carboni, M. Pittau, F. Feliziani, J.M. Sanchez-Vizcaino, C. Jurado, V. Guberti, M. Chessa, M. Muzzeddu, D. Sardo, S. Borrello, D. Mulas, G. Salis, P. Zinzula, S. Piredda, A. De Martini, and F. Sgarangella. Surveillance and control of African swine fever in free-ranging pigs in Sardinia. *Transboundary and Emerging Diseases*, 66:1114–1119, 2019.

[28] K. Depner, C. Gortázar, V. Guberti, M. Masiulis, S. More, E. Oļševskis, H-H. Thulke, A. Viltrop, G. Woźniakowski, J.C. Abrahantes, A. Gogin, F. Verdonck, and S. Dhollander. Scientific report on the epidemiological analyses of African swine fever in the Baltic states and Poland. *European Food Safety Authority Journal*, 15(11):1–59, 2017.

[29] Federal Research Institute for Animal Health. Animal disease situation: African swine fever. `https://www.fli.de/de/aktuelles/tierseuchengeschehen/afrikanische-schweinepest/`. Accessed: 2019-08-22.

[30] Y.-J. Kim, B. Park, and H.-E. Kang. Control measures to African swine fever outbreak: active response in South Korea, preparation for the future, and cooperation. *J. Vet. Sci.*, 22(1):e13, 2021.

[31] Y. Woonwong, D.D. Tien, and R. Thanawongnuwech. The future of the pig industry after the introduction of African swine fever into Asia. *Anim. Front.*, 10(4):30–37, 2020.

[32] X. Zhou, N. Li, Y. Luo, Y. Liu, F. Miao, T. Chen, S. Zhang, P. Cao, X. Li, K. Tian, H.J. Qiu, and R. Hu. Emergence of African swine fever in China, 2018. *Transboundary and Emerging Diseases*, 65(6):1482–1484, 2018.

[33] M.B. Barongo, R.P. Bishop, E.M. Févre, D.L. Knobel, and A. Ssematimba. A mathematical model that simulates control options for African swine fever virus (ASFV). *PLoS One*, 11(7):1–12, 2016.

[34] T. Vergne, F. Korennoy, L. Combelles, A. Gogin, and D.U. Pfeiffer. Modelling African swine fever presence and reported abundance in the Russian Federation

using national surveillance data from 2007 to 2014. *Spatial and Spatio-temporal Epidemiology*, 19:70–77, 2016.

[35] E. Chenais, K. Depner, V. Guberti, K. Dietze, A. Viltrop, and K. Ståhl. Epidemiological considerations on African swine fever in Europe 2014–2018. *Porcine Health Management*, 5(1):6, 2019.

[36] M.C. Gallardo, A. de la Torre Reoyo, J. Fernández-Pinero, I. Iglesias, M.J. Muñoz, and M.L. Arias. African swine fever: a global view of the current challenge. *Porcine Health Management*, 1(21):1–14, 2015.

[37] F.I. Korennoy, V.M. Gulenkin, J.B. Malone, C.N. Mores, S.A. Dudnikov, and M.A. Stevenson. Spatio-temporal modeling of the African swine fever epidemic in the Russian Federation, 2007–2012. *Spatial and Spatiotemporal Epidemiology*, 11:135–141, 2014.

[38] E. Simulundu, C.H. Lubaba, J. van Heerden, M. Kajihara, L. Mataa, H.M. Chambaro, Y. Sinkala, S.M. Munjita, H.M. Munang'andu, K.S. Nalubamba, K. Samui, G.S. Pandey, A. Takada, and A.S. Mweene. The epidemiology of African swine fever in "nonendemic" regions of Zambia (1989–2015): Implications for disease prevention and control. *Viruses*, 9(236):1–20, 2017.

[39] C. Berg, A. Bøtner, H. Browman, C. De Koeijer, M. Domingo, C. Ducrot, S. Edwards, C. Fourichon, F. Koenen, S. More, M. Raj, L. Sihvonen, H. Spoolder, J.A. Stegeman, H-H. Thulke, I. Vågsholm, A. Velarde, and P. Willeberg. African swine fever EFSA panel on animal health and welfare (AHAW). *EFSA Journal*, 13(7):101, 2015.

[40] K. Ståhl, S. Sternberg-Lewerin, S. Blome, A. Viltrop, M.L. Penrith, and E. Chenais. Lack of evidence for long term carriers of African swine fever virus - a systematic review. *Virus Research*, 272:197725, 2019.

[41] J.M. Sánchez-Vizcaíno, L. Mur, and B. Martínez-López. African swine fever: An epidemiological update. *Transboundary and Emerging Diseases*, 59:27–35, 2012.

[42] M.L. Penrith and W. Vosloo. Review of African swine fever: transmission, spread and control. *Journal of the South African Veterinary Association*, 80(2):58–62, 2009.

[43] S. More, M.A. Miranda, D. Bicout, A. Bøtner, A. Butterworth, P. Calistri, S. Edwards, B. Garin-Bastuji, M. Good, V. Michel, M. Raj, S.S. Nielsen, L. Sihvonen, H. Spoolder, J.A. Stegeman, A. Velarde, P. Willeberg, C. Winckler, K. Depner, V. Guberti, M. Masiulis, E. Oļševskis, P. Satran, M. Spiridon, H-H. Thulke, A. Vilrop, G. Woźniakowski, A. Bau, A. Broglia, J.C. Abrahantes, S. Dhollander, A. Gogin, I.M. Gajardo, F. Verdonck, L. Amato, and C. Gortázar. African swine fever in wild boar. *European Food Safety Authority Journal*, 16(7), 2018.

[44] J.A. Barasona, P. Acevedo, I. Díez-Delgado, J. Queiros, R. Carrasco-García, C. Gortázar, and J. Vicente. Tuberculosis-associated death among adult wild boars, Spain, 2009-2014. *Emerging Infectious Diseases*, 22(12):3, 2016.

[45] I. Barberis, N.L. Bragazzi, L. Galluzzo, and M. Martini. The history of tuberculosis: from the first historical records to the isolation of Koch's bacillus. *Journal of Preventative Medicine and Hygiene*, 58(1):E9–E12, 2017.

[46] M.V. Palmer and W.R. Waters. Bovine tuberculosis and the establishment of an eradication program in the United States: Role of veterinarians. *Veterinary Medicine International*, 2011:12, 2011.

[47] S. Fitzgerald and J. Kaneene. Wildlife reservoirs of bovine tuberculosis worldwide: hosts, pathology, surveillance, and control. *Veterinary Pathology*, 50:488–499, 2013.

[48] C. Gortázar, A. Che-Amat, and D. O'Brien. Open questions and recent advances in the control of a multi-host infectious disease: Animal tuberculosis. *Mammal Review*, 45:160–175, 2015.

[49] J.L. Hardstaff, G. Marion, M.R. Hutchings, and P.C.L. White. Evaluating the tuberculosis hazard posed to cattle from wildlife across Europe. *Research in Veterinary Science*, 97:S86–S93, 2014.

[50] P.C.L. White, M. Böhm, G. Marion, and M.R. Hutchings. Control of bovine tuberculosis in British livestock: there is no 'silver bullet'. *Trends in Microbiology*, 16(9):420–427, 2008.

[51] C. Gortázar, R. Delahay, R. McDonald, M. Boadella, G. Wilson, D. Gavier-Widen, and P. Acevedo. The status of tuberculosis in European wild mammals. *Mammal Review*, 42:193–206, 2012.

[52] V. Naranjo, C. Gortázar, J. Vicente, and J. De La Fuente. Evidence of the role of European wild boar as a reservoir of mycobacterium tuberculosis complex. *Veterinary Microbiology*, 127:1–9, 2008.

[53] N. Santos, C. Richomme, T. Nunes, J. Vicente, P. Alves, J. de la Fuente, M. Correia-Neves, M.-L. Boschiroli, R. Delahay, and C. Gortázar. Quantification of the animal tuberculosis multi-host community offers insights for control. *Pathogens*, 9(6):421, 2020.

[54] P. Andersen and J.S. Woodworth. Tuberculosis vaccines – rethinking the current paradigm. *Trends in Immunology*, 35(8):387–395, 2014.

[55] I. Smith. Mycobacterium tuberculosis pathogenesis and molecular determinants of virulence. *Clinical Microbiology Reviews*, 16(3):463–496, 2003.

[56] N. Fogel. Tuberculosis: A disease without boundaries. *Tuberculosis*, 95(5):527–531, 2015.

[57] S. Gagneux. Host-pathogen coevolution in human tuberculosis. *Phil. Trans. R. Soc. B*, 367(1590):850–859, 2012.

[58] C. Picasso-Risso, J. Alvarez, K. VanderWaal, A. Kinsley, A. Gil, S. Wells, and A. Perez. Modelling the effect of test-and-slaughter strategies to control bovine tuberculosis in endemic high prevalence herds. *Transboundary and Emerging Diseases*, 00:1–11, 2020.

[59] I. Schiller, R.W. Waters, M. Vordermeier, T. Jemmi, M. Welsh, N. Keck, A. Whelan, E. Gormley, M.L. Boschiroli, J.L. Moyen, C. Vela, M. Cagiola, B. Buddle,

M. Palmer, T. Thacker, and B. Oesch. Bovine tuberculosis in Europe from the perspective of an officially tuberculosis free country: Trade, surveillance and diagnostics. *Veterinary Microbiology*, 151:153–159, 2011.

[60] A. Kubik, B. Jakobsen, K. Mattfolk, K. Storup, C. Friel, A. do Jogo, X. Demarche, M. Dias, A. D'urrwanger, O. Dumitrescu, L. Gatter, M. Kerrigan, J. Kokot, M. Lanzutti, J. Otto, L. Rosca, and A. Zalega. Eradication, control and monitoring programmes to contain animal diseases. *European Court of Auditors*, 1(6):52, 2016.

[61] J. Barasona, V. VerCauteren, N. Saklou, C. Gortázar, and J. Vicente. Effectiveness of cattle operated bump gates and exclusion fences in preventing ungulate multi-host sanitary interaction. *Preventive Veterinary Medicine*, 111(1–2):42–50, 2013.

[62] M. Wilber, K. Pepin, H. Campa, S. Hygnstrom, M. Lavelle, T. Xifara, K.C. VerCauteren, and C. Webb. Modelling multi-species and multi-mode contact networks: Implications for persistence of bovine tuberculosis at the wildlife-livestock interface. *Journal of Applied Ecology*, 56(6):1471–1481, 2019.

[63] I. Díez-Delgado, I. Sevilla, B. Romero, E. Tanner, J. Barasona, A. White, P. Lurz, M. Boots, J. De La Feunte, L. Dominguez, J. Vicente, J. Garrido, R. Juste, A. Aranaz, and C. Gortázar. Impact of piglet oral vaccination against tuberculosis in endemic free-ranging wild boar populations. *Preventive Veterinary Medicine*, 155:11–20, 2018.

[64] J.L. Hardstaff, M.T. Bulling, G. Marion, M.R. Hutchings, and P.C.L. White. Modelling the impact of vaccination on tuberculosis in badgers. *Epidemiol. Infect.*, 141:1417–1427, 2013.

[65] M. Boadella, J. Vicente, F. Ruiz-Fons, J. de la Fuente, and C. Gortázar. Effects of culling Eurasian wild boar on the prevalence of Mycobacterium bovis and Aujeszky's disease virus. *Preventive Veterinary Medicine*, 107(3–4):214–221, 2012.

[66] E. Tanner, A. White, P. Acevedo, A. Balseiro, J. Marcos, and C. Gortázar. Wolves contribute to disease control in a multi-host system. *Scientific Reports*, 9:7940, 2019.

[67] European Food Safety Authority and European Centre for Disease Prevention and Control (EFSA and ECDC). The European Union one health 2018 Zoonoses report. *EFSA Journal*, 17(12):e05926, 2019.

[68] C. Gortázar, M.J. Torres, J. Vicente, P. Acevedo, M. Reglero, J. de la Fuente, J.J. Negro, and J. Aznar-Martín. Bovine tuberculosis in Doñana biosphere reserve: The role of wild ungulates as disease reservoirs in the last Iberian lynx strongholds. *PLoS One*, 3(7):e2776, 2008.

[69] N. Santos, M. Correia-Neves, S. Ghebremichael, G. Källenius, S.B. Svenson, and V. Almeida. Epidemiology of Mycobacterium bovis infection in wild boar (*Sus scrofa*) from Portugal. *Journal of Wildlife Diseases*, 45(4):1048–1061, 2009.

[70] J. Vicente, U. Höfle, J.M. Garrido, I.G. Fernández-de Mera, R. Juste, M. Barra, and C. Gortázar. Wild boar and red deer display high prevalences of tuberculosis-like lesions in Spain. *Veterinary Research*, 37(1):107–119, 2006.

[71] J. Barasona, C. Gortázar, J. de la Fuente, and J. Vicente. Host richness increases tuberculosis disease risk in game-managed areas. *Microorganisms*, 7(6):182, 2019.

[72] L. Burbaitė and S. Csányi. Red deer population and harvest changes in Europe. *Acta Zoologica Lituanica*, 20:179–188, 2010.

[73] E.W. Cupp. Biology of ticks. *Vet. Clin. North Am. Small Anim. Pract.*, 21(1):1–26, 1991.

[74] J.F. Anderson and L.A. Magnarelli. Biology of ticks. *Infectious Disease Clinics of North America*, 22(2):195–215, 2008.

[75] A. Nilsson and L. Lundqvist. Host selection and movements of ixodes ricinus (acari) larvae on small mammals. *Oikos*, 31(3):313–322, 1978.

[76] S. Rahlenbeck, V. Fingerle, and S. Doggett. Prevention of tick-borne diseases: an overview. *British Journal of General Practice*, 66(650):492–494, 2016.

[77] A. Gayle and E. Ringdahl. Tick-borne diseases. *Am. Fam. Physician*, 64(3):461–466, 2001.

[78] F. Jongejan and G. Uilenberg. The global importance of ticks. *Parasitology*, 129:S3–S14, 2004.

[79] N. Perveen, S.B. Muzaffar, and M.A. Al-Deeb. Ticks and tick-borne diseases of livestock in the Middle East and North Africa: A review. *Insects*, 12(1):83, 2021.

[80] A.A. Cunningham, P. Daszak, and J.L.N. Wood. One health, emerging infectious diseases and wildlife: two decades of progress? *Phil. Trans. R. Soc. B*, 372(20160167):8, 2017.

[81] A. Michelitsch, K. Wernike, C. Klaus, G. Dobler, and M. Beer. Exploring the reservoir hosts of tick-borne encephalitis virus. *Viruses*, 11(7):669, 2019.

[82] R. Norman, R.G. Bowers, M. Begon, and P.J. Hudson. Persistence of tick-borne virus in the presence of multiple host species: Tick reservoirs and parasite mediated competition. *Journal of Theoretical Biology*, 200(1):111–118, 1999.

[83] R. Rosá and A. Pugliese. Effects of tick population dynamics and host densities on the persistence of tick-borne infections. *Math Biosci.*, 208(1):216–240, 2007.

[84] J. Switkes, B. Nannyonga, J.Y.T. Mugisha, and J. Nakakawa. A mathematical model for Crimean-Congo haemorrhagic fever: tick-borne dynamics with conferred host immunity. *Journal of Biological Dynamics*, 10(1):59–70, 2016.

[85] R. Rosá, A. Pugliese, R. Norman, and P.J. Hudson. Thresholds for disease persistence in models for tick-borne infections including non-viraemic transmission, extended feeding and tick aggregation. *Journal of Theoretical Biology*, 224(3):359–376, 2003.

[86] A. Pugliese and R. Rosá. Effect of host populations on the intensity of ticks and the prevalence of tick-borne pathogens: how to interpret the results of deer exclosure experiments. *Parasitology*, 135(13):1531–1544, 2008.

[87] L.G. Ixaru and G. Vanden Berghe. *Exponential Fitting*, chapter 6. Runge-Kutta Solvers for Ordinary Differential Equations. Springer Science, 2004.

[88] K.M. Kamina, S. Mwalili, and A. Wanjoya. The modeling of a stochastic SIR model for HIV/AIDS epidemic using Gillespie's algorithm. *International Journal of Data Science and Analysis*, 5(6):117–122, 2019.

[89] A. White, S. Bell, P. Lurz, and M. Boots. Conservation management within strongholds in the face of disease-mediated invasions: red and grey squirrels as a case study. *Journal of Applied Ecology*, 51:1631–1642, 2014.

[90] O. Diekmann, J.A.P. Heesterbeek, and M.G. Roberts. The construction of next-generation matrices for compartmental epidemic models. *J. R. Soc. Interface*, 7:873–885, 2010.

[91] M.M. Rossi and S. Ternes. Simple linearization procedure for obtaining r_0 from invasive epidemic models. *Natural Resource Modeling*, 29(4):600–609, 2016.

[92] P. van den Driessche. Reproduction numbers of infectious disease models. *Infectious Disease Modelling*, 2(3):288–303, 2017.

[93] M.J. Keeling and P. Rohani. Modelling infectious diseases in humans and animals. *Princeton Unviersity Press*, 2008.

[94] T. Halasa, A. Boklund, A. Bøtner, N. Toft, and H-H. Thulke. Simulation of spread of African swine fever including the effects of residues from dead animals. *Frontiers in Veterinary Science*, 3(6), 2016.

[95] T. Halasa, A. Bøtner, S. Mortensen, H. Christensen, S.B. Wulff, and A. Boklund. Modelling the effects of duration and size of the control zones on the consequences of a hypothetical African swine fever epidemic in Denmark. *Frontiers in Veterinary Science*, 5(49):7, 2018.

[96] L. Mur, J.M. Sánchez-Vizcaíno, E. Fernández-Carrión, C. Jurado, S. Rolesu, F. Feliziani, A. Laddomada, and B. Martínez-López. Understanding African swine fever infection dynamics in Sardinia using a spatially explicit transmission model in domestic pig farms. *Transboundary and Emerging Diseases*, 65:123–134, 2018.

[97] S. Ito, C. Jurado, J.M. Sánchez-Vizcaíno, and N. Isoda. Quantitative risk assessment of African swine fever virus introduction to Japan via pork products brought in air passengers' luggage. *Transboundary and Emerging Diseases*, 67(2):894–905, 2019.

[98] Y. Lu, X. Deng, J. Chen, J. Wang, Q. Chen, and B. Niu. Risk analysis of African swine fever in Poland based on spatio-temporal pattern and Latin hypercube sampling, 2014–2017. *BMC Veterinary Research*, 15:160, 2019.

[99] R. Liang, Y. Lu, X. Qu, Q. Su, C. Li, S. Xia, Y. Liu, Q. Zhang, X. Cao, Q. Chen, and B. Niu. Prediction for global African swine fever outbreaks based on a combination of random forest algorithms and meteorological data. *Transboundary and Emerging Diseases*, 67(2):935–946, 2020.

[100] S.S. Nielsen, J. Alvarez, D. Bicout, P. Calistri, K. Depner, J.A. Drewe, B. Garin-Bastuji, J.L.G. Rojas, V. Michel, M.A. Miranda, H. Roberts, L. Sihvonen, H. Spoolder, K. Ståhl, A. Viltrop, C. Winckler, A. Boklund, A. Bøtner, J.L.G. Rojas, S.J. More, H-H. Thulke, S-E. Antoniou, J.C. Abrahantes, S. Dhollander, A. Gogin, A. Papanikolaou, L.C.G. Villeta, and C. Gortázar. Risk assessment of African swine fever in the south-eastern countries of Europe. *EFSA Journal*, 17(11):5861, 2019.

[101] K. Petit, C. Dunoyer, C. Fischer, J. Hars, E. Baubet, J.R. López-Olvera, S. Rossi, E. Collin, M-F. Le Potier, C. Belloc, C. Peroz, N. Rose, J-P. Vaillancourt, and C. Saegerman. Assessment of the impact of forestry and leisure activities on wild boar spatial disturbance with a potential application to asf risk of spread. *Transboundary and Emerging Diseases*, 67(3):1164–1176, 2020.

[102] V. Sidorovich, A.E. Schnitzler, C. Schnitzler, I. Rotenko, and Y. Holikava. Responses of wolf feeding habits after adverse climatic events in central-western Belarus. *Mammalian Biology*, 83:44–50, 2017.

[103] R.M. Anderson and R.M. May. The population dynamics of microparasites and their invertebrate hosts. *Phil. Trans. R. Soc. Lond. B.*, 291:451–524, 1981.

[104] E. Tanner, A. White, P. Lurz, C. Gortázar, I. Díez-Delgado, and M. Boots. The critical role of infectious disease in compensatory population growth in response to culling. *American Naturalist*, 194(1):E1–E12, 2019.

[105] A. Malmsten and A.M. Dalin. Puberty in female wild boar (*Sus scrofa*) in Sweden. *Acta Veterinaria Scandinavica*, 58(55):7, 2016.

[106] O. Keuling, E. Baubet, A. Duscher, C. Ebert, C. Fischer, A. Monaco, T. Podgórski, C. Prevot, K. Ronnenberg, G. Sodeikat, N. Stier, and H. Thurfjell. Mortality rates of wild boar *Sus scrofa* L. in central Europe. *European Journal of Wildlife Research*, 59:805–814, 2013.

[107] R. Carrasco-Garcia. *Factores de riesgo de transmisión de enfermedades en ungulados cinegéticos del centro y sur de España*. PhD thesis, Instituto de Investigación en Recursos Cinegéticos, 2015.

[108] P. Acevedo, J. Vicente, H. Höfle, J. Cassinello, F. Ruiz-Fons, and C. Gortázar. Estimation of European wild boar relative abundance and aggregation: a novel method in epidemiological risk assessment. *Epidemiology and Infection*, 135(3):519–527, 2007.

[109] R. Carrasco-Garcia, P. Barroso, J. Perez-Olivares, V. Montoro, and J. Vicente. Consumption of big game remains by scavengers: A potential risk as regards disease transmission in central Spain. *Frontiers in Veterinary Science*, 5(4):10, 2018.

[110] C. Gallardo, A. Soler, R. Nieto, M.A. Sánchez, C. Martins, V. Pelayo, A. Carrascosa, Y. Revilla, A. Simón, V. Briones, J.M. Sánchez-Vizcaíno, and M. Arias. Experimental transmission of African swine fever (ASF) low virulent isolate NH/P68 by surviving pigs. *Transboundary and Emerging Diseases*, 62:612–622, 2015.

[111] E. Oļševskis, V. Guberti, M. Seržants, J. Westergaard, C. Gallardo, I. Rodze, and K. Depner. African swine fever virus introduction into the EU in 2014: Experience of Latvia. *Research in Veterinary Science*, 105:28–30, 2016.

[112] P.L. Eblé, T.J. Hagenaars, E. Weesendorpa, S. Quak, H.W. Moonen-Leusen, and W.L.A. Loeffena. Transmission of African swine fever virus via carrier (survivor) pigs does occur. *Veterinary Microbiology*, page 33, 2019.

[113] C. Probst, J. Gethmann, J. Amendt, L. Lutz, J.P Teifke, and F.J. Conraths. Estimating the postmortem interval of wild boar carcasses. *Veterinary Sciences*, 7(1):1–22, 2020.

[114] C. Probst, J. Gethmann, S. Amler, A. Globig, B. Knoll, and F.J. Conraths. The potential role of scavengers in spreading African swine fever among wild boar. *Scientific Reports*, 9(11450):13, 2019.

[115] A. Margalida and D. Ogada. Old world vultures in a changing environment. *Birds of Prey: Biology and Conservation in the XXI century*, pages 457–471, 2018.

[116] M. Boadella, P. Acevedo, J. Vicente, G. Mentaberre, A. Balseiro, M.C. Arnal, D. Martínez, I. García-Bocanegra, C. Casal, J. Álvarez, A. Oleaga, S. Lavín, M. Muñoz, J.L. Sáez-Llorente, J. de la Fuente, and C. Gortázar. Spatio-temporal trends of Iberian wild boar contact with Mycobacterium tuberculosis complex detected by ELISA. *EcoHealth*, 8(4):478–484, 2011.

[117] M. Boadella, J.F. Ruiz-Fons, J. Vicente, M. Martín, J. Segalés, and C. Gortázar. Seroprevalence evolution of selected pathogens in Iberian wild boar. *Transboundary and Emerging Diseases*, 59(5):395–404, 2012.

[118] B. Márton, D. Atilla, I.B. Csaba, and O. László. The economic impact of African swine fever on game management in the north-eastern part of pest county and Nógrád county, with special regard to the earlier experiences relating to classical swine fever eradication. *Magyar Allatorvosok Lapja*, 141:27–38, 2019.

[119] N. Beeton and H. McCallum. Models predict that culling is not a feasible strategy to prevent extinction of Tasmanian devils from facial tumour disease. *Journal of Applied Ecology*, 48:1315–1323, 2011.

[120] M. Artois, R. Delahay, V. Guberti, and C. Cheeseman. Control of infectious diseases of wildlife in Europe. *he Veterinary Journal*, 162:141–152, 2001.

[121] N.D. Barlow. Bovine tuberculosis in New Zealand: epidemiology and models. *Trends in Microbiology*, 2(4):119–124, 1994.

[122] C.A. Donnelly, R. Woodroffe, D.R. Cox, F.J. Bourne, C.L. Cheeseman, R.S. Clifton-Hadley, G. Wei, G. Gettinby, P. Gilks, H. Jenkins, W.T. Johnston, A.M. Le Fevre, J.P. McInerney, and W.I. Morrison. Positive and negative effects of widespread badger culling on tuberculosis in cattle. *Nature*, 439:843—-846, 2006.

[123] When to kill a cull: factors affecting the success of culling wildlife for disease control. Prentice, j.c. and fox, n.j. and hutchings, m.r. and white, p.c.l. and davidson, r.s. and marion, g. *J. R. Soc. Interface*, 16:20180901, 2019.

[124] F.A.M. Tuyttens, R.J. Delahay, D.W. MacDonald, C.L. Cheeseman, B. Long, and C.A. Donnelly. Spatial perturbation caused by a badger (Meles meles) culling operation: implications for the function of territoriality and the control of bovine tuberculosis (mycobacterium bovis). *Journal of Animal Ecology*, 69:815–828, 2000.

[125] S. Blome, K. Franzke, and M. Beer. African swine fever – a review of current knowledge. *Virus Research*, 287:198099, 2020.

[126] C. Jurado, M. Martínez-Avilés, A. De La Torre, M. Štukelj, H. Cardoso de Carvalho Ferreira, M. Cerioli, J. Sánchez-Vizcaíno, , and S. Bellini. Relevant measures to prevent the spread of African swine fever in the European Union domestic pig sector. *Frontiers in Veterinary Science*, 5(77):16, 2018.

[127] J. Sánchez-Vizcaíno, L. Mur, and B. Lopez. African swine fever (ASF): Five years around Europe. *Veterinary Microbiology*, 165(1–2):45–50, 2013.

[128] A. Linden, A. Licoppe, R. Volpe, J. Paternostre, C. Lesenfants, D. Cassart, M. Garigliany, M. Tignon, T. van den Berg, D. Desmecht, and A.B. Cay. Summer 2018: African swine fever virus hits north-western Europe. *Transboundary and Emerging Diseases*, 66(1):54–55, 2019.

[129] N. Mazur-Panasiuk, M. Walczak, M. Juszkiewicz, and G. Wozniakowski. The spillover of African swine fever in Western Poland revealed its estimated origin

on the basis of O174L, K145R, MGF 505-5R and IGR I73R/I329L genomic sequences. *Viruses*, 12(10):1094, 2020.

[130] A. Miteva, A. Papanikolaou, A. Gogin, A. Boklund, A. Bøtner, A. Linden, A. Viltrop, C. Gortázar, C. Ivanciu, D. Desmecht, D. Korytarova, E. Olševskis, G. Helyes, G. Woźniakowski, H.-H. Thulke, H. Roberts, J. Abrahantes, K. Ståhl, K. Depner, L. Gonzalez Villeta, M. Spiridon, S. Ostojic, S. More, T. Vasile, V. Grigaliuniene, V. Guberti, and R. Wallo. Scientific report on the epidemiological analyses of African swine fever in the European Union (November 2018 to October 2019). *EFSA Journal*, 18(1):5996, 2020.

[131] C. Sauter-Louis, J.H. Forth, C. Probst, C. Staubach, A. Hlinak, A. Rudovsky, D. Holland, P. Schlieben, M. Göldner, J. Schatz, S. Bock, M. Fischer, K. Schulz, T. Homeier-Bachmann, R. Plagemann, U. Klaaß, R. Marquart, T.C. Mettenleiter, M. Beer, F.J. Conraths, and S. Blome. Joining the club: First detection of African swine fever in wild boar in Germany. *Transboundary and Emerging Diseases*, 00:1–9, 2020.

[132] FAO Agriculture and Consumer Protection Department: Animal Production and Health. ASF situation in Asia update. `http://www.fao.org/ag/againfo/programmes/en/empres/ASF/situation_update.html`. Accessed: 2020-02-28.

[133] N. Barlow. The ecology of wildlife control: simple models revisited. *Journal of Applied Ecology*, 33:303–314, 1996.

[134] R. Woodroffe. Managing disease threats to wild mammals. *Animal Conservation*, 2(3):185–193, 1999.

[135] K. Morelle, J. Bubnicki, M. Churski, J. Gryz, T. Podgórski, and D.P.J. Kuijper. Disease-induced mortality outweighs hunting in causing wild boar population crash after African swine fever outbreak. *Frontiers in Veterinary Science*, 7:378, 2020.

[136] M. Martín-Hernando, U. Höfle, J. Vicente, F. Ruiz-Fons, D. Vidal, M. Barral, J. Garrido, J. De La Fuente, and C. Gortázar. Lesions associated with mycobac-

terium tuberculosis complex infection in the European wild boar. *Tuberculosis*, 87:360–367, 2007.

[137] M. Muñoz Mendoza, N. Marreros, M. Boadella, C. Gortázar, S. Menéndez, L. de Juan, J. Bezos, B. Romero, M. Copano, J. Amado, J. Sáez, J. Mourelo, and A. Balseiro. Wild boar tuberculosis in Iberian Atlantic Spain: a different picture from Mediterranean habitats. *BMC Veterinary Research*, 9:176, 2013.

[138] J. Vicente, J. Barasona, P. Acevedo, J. Ruiz-Fons, M. Boadella, I. Diez-Delgado, B. Beltran-Beck, D. González-Barrio, J. Queirós, V. Montoro, J. de la Fuente, and C. Gortázar. Temporal trend of tuberculosis in wild ungulates from Mediterranean Spain. *Transboundary and Emerging Diseases*, 60:92–103, 2013.

[139] L. Mur, M. Boadella, B. Martínez-López, C. Gallardo, C. Gortázar, and J. Sánchez-Vizcaíno. Monitoring of African swine fever in the wild boar population of the most recent endemic area of Spain. *Transboundary and Emerging Diseases*, 59(6):526–531, 2012.

[140] Y. Jo and C. Gortázar. African swine fever in wild boar, South Korea, 2019. *Transboundary and Emerging Diseases*, 67:1776–1780, 2020.

[141] H. Bremermann and H. Thieme. A competitive exclusion principle for pathogen virulence. *Journal of Mathematical Biology*, 27:179–190, 1989.

[142] R. Bowers and M. Boots. Baseline criteria and the evolution of hosts and parasites: D0, R0 and competition for resources between strains. *Journal of Theoretical Biology*, 223(3):361–365, 2003.

[143] M. Begon and R.G. Bowers. *Beyond Host-Pathogen Dynamics*, pages 478–509. Publications of the Newton Institute. Cambridge University Press, 1995.

[144] M. Hochberg and R. Holt. The coexistence of competing parasites. I. The role of cross-species infection. *The American Naturalist*, 136(4):517–541, 1990.

[145] S. Levin and D. Pimentel. Selection of intermediate rates of increase in parasite-host systems. *The American Naturalist*, 117(3):308–315, 1981.

[146] M. Nowak and R. May. Superinfection and the evolution of parasite virulence. *Proceedings of the Royal Society B*, 255:81–89, 1994.

[147] P.C. Cross, J.O. Lloyd-Smith, P.L.F. Johnson, and W.M. Getz. Duelling timescales of host movement and disease recovery determine invasion of disease in structured populations. *Ecology Letters*, 8:587–595, 2005.

[148] M. Macpherson, R. Davidson, D. Duncan, P. Lurz, A. Jarrott, and A. White. Incorporating habitat distribution in wildlife disease models: conservation implications for the threat of squirrelpox on the Isle of Arran. *Animal Conservation*, 19(1):3–14, 2015.

[149] I. Nurmoja, K. Mõtus, M. Kristian, T. Niine, K. Schulz, K. Depner, and A. Viltrop. Epidemiological analysis of the 2015-2017 African swine fever outbreaks in Estonia. *Preventive Veterinary Medicine*, 181:104556, 2020.

[150] S. Bellini, D. Rutili, and V. Guberti. Preventive measures aimed at minimizing the risk of African swine fever virus spread in pig farming systems. *Acta Veterinaria Scandinavica*, 58(82):10, 2016.

[151] F. Vial, E. Miguel, W. Johnston, A. Mitchell, and C. Donnelly. Bovine tuberculosis risk factors for British herds before and after the 2001 Foot-and-Mouth epidemic: What have we learned from the TB99 and CCS2005 studies? *Transboundary and Emerging Diseases*, 62:505–515, 2013.

[152] C. Gortázar and J. de la Fuente. COVID-19 is likely to impact animal health. *Preventive Veterinary Medicine*, 180:105030, 2020.

[153] R.M. Anderson and R.M. May. *Infectious Diseases of Humans: dynamics and control*. Oxford University Press, 1992.

[154] M. Aliee, K.S. Rock, and M.J. Keeling. Estimating the distribution of time to extinction of infectious diseases in mean-field approaches. *J. R. Soc. Interface*, 17:1–7, 2020.

[155] J.O. Lloyd-Smith, P.C. Cross, C.J. Briggs, M. Daugherty, W.M. Getz, J. Latto, M.S. Sanchez, A.B. Smith, and A. Swei. Should we expect population thresholds for wildlife disease? *Trends in Ecology and Evolution*, 20(9):511–9, 2005.

[156] I. Nåsell. A new look at the critical community size for childhood infections. *Journal of Theoretical Population Biology*, 67:203–216, 2005.

[157] G. Garnett, S. Cousens, T. Hallet, R. Steketee, and N. Walker. Mathematical models in the evaluation of health programmes. *Lancet*, 378(9790):515–525, 2011.

[158] I. Nåsell. On the time to extinction in recurrent epidemics. *Journal of the Royal Statistical Society*, 61(2):309–330, 1999.

[159] H. Andersson and B. Djehiche. A threshold limit theorem for the stochastic logistic epidemic. *Journal of Applied Probability*, 35(3):662–670, 1998.

[160] F. Ball, T. Britton, and P. Neal. On expected durations of birth-death processes with applications to branching processes and SIS epidemics. *Journal of Applied Probability*, 53(1):203–215, 2016.

[161] L.J.S. Allen and A.M. Burgin. Comparison of deterministic and stochastic SIS and SIR models in discrete time. *Mathematical Biosciences*, 163:1–33, 2000.

[162] D. Clancy and S.T. Mendy. The effect of waning immunity on long-term behaviour of stochastic models for the spread of infection. *Journal of Mathematical Biology*, 61:527–544, 2010.

[163] F. Brauer and C. Castillo-Chavez. *Mathematical Models in Population Biology and Epidemiology*, volume 2 of *Texts in Applied Mathematics*. Springer, 2012.

[164] D.B. George, C.T. Webb, M.L. Farnsworth, T.J. O'Shea, R.A. Bowen, D.L. Smith, T.R. Stanley, L.E. Ellison, and C.E. Rupprecht. Host and viral ecology determine bat rabies seasonality and maintenance. *Proc. Natl. Acad. Sci. U.S.A*, 108(25):10208–10213, 2011.

[165] H.H.Jr. Balfour, S.K. Dunmire, and K.A. Hogquist. Infectious mononucleosis. *Clinical and Translational Immunology*, 4(2):e33, 2015.

[166] World Health Organisation. Coronavirus disease 2019 (COVID-19): situation report, 73. Technical documents, World Health Organisation, 2020.

[167] D. Ebert, M. Lipsitch, and K.L. Mangin. The effect of parasites on host population density and extinction: experimental epidemiology with Daphnia and six microparasites. *The American Naturalist*, 156(5):459–477, 2000.

[168] J.J. Ryder, M.R. Miller, A. White, R.J. Knell, and M. Boots. Host-parasite population dynamics under combined frequency- and density-dependent transmission. *Oikos*, 116:2017–2026, 2007.

[169] D.T. Gillespie. Exact stochastic simulation of coupled chemical reactions. *The Journal of Physical Chemistry*, 81(25):2340–2361, 1977.

[170] E. Renshaw. *Modelling Biological Populations in Space and Time*. Cambridge University Press, 1991.

[171] J.R. Norris. *Markov Chains*, chapter 3. Cambridge University Press, 1997.

[172] N.T.J. Bailey. *The Mathematical Theory of Infectious Diseases*. Griffin, 1975.

[173] H.A. McCallum, M. Jones, C. Hawkins, R. Hamede, S. Lachish, D.L. Sinn, N. Beeton, and B. Lazenby. Transmission dynamics of Tasmanian devil facial tumor disease may lead to disease-induced extinction. *Ecology*, 90(12):3379–92, 2009.

[174] L. Peng, W. Yang, D. Zhang, C. Zhuge, and L. Hong. Epidemic analysis of COVID-19 in China by dynamical modeling. *MedRxiv*, 2020.

[175] Z. Yang, Z. Zeng, K. Wang, S.S. Wong, W. Liang, M. Zanin, P. Liu, X. Cao, Z. Gao, Z. Mai, J. Liang, X. Liu, S. Li, Y. Li, F. Ye, W. Guan, Y. Yang, F. Li, S. Luo, Y. Xie, B. Liu, Z. Wang, S. Zhang, Y. Wang, N. Zhong, and J. He. Modified SEIR and AI prediction of the epidemics trend of COVID-19 in China under public health interventions. *Journal of Thoracic Disease*, 12(3):165–174, 2020.

[176] J.S. Gray. The ecology of ticks transmitting Lyme borreliosis. *Experimental and Applied Acarology*, 22:249–258, 1998.

[177] N. Nyangiwe, M. Yawa, and V. Muchenje. Driving forces for changes in geographic range of cattle ticks (acari: Ixodidae) in Africa: A review. *South African Journal of Animal Science*, 48(5):13, 2018.

[178] Y. Rechav, M.M. Knight, and R.A.I. Norval. Life cycle of the tick *Rhipicephalus evertsi evertsi* neumann (acarina: ixodidae) under laboratory conditions. *The Journal of Parasitology*, 63(3):575–579, 1977.

[179] J. Shi, Z. Hu, F. Deng, and S. Shen. Tick-borne viruses. *Virologica Sinica*, 33(1):21–43, 2018.

[180] S.K. Wikel. Ticks and tick-borne infections: Complex ecology, agents, and host interactions. *Veterinary Science*, 5(2):60, 2018.

[181] L. Ferreri, P. Bajardi, and M. Giacobini. Non-systemic transmission of tick-borne diseases: A network approach. *Commun Nonlinear Sci Numer Simulat*, 39:149–155, 2016.

[182] T.C. Moore, L.A. Pulscher, L. Caddell, M.E. von Fricken, B.D. Anderson, B. Gonchigoo, and G.C. Gray. Evidence for transovarial transmission of tick-borne rickettsiae circulating in Northern Mongolia. *PLOS Neglected Tropical Diseases*, 12(8):e0006696, 2018.

[183] C.D. Paddock, R.S. Lane, J.E. Staples, and M.B. Labruna. *Changing paradigms for tick-borne diseases in the Americas*, chapter A8, pages 221–257. National Academies Press, 2016.

[184] N. Boulanger and S. Wikel. Induced transient immune tolerance in ticks and vertebrate host: A keystone of tick-borne diseases? *Frontiers in Immunology*, 12:284, 2021.

[185] A. Mysterud, V.M. Stigum, I.V. Seland, A. Herland, W.R. Easterday, S. Jore, O. Østerås, and H. Viljugrein. Tick abundance, pathogen prevalence, and disease incidence in two contrasting regions at the northern distribution range of Europe. *Parasites and Vectors*, 11(1):1–11, 2018.

[186] C. Bouchard, A. Dibernardo, J. Koffi, P.A. Leighton, and L.R. Lindsay. Increased risk of tick-borne diseases with climate and environmental changes. *Can. Commun. Dis Rep.*, 45(4):83–89, 2019.

[187] A. Estrada-Peña. Tick-borne pathogens, transmission rates and climate change. *Frontiers in Bioscience*, 14:2674–2687, 2009.

[188] L. Gilbert. Altitudinal patterns of tick and host abundance: a potential role for climate change in regulating tick-borne diseases? *Oecologia*, 162(1):217–225, 2010.

[189] L.K. Jackson, D.M. Gaydon, and J. Goddard. Seasonal activity and relative abundance of amblyomma americanum in Mississippi. *J. Med. Entomol.*, 33(1):128–131, 1996.

[190] A. Mysterud, W.R. Easterday, V.M. Stigum, A.B. Aas, E.L. Meisingset, and H. Viljugrein. Contrasting emergence of Lyme disease across ecosystems. *Nature Communincations*, 7(11882):11, 2016.

[191] J.M. Olwoch, A.S. Van Jaarsveld, C.H. Scholtz, and I.G. Horak. Climate change and the genus Rhipicephalus (acari: Ixodidae) in Africa. *Onderstepoort Journal of Veterinary Research*, 74(1):45–72, 2007.

[192] S.E. Randolph. Dynamics of tick-borne disease systems: minor role of recent climate change. *Rev. Sci. Tech. Off. Int. Epiz.*, 27(2):367–381, 2008.

[193] J.P.W. Scharlemann, P.J. Johnson, A.A. Smith, D.W. Macdonald, and S.E. Randolph. Trends in ixodid tick abundance and distribution in Great Britain. *Medical and Veterinary Entomology*, 22(3):238–247, 2008.

[194] M. Begon. *Effects of Host Diversity on Disease Dynamics*, chapter 1, pages 187–221. Princeton University Press, 2008.

[195] P.T. Johnson and D.W. Thieltges. Diversity, decoys and the dilution effect: how ecological communities affect disease risk. *Journal of Experimental Biology*, 213(6):961–970, 2010.

[196] C.A. Cobbold, J. Teng, and J.S. Muldowney. The influence of host competition and predation on tick densities and management implications. *Theoretical Ecology*, 8:349–368, 2015.

[197] Y. Lou and J. Wu. Tick seeking assumptions and their implications for Lyme disease predictions. *Ecological Complexity*, 17:99–106, 2014.

[198] Y. Lou, J. Wu, and X. Wu. Impact of biodiversity and seasonality on Lyme-pathogen transmission. *Theoretical Biology and Medical Modelling*, 11(50):25, 2014.

[199] M. Brossard and S.K. Wikel. Tick immunobiology. *Parasitology*, 129(S1):S161–S176, 2004.

[200] S.K. Wikel. Host immunity to ticks. *Annu. Rev. Entomol.*, 41:1–22, 1996.

[201] L. Fajs, I. Humolli, A. Saksida, N. Knap, M. Jelovšek, M. Korva, I. Dedushaj, and T. Avšič-Županc. Prevalence of Crimean-Congo haemorrhagic fever virus in healthy population, livestock and ticks in Kosovo. *PLoS One*, 9(11):1–6, 2014.

[202] A. Moming, X. Yue, S. Shen, C. Chang, C. Wang, T. Luo, Y. Zhang, R2. Guo, Z. Hu, Y. Zhang, F. Deng, and S. Sun. Prevalence and phylogenetic analysis of Crimean-Congo hemorrhagic fever virus in ticks from different ecosystems in Xinjiang, China. *Virologica Sinica*, 33(1):67–73, 2018.

[203] S. Randolph. Tick ecology: Processes and patterns behind the epidemiological risk posed by ixodid ticks as vectors. *Parasitology*, 129(S1):S37–S65, 2004.

[204] K. Anderson, V.O. Ezenwa, and A.E. Jolles. Tick infestation patterns in free ranging African buffalo (*Syncercus caffer*): Effects of host innate immunity and niche segregation among tick species. *International Journal for Parasitology: Parasites and Wildlife*, 2:1–9, 2013.

[205] G.B. Schoeler and S.K. Wikel. Modulation of host immunity by haematophagous arthropods. *Annals of Tropical Medicine and Parasitology*, 95(8):755–771, 2001.

[206] Y. Lou and J. Wu. Modeling Lyme disease transmission. *Infectious Disease Modelling*, 2(2):229–243, 2017.

[207] M. Maliyoni, F. Chirove, H.D. Gaff, and K.S. Govinder. A stochastic tick-borne disease model: Exploring the probability of pathogen persistence. *Bull Math Bio.*, 79:1999–2021, 2017.

[208] H.D. Gaff and L.J. Gross. Modeling tick-borne disease: A metapopulation model. *Bulletin of Mathematical Biology*, 69(1):265–288, 2007.

[209] H. Gómez-Acevedo. Global stability in a model for diseases transmitted by ixodid ticks. *Canadian Applied Mathematics Quarterly*, 11(1):81–92, 2003.

[210] P.J. Hudson, R. Norman, M.K. Laurenson, D. Newborn, M. Gaunt, L. Jones, H. Reid, E. Gould, R. Bowers, and A. Dobson. Persistence and transmission of tick-borne viruses: Ixodes ricinus and louping-ill virus in red grouse populations. *Parasitology*, 111:S49–S58, 1995.

[211] T. Hoch, E. Breton, and Z. Vatansever. Dynamic modeling of Crimean-Congo Hemorrhagic Fever virus (CCHFv) spread to test control strategies. *Journal of Medical Entomology*, 55(5):1124–1132, 2018.

[212] S. Li, L. Gilbert, P.A. Harrison, and M.D.A. Rounsevell. Modelling the seasonality of Lyme disease risk and the potential impacts of a warming climate within the heterogeneous landscapes of Scotland. *J. R. Soc. Interface*, 13:20160140, 2016.

[213] S.M. Moore, R.J. Eisen, A. Monaghan, and P. Mead. Meteorological influences on the seasonality of Lyme disease in the United States. *Am. J. Trop. Med. Hyg.*, 90(3):486–496, 2014.

[214] A.L. Reye, J.M. Hübschen, A. Sausy, and C.P. Muller. Prevalence and seasonality of tick-borne pathogens in questing ixodes ricinus ticks from Luxembourg. *App. and Env. Microbiology*, 76(9):2923–2931, 2010.

[215] A. Roome, R. Spathis, L. Hill, J.M. Darcy, and R.M. Garruto. Lyme disease transmission risk: Seasonal variation in the built environment. *Healthcare*, 6(3):84, 2018.

[216] Z.Y.X. Huang, F. Van Langevelde, A. Estrada-Peña, G. Suzán, and W.F. De Boer. The diversity–disease relationship: evidence for and criticisms of the dilution effect. *Parasitology*, 143(9):1075–86, 2016.

[217] T. Levi, F. Keesing, R.D. Holt, M. Barfield, and R.S. Ostfield. Quantifying dilution and amplification in a community of hosts for tick-borne pathogens. *Ecological Applications*, 26(2):484–498, 2016.

[218] K. Nah, F.M.G. Magpantay, Á. Bede-Fazekas, G. Röst, A.J. Trájer, X. Wu, X. Zhang, and J. Wu. Assessing systemic and non-systemic transmission risk of tick-borne encephalitis virus in Hungary. *PLoS One*, 14(6):e0217206, 2019.

[219] E. Nonaka, G.D. Ebel, and H.J. Wearing. Persistence of pathogens with short infectious periods in seasonal tick populations: The relative importance of three transmission routes. *PLoS One*, 5(7):e11745, 2010.

[220] L. Eisen and R.S. Lane. *Lyme Borreliosis Biology, Epidemiology and Control*, chapter 4: Vectors of Borrelia burgdorferi sensu lato. Centre for Agriculture and Bioscience (CAB), 2002.

[221] E.I. Korenberg. Comparative ecology and epidemiology of Lyme disease and tick-borne encephalitis in the Former Soviet Union. *Parasitology Today*, 10(4):157–160, 1994.

[222] R.C. Falco, D.F. McKenna, T.J. Daniels, R.B. Nadelman, J. Nowakowski, D. Fish, and G.P. Wormser. Temporal relation between ixodes scapularis abundance and risk for Lyme disease associated with erythema migrans. *Am. J. of Epidemiol.*, 149(8):771–776, 1989.

[223] K.A. Orloski, E.B. Hayes, G.L. Campbell, and D.T. Dennis. Surveillance for Lyme disease - United States, 1992–1998. *Surveillance Summaries*, 49(SS03):1–11, 2000.

[224] V. Cairns, C. Wallenhorst, S. Rietbrock, and C. Martinez. Incidence of Lyme disease in the UK: a population-based cohort study. *BMJ Open*, 9:e025916, 2019.

[225] K. Lihou, H.R. Vineer, and R. Wall. Distribution and prevalence of ticks and tick-borne disease on sheep and cattle farms in Great Britain. *Parasites Vectors*, 13(406):10, 2020.

[226] A. Grochowska, R. Milewski, S. Pancewicz, J. Dunaj, P. Czupryna, A.J. Milewska, M. Róg-Makal, S. Grygorczuk, and A. Moniuszko-Malinowska. Comparison of tick-borne pathogen prevalence in ixodes ricinus ticks collected in urban areas of Europe. *Scientific Reports*, 10(6975):9, 2020.

[227] G.-P. Zhao, Y.-X. Wang, Z.-W. Fan, Y. Ji, M. Liu, W.-H. Zhang, X.-L. Li, S.-X. Zhou, H. Li, S. Liang, W. Liu, Y. Yang, and L.-Q. Fang. Mapping ticks and tick-borne pathogens in China. *Nature Communications*, 12(1075):13, 2021.

[228] L.A. Pulscher, T.C. Moore, L. Caddell, L. Sukhbaatar, M.E. von Fricken, B.D. Anderson, B. Gonchigoo, and G.C. Gray. A cross-sectional study of small mammals for tick-borne pathogen infection in northern Mongolia. *Inf. Ecol. and Epidem.*, 8(1):1450591, 2018.

[229] H. Nasirian. New aspects about Crimean-Congo hemorrhagic fever (CCHF) cases and associated fatality trends: A global systemic review and met-analysis. *Comparative Immunology, Microbiology and Infectious Diseases*, 69:101429, 2020.

[230] J.R. Spengler, E. Bergeron, and C.F. Spiropoulou. Crimean-Congo hemorrhagic fever and expansion from endemic regions. *Current Opinion in Virology*, 34:70–78, 2019.

[231] I. Dumic and E. Severnini. "Ticking Bomb": The impact of climate change on the incidence of Lyme disease. *Canadian Journal of Infectious Diseases and Medical Microbiology*, 2018:10, 2018.

[232] F. Keesing, J. Brunner, S. Duerr, M. Killilea, K. LoGiudice, K. Schmidt, H. Vuong, and R.S. Ostfeld. Hosts as ecological traps for the vector of Lyme disease. *Proc. R. Soc. B*, 276:3911–3919, 2009.

[233] R.S. Ostfeld, O.M. Cepeda, K.R. Hazler, and M.C. Miller. Ecology of Lyme disease: Habitat associations of ticks (ixodes scapularis) in a rural landscape. *Ecological Applications*, 5(2):353–361, 1995.

[234] R.E.L. Paul, M. Cote, E.L. Naour, and S.I. Bonnet. Environmental factors influencing tick densities over seven years in a French suburban forest. *Parasites and Vectors*, 9(309):10, 2016.

[235] S. Thamm, E.K.V. Kalko, and K. Wells. Ectoparasite infestations of hedgehogs (*Erinaceus europaeus*) are associated with small-scale landscape structures in an urban–suburban environment. *EcoHealth*, 6(3):404–413, 2009.

[236] T. Borowik, T. Cornulier, and B. Jedrzejewska. Environmental factors shaping ungulate abundances in Poland. *Acta Theriol.*, 58:403–413, 2013.

[237] S.L. Gilbert, K.J. Hundertmark, M.S. Lindberg, D.K. Person, and M.S. Boyce. The importance of environmental variability and transient population dynamics for a northern ungulate. *Front. Ecol. Evol.*, 8:380, 2020.

[238] D. Desmecht, G. Gerbier, C. Gortázar, V. Grigaliuniene, G. Helyes, M. Kantere, D. Korytarova, A. Linden, A. Miteva, I. Neghirla, E. Olsevskis, S. Ostojic, T. Petit, C. Staubach, H.-H. Thulke, A. Viltrop, W. Richard, G. Wozniakowski, J. Abrahantes Cortiñas, A. Broglia, S. Dhollander, E. Lima, A. Papanikolaou, Y. Van der Stede, and K. Ståhl. Epidemiological analysis of African swine fever in the European Union (September 2019 to August 2020). *EFSA Journal*, 19(5):6572, 2021.

[239] S.S. Nielsen, J. Alvarez, D.J. Bicout, P. Calistri, K. Depner, J.A. Drewe, B. Garin-Bastuji, J.L.G. Rojas, C. Gortázar, M. Herskin, V. Michel, M.A.M. Chueca, P. Pasquali, H.C. Roberts, L.H. Sihvonen, H. Spoolder, K. Ståhl, A. Velarde, C. Winckler, J.C. Abrahantes, S. Dhollander, C. Ivanciu, A. Papanikolaou, Y. Van der Stede, S. Blome, V. Guberti, F. Loi, S. More, E. Olsevskis, H.-H. Thulke, and A. Viltrop. ASF exit strategy: Providing cumulative evidence of the absence of African swine fever virus circulation in wild boar populations using standard surveillance measures. *EFSA Journal*, 19(3):6419, 2021.

[240] T. Xiong, W. Zhang, and C.-T. Chen. A fortune from misfortune: Evidence from Hog Firms' stock price responses to China's African swine fever. *CARD Working Papers*, 619, 2020.

[241] Y.-S. Jo and C. Gortázar. African swine fever in wild boar: Assessing interventions in South Korea. *Transboundary and Emerging Diseases*, 00:1–12, 2021.

[242] J.-S. Lim, T. Vergne, S.-I. Pak, and E. Kim. Modelling the deathbed of ASF-infected wild boars in South Korea using 2019-2020 national surveillance data. *Animals*, 11:1208, 2021.

[243] D. Anderson, Y. Negishi, H. Ishiniwa, K. Okuda, T.G. Hinton, R. Toma, J. Nagata, H.B. Tamate, and S. Kaneko. Introgression dynamics from invasive pigs into wild boar following the March 2011 natural and anthropogenic disasters at Fukushima. *Proc. R. Soc. B*, 288:20210874, 2021.

[244] Y. Yang and H. Nishiura. Assessing the geographic range of classical swine fever vaccinations by spatiotemporal modelling in Japan. *Transboundary and Emerging Diseases*, pages 1–10, 2021.

[245] M. Frant, A. Gal, Ł. Bocian, A. Ziętek-Barszcz, K. Niemczuk, and G. Wozniakowski. African swine fever virus (ASFV) in Poland in 2019—wild boars: Searching pattern. *Agriculture*, 11(1):45, 2021.

[246] S.S. Nielsen, J. Alvarez, D.J. Bicout, P. Calistri, K. Depner, J.A. Drewe, B. Garin-Bastuji, J.L.G. Rojas, C. Gortázar, M. Herskin, V. Michel, P. Pasquali, H.C. Roberts, L.H. Sihvonen, H. Spoolder, K. Ståhl, A. Velarde, C. Winckler, S. Blome, A. Boklund, A. Bøtner, S. Dhollander, C. Rapagnà, Y. Van der Stede, and M.A.M. Chueca. Research priorities to fill knowledge gaps in the control of African swine fever: possible transmission of African swine fever virus by vectors. *EFSA Journal*, 19(6):6676, 2021.

[247] S.S. Nielsen, J. Alvarez, D.J. Bicout, P. Calistri, K. Depner, J.A. Drewe, B. Garin-Bastuji, J.L.G. Rojas, C. Gortázar, M. Herskin, V. Michel, P. Pasquali, H.C. Roberts, L.H. Sihvonen, H. Spoolder, K. Ståhl, A. Velarde, C. Winckler, S. Blome,

A. Boklund, A. Bøtner, S. Dhollander, Y. Van der Stede, and M.A.M. Chueca. Research priorities to fill knowledge gaps on ASF seasonality that could improve the control of ASF. *EFSA Journal*, 19(4):6550, 2021.

[248] A. Boklund, A. Bøtner, T.V. Chesnoiu, K. Depner, D. Desmecht, V. Guberti, G. Helyes, D. Korytarova, A. Linden, A. Miteva, S. More, E. Olsevskis, S. Ostojic, H. Roberts, M. Spiridon, K. Ståhl, H.-H. Thulke, G. Vilija, A. Viltrop, R. Wallo, G. Wozniakowski, J. Abrahantes Cortiñas, S. Dhollander, A. Gogin, C. Ivanciu, A. Papanikolaou, L.C.G. Villeta, and C. Gortázar. Epidemiological analyses of African swine fever in the European Union (November 2018 to October 2019). *EFSA Journal*, 18(1):5996, 2020.

[249] A. Boklund, B. Cay, K. Depner, Z. Földi, V. Guberti, M. Masiulis, A. Miteva, S. More, E. Olevskis, P. Šatrán, M. Spiridon, K. Ståhl, H.-H. Thulke, A. Viltrop, G. Wozniakowski, A. Broglia, J.C. Abrahantes, S. Dhollander, A. Gogin, F. Verdonck, L. Amato, A. Papanikolaou, and C. Gortázar. Epidemiological analyses of African swine fever in the European Union (November 2017 until November 2018). *EFSA Journal*, 16(11):5494, 2018.

[250] M.L. Penrith. Current status of African swine fever. *CABI Agric. Biosci.*, 1:11, 2020.

[251] E. Mighell and M.P. Ward. African swine fever spread across Asia, 2018–2019. *Transboundary and Emerging Diseases*, 00:1–11, 2021.

[252] D. Tao, D. Sun, Y. Liu, S. Wei, Z. Yang, T. An, F. Shan, Z. Chen, and J. Liu. One year of African swine fever outbreak in China. *Acta Tropica*, 211:105602, 2020.

[253] E. Denstedt, A. Porco, J. Hwang, N.T.T. Nga, P.T.B. Ngoc, S. Chea, K. Khammavong, P. Milavong, S. Sours, K. Osbjer, S. Tum, B. Douangngeun, W. Theppanya, N.V. Long, N.T. Phuong, L.T.V. Quang, V.V. Hung, N.T. Hoa, D.L. Anh, A. Fine, and M. Pruvot. Detection of African swine fever virus in free-ranging wild boar in Southeast Asia. *Transboundary and Emerging Diseases*, 00:1–7, 2021.

[254] D.N. Schettino, S.K. Abdrakhmanov, K.K. Beisembayev, F.I. Korennoy, A.A. Sultanov, Y.Y. Mukhanbetkaliyev, A.S. Kadyrov, and A.M. Perez. Risk for African swine fever introduction into Kazakhstan. *Front. Vet. Sci.*, 8:605910, 2021.

[255] A.R. Cook, W. Otten, G. Marion, G.J. Gibson, and C.A. Gilligan. Estimation of multiple transmission rates for epidemics in heterogeneous populations. *Proc. Nat. Aca. Sc. U.S.A*, 104(51):20392–20397, 2007.